IMPACT OF PVT PROPERTIES OF THE FLUID ON THE LBM SCHEME WITHIN THE SCALE INTEGRATION FOR SHALE RESERVOIRS

A Thesis

by

ALEXANDER TARAKANOV

Submitted to the Office of Graduate and Professional Studies of
Texas A&M University
in partial fulfillment of the requirements for the degree of

DOCTOR OF PHILOSOPHY

Chair of Committee,	Eduardo Gildin
Committee Members,	Hadi Nasrabadi
	Michael King
	Yalchin Efendiev
Head of Department,	Daniel Hill

December 2017

Major Subject: Petroleum Engineering

ABSTRACT

Modelling of the performance of shale gas reservoirs is known for the presence of multiple scales. The latter includes pore-scale, fracture scale and field scale. The nature of flow-mechanisms at various scales is different. Therefore, separate treatment of the physical processes is required. On the other hand, an integrated approach is highly beneficial for practical implementation. One of the candidates for seamless integration concerned is the Lattice-Boltzmann Method. The latter fact together with the demands of the industry provides the major motivation for the present work.

In this study the novel Lattice-Boltzmann Model for pore-scale simulations has been introduced. The major advantage of the approach concerned is that the mathematical formulation of the model has a high degree of self-consistency. The latter means that it does not have an artificially introduced terms like pseudo-potentials, which are common for conventional Lattice-Boltzmann schemes. Despite the advantages of the approach in terms of mathematical formulation, there exist certain limitations because of the issues with numerical stability. One of the most important results of the present work is that the issues concerned can not be resolved by the reasonable increase of the number of lattice vectors in the model. The limitations involved make the scheme impractical for field-scale simulations. Therefore, an alternative formulation of Lattice-Boltzmann method for reservoir modelling is required.

In the present work, a novel pseudo-potential model for field-scale simulations has been introduced. The model concerned demonstrates a reasonable agreement with the analytical techniques in the case of steady-state flow. However, further investigation shows significant deviations because of the numerical diffusion. Moreover, it has been shown that significant numerical diffusion is a feature of the majority of the existent pseudo-potential

models. The numerical effect concerned is critically important in the case of the multi-phase flow, because it can lead to non-physical solutions. In order to resolve the problem concerned a novel Lattice-Boltzmann Scheme has been introduced. The scheme demonstrates reasonable agreement with analytical methods and with simulations performed with trusted programs for reservoir modelling.

Finally, the major contribution of the present work includes the development of self-consistence approach for simulations at pore-scale, the proof of fundamental limitations of the model introduced, observation of numerical diffusion in pseudo-potential Lattice-Boltzmann Methods, and the solution of the latter issue through the development of the novel Lattice-Boltzmann scheme for field-scale simulations.

ACKNOWLEDGMENTS

I would like to express my very great appreciation to Dr. Eduardo Gildin for the guidance in the research and for the invaluable support of me as a student.

Dr. Eduardo Gildin, Dr. Hadi Nasrabadi, Dr. Michael King and Dr. Yalchin Efendief are greatly acknowledged for the suggestions for the research.

I am particularly grateful for the assistance given by Dr. Zachary Benamram and Kingsley Madiebo for long discussions on Lattice-Boltzmann Method.

CONTRIBUTORS AND FUNDING SOURCES

Contributors

This work was supported by a thesis committee consisting of Professors Dr. Eduardo Gildin, Dr. Hadi Nasrabadi and Dr. Michael King of the Department of Petroleum Engineering and Professor Dr. Yalchin Efendiev of the Department of Mathematics.

All other work conducted for the thesis (or) dissertation was completed by the student independently.

Funding Sources

Graduate study was supported by a fellowship from the Crisman Research Institute.

NOMENCLATURE

LBM	Lattice-Boltzmann Method
DKE	Discrete Kinetic Equation
BGK	BhatnagarGrossKrook
ODE	Ordinary Differential Equations
PDE	Partial Derivatives Equations
PVT	Pressure Volume Temperature
EOS	Equation of State
FV	Finite Volume
FE	Finite Element
MCM	Multiple Continuum Model
DFN	Discrete Fracture Network

TABLE OF CONTENTS

Page

LIST OF FIGURES

FIGURE Page

LIST OF TABLES

TABLE Page

1. INTRODUCTION

At the beginning of the 20th century, the breakthrough in the technology of hydraulic fracturing has made it possible to produce hydrocarbons from shale reservoirs in the economically efficient way. Despite the challenges in the application of the technology concerning hydraulic fracturing and relatively low quality of the shale reservoirs, they are considered as one of the most important sources of energy in the future. There are two reasons for that. The first one is the growth of human population [1] and in turn, the increase of the overall energy demands [2] and [3]. The second cause is the depletion of oil and gas reservoirs of high quality. That latter serves as the backbone to increase the role of shale reservoirs given that the total amount of hydrocarbons stored in shale reservoirs is significantly greater if compared with conventional high quality reservoirs [4].

The conclusion of the discussion above is that, despite the recent drop of the oil-price, the prospects of production from shale reservoirs are still promising. This gives a motivation for the research in this area, and particularly in the numerical solution of the complex interplay between the mechanisms of a production in shale reservoirs with further application to the problems of the production forecast and analysis of transport phenomena in such reservoirs.

The main reason why the predictive modelling of shale reservoirs is still challenging nowadays is the complicated interaction of different scales that represent the structural features of these rocks. The vast majority of conventional reservoir simulation tools have not been designed to address the impact of multiple scales. Therefore, a lot of effort have been taken in order to develop an integrated approach to the modelling of shale reservoirs. To the best of the author's knowledge, the issue concerned has been partially addressed. However, there is a need for the method that allows one to perform this integration seam-

lessly, i.e. within a single algorithm for the numerical modelling of all of the scales. This is the first reason that makes the Lattice-Boltzmann Method (LBM) a promising tool for the simulation of shale reservoirs. In the present work it is shown that the integration concerned can be made naturally with LBM, because of both kinetic nature of the method and its outstanding flexibility.

The second reason is properties of LBM as an algorithm for numerical simulations. Various studies indicate that LBM has a remarkable efficiency for GPU-based parallel computing [5]. From practical point of view, this means that LBM has a potential to work better for massive calculations if compared with conventional reservoir simulation tools.

The reasoning above shows that LBM has very promising prospects in the integrated shale reservoir modelling. The investigation of such prospectives is the main motivation of the present work. For that purpose, a fully-coupled model has been developed. There are several main issues that has been addressed in the following work. The first one is the upscaling of PVT properties of the fluid inside the nano-pores. The second issue is consequent treatment of equation of state for nano-scale simulations. Finally, a new approach for EOS integration into field-scale simulations has been developed. The need for two different treatments of EOS at different scales is discussed later. The main scientific value of the present work is that the tools for EOS modelling preserve the computational efficiency of the method and significantly improve its stability.

1.1 Challenges in Simulation of Shale Reservoirs and Literature Review

Despite the long history of production from shale reservoirs, there is no universal approach for the modelling of unconventional oil and gas fields. This may be due to the higher degree of complexity of physics of shale reservoirs if compared with conventional ones. In general, a shale gas reservoir is a highly heterogeneous source rock with a well-developed network of natural fractures. The typical size of the pores in such rocks varies

from 10 to 100 of nanometers [6], [7]. Because of such small pores, permeability of the rock is extremely low if compared with conventional reservoirs [8]. The other factor that has a significant impact on the mechanism of fluid flow is the notable amount of kerogen, which affects both connectivity of the pore space and apparent permeability [9]. In addition, shale reservoirs are well-known for the high degree of heterogeneity of rock properties [10].

The combination of these factors cause significant difficulties for understanding of flow mechanism in shales. Nowadays, the majority of engineers believe that in shale reservoirs hydrocarbons migrate from source rock to the well only through the fracture network [11]. In other words, the presence and the quality of the fracture network is critical for the production from shale reservoirs. Creating models for handling this complex flow mechanism brings several challenges for simulations.

The first challenge is the geometry of such reservoirs. Nowadays, the only economical way of production from shales is through the use of multiple hydraulic fracturing. Even with such technology, it is necessary to have a wide network of natural fractures to have reasonable production rates. Different authors indicate that interaction of natural fractures with the artificial hydraulic fractures created by the process, can be extremely complicated and results in a non-trivial geometry of the fracture network [12], [13], [14]. Moreover, various studies show that conductivity and effective permeability of fracture network is highly sensitive to the stress pattern. This means that for the accurate simulations, coupling of fluid dynamics with geomechanics is necessary [15]. On the other hand, attention should be paid to the cross-flow between the fracture network and solid matrix.

The second challenge is caused by the sizes of the pore network, which may be in the range of nanometers. Actually, it is not a single problem, but a set of problems. To this end, phase behaviour of fluids in nano-pores that can be different from the traditional one. Simple calculation shows that there could be around 100 to 10000 molecules in a

single pore of shale matrix. For such systems, the difference between the fluid and gas phase can be extremely subtle. Moreover, the interaction of molecules of the fluid with the surface of the pore becomes more significant if compared with fluid under normal conditions. In addition, high capillary pressures and interaction with kerogen can cause significant deviations from the traditional equation of state (EOS). Finally, such effects like adsorption contribute a lot to the overall flow pattern. The significance of some of these effects has been studied in [16], [17].

The third challenge that should be addressed is called the Klinkenberg effect [18]. The physics behind the phenomenon concerned is that inside the pores of small diameter, molecules of the fluid start to interact more intense with the surface in comparison with fluid in a macroscopic volume. This is due to the fact that the apparent viscosity of the fluid becomes different from those measured for the flow in traditional experiments.

Summarizing the challenges listed above, it is clear that the problems with simulation of unconventional reservoirs are caused by two reasons: flow in the network of natural fractures and physics of fluid behaviour in nano-pores. In order to address the first issue, standard methods for simulation of fractured reservoirs can be applied. The second issue can be reformulated in terms of modification of PVT properties. Existent approaches for simulation of shale reservoirs will be discussed in the next section.

1.2 Present Methodologies of Shale Reservoirs Modelling

The problem of simulation of shale reservoirs is not new to the industry. Therefore, the presence of great variety of tools for simulation of transport in shale rocks is not surprising. For the author's concern, most of the works about shale reservoirs are focused only on one of the part of problem of simulation of shale reservoirs. For example, only PVT properties of fluids inside small pores are studied, or only the transport in fractured media is considered. At the same time, there are studies where all the aspects of simulations

of shale reservoirs are integrated. The approaches are different in the robustness, in the type of data required, and in the accuracy of the solution. In the present section the most well-known techniques are discussed.

Proxy models are one of the popular tools for simulation of unconventional reservoirs [19], [20]. The foundation of the techniques involved can vary from analytical models [21], that make an attempt to capture all or at least the most essential physical processes, to artificial intelligence and machine learning. The obvious advantage of the methods concerned is absence of need for full 3D reservoir simulations and relatively small computational time as a consequence. By the definition, proxy modelling relies heavily on the available data. As a consequence, that models have limited application for the prediction of hydrocarbons production for a new well.

An accurate numerical simulation, which captures multi-scale and multi-physics phenomena, seems to be the most favourable tool for the forecast of the production of a new well in a field. Nowadays, the commercial reservoir simulators have certain limitations for applications to multi-scale problems. Therefore, the development of alternative techniques together with the improvement of the present ones is an important problem to be addressed. For the purposes of addressing the issue concerned, one needs to take into account the specific properties of shale reservoirs mentioned before. The latter has given birth to a plenty of excellent works on physics of shale reservoirs. The works concerned can be roughly divided into two categories: integrated approaches, and studies that are focused on a particular aspect of the problem, like fluid behaviour inside nano-scale pores or flow in fractured porous media. Because of this division, it is reasonable to organize the review with the same principle.

It has been mentioned that fluid properties or PVT properties may differ significantly from those under conditions of conventional reservoirs. It is well known that PVT has a significant impact on both reserves and fluid flow. Therefore, accurate representation of

PVT properties in the numerical scheme is important. The most common way to address the issue concerned is Klinkenberg's correction formula and Langmuir's isotherm [22]. In general, such methods can make a forecast of the production with reasonable accuracy; however, under certain conditions the corrections may misrepresent real behaviour of fluids. One of the possible reasons for that is that correction formulas have been derived under assumptions that might be no longer valid under reservoir conditions. Moreover, several experimental studies demonstrate the deviation of measured fluid properties from the computed ones it directly [23].

One of the possible solutions to the problem involved is direct numerical simulation of processes in nano-scale pores. Typically , slippage effect and adsorption are estimated independently. For instance, Klinkenberg's correction can be derived from flow simulations in porous media performed with commercial hydrodynamic simulators COMSOL [24]. Despite the atomistic level of the effect, conventional approaches for continuous media simulation can be applied if boundary conditions have been modified properly [25]. Mesoscopic methods or Lattice-Boltzmann Method in particular, are ratther popular [26]. In some cases Molecular Dynamic simulation tools are applicable [27]. For the corrections to the adsorption isotherm Molecular Dynamic simulations are used predominantly [28], [29]. However, it is possible to evaluate adsorption and slippage effects within a single simulation work flow [30]. Therefore, there exist plenty of reliable tools that can represent pore-scale physics effectively and accurately.

The discussion above can be formulated simply as: apply Klinkenberg's correction formula together with Langmuir isotherm, because those tools perform well in general. If this is not the case, then more detailed simulation of physics in small pores gives desired accuracy. The situation with simulation of impact of fracture network is not so clear and there is no widely recognized approach for numerical modelling of the systems concerned. Moreover, motivation for modelling can be different leading to distinct methods. For example,

a variety of semi-analytical models have been developed in the past for understanding the key parameters that control the behavior of shale reservoirs [31], [32]. Semi-analytical and analytical tools can be applied for the production data analysis of shale reservoirs as well [33]. Despite the advantages of analytical tools, the the applicability is limited by the complexity of the problem and desired accuracy of the solution.

Because of the present state of mathematics, the only way to avoid the restrictions concerned is numerical modelling. The great diversity of techniques can be observed in this field. There exist a variety of approaches that are still simple but expand the horizons of analytical tools. Typically, such methods are applied to simulations of flow in homogeneous reservoirs. The fracture network is represented by the set of straight fractures that are either parallel or perpendicular to each other. The motivation for applications of these methods is again understanding of physics in shales and sensitivity analysis for the relatively small computational price [34]. Because of the complexity of the shale reservoirs, there is a variety of studies focused on the particular aspect of flow, like fluid-fluid interaction. The object of the research in such works is physics of fluid motion. Therefore, computations are usually made for homogeneous or even one-dimensional reservoirs [35].

It has been mentioned earlier that shale reservoirs are characterized by high level of heterogeneity. Therefore for the practical purposes more involved techniques should be used. The most popular tools are Multiple Continuum Models (MCM) and Discrete Fracture Network (DFN). In the first family of methods, reservoir rock is represented by several porous rocks that can participate into mutual mass exchange. For the shale reservoirs one porous rock is typically the fracture network itself, and the other continuum is usually solid matrix with nano-pores. However the total number of medias can vary [36], [37]. In MCM models fracture network is represented as an effective media. Therefore, the advantage of the method is its relatively small computational cost because fractures are not resolved by the mesh. In other words, fracture network is upscaled to additional con-

tinuum. The disadvantage of the approach concerned comes from the coefficients that describe mass exchange between elements of MCM. Currently, the reasonable determination of the magnitudes of the coefficients still remains rather involved. In addition, several studies indicate that MCM models can not capture correct physical behavior in certain cases [38] and DFN models perform better. The idea behind DFN models is explained in the name of the method. Fracture network in DFN is given as a finite set of fractures. The computational mesh is generated in such a way that it is capable for resolving each individual fracture. Typically, that leads to very tiny mesh. As a result, DFN models typically have high accuracy but are extremely expensive from computational point of view. Because of those reasons, DFN models are rarely applied in field-scale calculations [39], but they are applied in the upscaling calculations for building MCM model [40]. From the above discussion it follows that DFN and MCM suffer from the classic trade-of in numerical methods: compromise between accuracy and computational time. As it usually happens in such cases, the truth is somewhere in the middle. In other words, the modern tendency in simulation of fractured and shale reservoirs is the combination of DFN and MCM. The goal is to resolve certain fractures via grid geometry, and simulate others as effective media [41]. Recent research demonstrates that such techniques have improved accuracy if compared with pure MCM and lower computational cost of than pure DFN [42].

1.3 Thesis Scope and Objectives

The main focus of the present study is the modelling of the flow of the fluid with prescribed EOS. Therefore, the EOS is a sort of the input data for LBM simulations presented here. This is the reason why the EOS is assumed to have a certain degree of generality. It has been mentioned that the linear EOS is natural for LBM schemes. The treatment of non-linear in LBM is not a trivial task. Moreover, the strong connection of the EOS with

the parameters of the spatial resolution has been observed.

The first important result of the present work is the development of the self-consistent LBM model for the numerical solution of the compressible version of the Navier-Stokes equations. The model concerned is capable to simulate the flow of the fluid with the given EOS. The first advantage of the model is the mathematical form of the equations. There are no artificially introduced terms like pseudo-potentials. This is the reason why in the present work, this model is referred to as a self-consistent approach. The second advantage of the developed approach is potential for efficient parallel computing. The method is self-consistent, therefore, there are no time expenses on sending the values of pseudo-potentials. This can speed up the simulation in parallel significantly.

The second result of the work is the demonstration of the capability of the novel self-consistent approach to be applied to the upscaling of PVT properties of the fluid inside the nano-pores. For the purposes of the proof of concept, corrections to the PVT properties of methane has been derived through the numerical simulations with LBM.

The third group of the results is related to the stability and to the accuracy of the method. It has been shown that the the novel self-consistent method has both the upper and the lower bound for the time step. This situation is unusual for numerical methods. In the present work it is shown that this issue is inherit for LBM self-consistent schemes and can not be addressed through the increase of the number of the lattice vectors.

These restrictions on the time step are related to the speed of sound of the fluid. This leads to the impractically small time steps for reservoir simulations with self-consistent model. Therefore, the novel pseudo-potential LBM scheme has been introduced. The model concerned has an acceptable level of accuracy for the simulation of steady-state flow. The issues with transient processes has been observed. Moreover, it has been demonstrated that the numerical diffusion is unavoidable for pseudo-potential methods.

Finally, in order to address the issue with the numerical diffusion a conceptually new

LBM scheme has been proposed for the reservoir simulations at the field scale. The novel approach is not as flexible as the traditional LBM in the sense that it can be applied only to the flow governed by the Darcy law. The additional work required to make it capable for solving of the Navier-Stokes equation. However, the method has a scientific value as a revision of the foundations of LBM.

1.4 Organization of the Work

This thesis is organized as follows: in chapter 1 the introduction to the present stage of shale reservoirs simulation together with the literature review of this field is given. Chapter 2 serves as a brief introduction to LBM.

In chapter 3 the model for the pore scale simulations with LBM is derived. The potential of the application of this model to the upscaling of PVT properties of the fluid inside the nano pores is demonstrated.

In chapter 4 is devoted to the observation of the capabilities of LBM as a computational method. First of all, the fundamental limitations of the proposed approach is shown. The need for pseudo-potential LBM models for field-scale simulations is discussed. A novel pseudo-potential LBM model is introduced. It is demonstrated, that pseudo-potential LBM models have certain limitations caused by the numerical diffusion.

In chapter 5 a conceptually new LBM scheme has been presented. The validation of the new method together with the prospects for further research are discussed.

In chapter 6 the results of the work are analysed. Directions for the future research are explored.

2. INTRODUCTION TO LATTICE-BOLTZMANN METHOD

2.1 Modelling of Continuous Media

There is no doubt that numerical simulation of physical systems is highly valuable for modern industry, especially in the cases when it is either too difficult or too expensive to make a reliable experimental study. Therefore, a vast majority of approaches have been developed. Despite the diversity of the methods all of them start from the equations that describe real physical systems. The appropriate choice of the equations is usually determined by the desired level of accuracy and by the scale of the system. The most common model is called continuous media approximation. In this framework, the system is described by the finite numbers of functions like density, pressure, temperature among others. The evolution of the system is normally governed by mass, momentum and energy conservation laws. One of the most popular examples is equations from fluid dynamics [45]:

$$\begin{aligned} \frac{\partial \rho}{\partial t} + \frac{\partial \rho u^\alpha}{\partial x^\alpha} &= 0 \\ \frac{\partial \rho u^\alpha}{\partial t} + \frac{\partial \rho u^\alpha u^\beta}{\partial x^\beta} + \frac{\partial \Pi^{\alpha\beta}}{\partial x^\beta} &= F^\alpha \end{aligned} \tag{2.1}$$

Here ρ is the density of the fluid, u^α is the velocity, $\Pi^{\alpha\beta}$ is the stress-tensor, F^α is vector of forces. In order to make a complete system of equations one should introduce closure relations. In the case of fluid dynamics it could be the expression for the stress-tensor and equation of state:

$$\begin{aligned} \Pi^{\alpha\beta} &= P\delta^{\alpha\beta} \\ P &= P(\rho) \end{aligned} \tag{2.2}$$

Here $P(\rho)$ is fluid pressure as function of density of the fluid. Physical systems with the characteristic scale of 1 μm and higher can be simulated with a reasonable accuracy

with continuous media models. This is the reason why such models are referred to as macroscopic models.

The other well-known approach that is heavily used in industry is molecular dynamic simulations or MD [46]. The area of application of the method concerned varies from the estimation of the energy of a given molecule to simulation of the evolution of the population of molecules. The governing equation in this case is the Schröedinger equation [47]:

$$i\hbar\frac{\partial\Psi}{\partial t} = -\frac{\hbar}{2m}\Delta\Psi + V\Psi \tag{2.3}$$

Here Ψ is the wave-function, V is the potential energy, m is the mass of the particle, and $\hbar$ is the Plank Constant. In theory, MD is based on the fundamental principles and equations of molecular motion. Therefore, the set of physical systems that MD can describe contains the world of macroscopic equations as well. In other words, one can replace the solver for macroscopic equations by MD simulation with huge amount of particles. Unfortunately, this is not feasible because the typical number of molecules in macroscopic system is approximately equal to the Avogadro Constant: $N_A = 6 \cdot 10^{23}$. That is very huge number and it is beyond the available computational resources. The typical size of the system for MD simulations varies in the range: $10^4 - 10^5$ [48]. That means that there is a huge gap between MD and macroscopic physical systems. In that intermediate case, kinetic theory approach can be used. The primary object of the theory concerned is a distribution function $f(t, x, v)$, which is a normalized number of particles that have velocity v at the point x at moment t. The evolution equation of the system is Boltzmann kinetic equation [49]:

$$\frac{\partial f(t,x,v)}{\partial t} + v^\alpha\frac{\partial f(t,x,v)}{\partial x^\alpha} + \frac{F^\beta}{m}\frac{\partial f(t,x,v)}{\partial v^\beta} = \Omega(f) \tag{2.4}$$

Here F describes external forces and m is the mass of a single particle or molecule. The special attention is required to $\Omega(f)$. This term is called collision integral. Actually, it is not a function but a functional, because its argument is the distribution function itself. $\Omega(f)$ describes the change of the distribution function due to mutual collisions of particles.

Distribution function can be used for calculation of macroscopic or measurable properties like density, momentum and stress-tensor:

$$\begin{aligned} \rho &= \int f(t,x,v)dv \\ \rho u^{\alpha} &= \int f(t,x,v)v^{\alpha}dv \\ \rho u^{\alpha}u^{\beta} + \Pi^{\alpha\beta} &= \int f(t,x,v)v^{\alpha}v^{\beta}dv \end{aligned} \tag{2.5}$$

Here ρ is the density, u is velocity $\Pi^{\alpha\beta}$ is a stress tensor. The latter is related to pressure and to viscous friction in gases and fluids.

The important concept of the formalism concerned is equilibrium distribution. It is nothing but the solution for:

$$\Omega(f_0) = 0 \tag{2.6}$$

In this work it is referred to as f^{eq}. Actually, if the system is uniform in space and time and there are no external forces, than f^{eq} is a solution for (2.4). There are several examples of equilibrium distribution functions. One of them is Maxwell distribution. The importance of the equilibrium distribution function comes from the connection between kinetic theory and thermodynamics. Primary variables in thermodynamic theory are such macroscopic quantities as density, pressure and temperature. The central concept of thermodynamics is the idea of equilibrium. That means that all the properties mentioned before should be measured after all transitional processes have finished. In the present study, this state is referred to as equilibrium limit. Therefore, equilibrium distribution function corresponds

to a well-known macroscopic physical system with well-defined densities, pressures etc. That indicates the importance of f^{eq} and $\Omega(f)$: the first one determines a physical system and the latter describes how the system evolves to its equilibrium state.

Therefore, choice of the numerical method and the set of equations that are planned to be solved is significantly affected by the scale of the physical system. For instance, behaviour of small groups of particles is best described by MD macroscopic systems are represented well with continuous media approach, intermediate or meso-scale systems could modelled with kinetic equation with reasonable accuracy. The following statement can be illustrated in Figure (2.1):

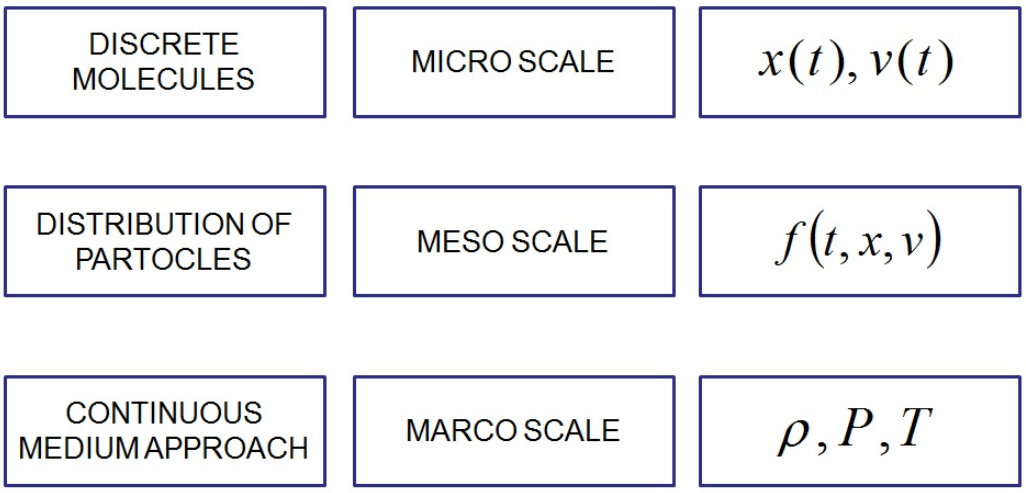

Figure 2.1: Diagram of models of media at different scales. The set of primary variables for each of the model is shown.

2.2 Lattice, Particles and Equations

There are many different ways to think about Lattice-Boltzmann Method (LBM). The simplest from mathematical point of view, is the interpretation of LBM as the discretization of kinetic equation both in velocity and coordinate spaces, therefore the total number

of velocities available for particles is finite. In such a setting, the primary object is a distribution function $f_i(t, x)$ that is proportional to the number of particles that have velocity v_i at the point x at the moment t. Here i is an index that runs over the whole finite set of all possible velocities in the model. Elements of the set concerned are denoted as c_i. Typically, the velocities concerned are related to geometric objects, for instance to square in 2D or the cube in 3D. In this example, lattice velocities are parallel to vectors that connect the center of the cube with all or some of centers of faces, edges and vertexes. The common notation for such type of lattices is Dn_1Qn_2. Here n_1 is the dimension of the space and n_2 is the number of selected vectors. For example, the set of lattice velocities for D2Q9 and D3Q27 is shown in Figure (2.2). More details about D2Q9 and D3Q27 lattices can be found in [50] and [51].

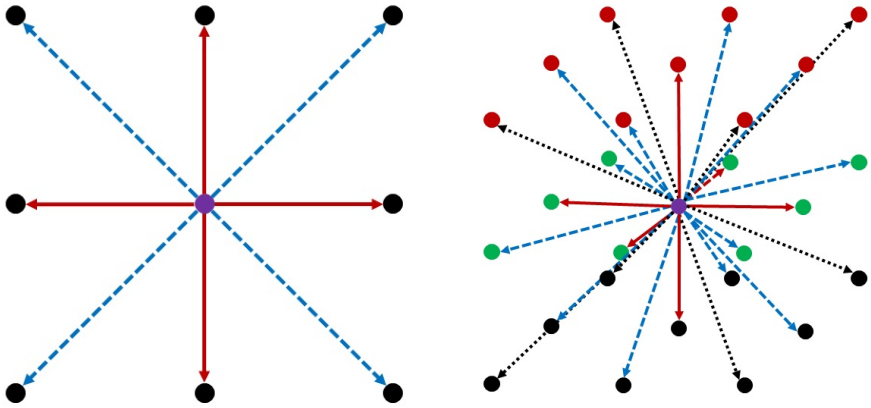

Figure 2.2: Set of lattice velocities for D2Q9 (left) and D3Q27 (right) lattices. Zero velocity vector is not shown.

It is traditionally to work in dimensionless units in LBM. Namely, if ΔX and ΔT are representative spatial and temporal scale of the system, then lattice velocities are typically

expressed in the form of dimensionless vectors e_i:

$$c_i^\alpha = \frac{\Delta X}{\Delta T} e_i^\alpha \tag{2.7}$$

In this work, e_i^α can take only one of three values $-1, 0, +1$. The exact definition of ΔX and ΔT varies from problem to problem and can be absolutely non-trivial in general. However, in numerical analysis ΔX and ΔT are simply spatial and temporal time steps respectively. Here and later in the text, ΔX and ΔT are referred only to spatial and temporal steps. By the analogy with continuous case, it is possible to introduce the evolution equation:

$$\frac{\partial f_i}{\partial t} + c_i^\alpha \frac{\partial f_i}{\partial x^\alpha} + F_i = \Omega_i(f) \tag{2.8}$$

Here again Ω_i is a collision integral or collision term. F_i represents external forces. In the case of discrete kinetic equation $\Omega_i(f)$ is the finite family of ordinary functions, therefore, it is no longer a functional [52].

The discretization in velocity space can be considered as the replacement of classic Boltzmann equation by the discrete analog: Discrete Kinetic Equation (DKE). However, in order to come up with the LBM scheme an additional step is required: discretization in space and time. This can be made by setting the whole system on the lattice. This procedure is equivalent to the simplest uniform discretization in space and time. As long as there is not much sense in having derivatives in discrete space, they should be replaced by the numerical analog, for instance with finite differences. Therefore, it is possible to consider LBM as a numerical scheme for DKE with uniform spatial and temporal discretization and finite difference approximation of derivatives:

$$f_i(t + \Delta T, x + e_i \Delta X) - f_i(t, x) + F_i \Delta T = \Omega_i(f) \Delta T \tag{2.9}$$

Equation (2.9) and its numerical scheme has a meaningful graphical interpretation. Namely, the scheme can be divided into two steps. The first one is the evaluation of the following expression:

$$\hat{f}_i(t,x) = f_i(t,x) - F_i\Delta T + \Omega_i(f)\Delta T$$

This step is called the collision step. The next step is an update of distribution functions using following rule:

$$f_i(t+\Delta T, x+e_i\Delta X) = \hat{f}_i(t,x)$$

This step is called streaming step. It simply states that nodes of the lattice exchange distribution functions with neighbours. The pictorial representation of streaming and collision steps is shown below (2.3).

This is the mathematical way of thinking about LBM. However, it is useful to look at LBM from another prospective. According to the definition, distribution functions in continuous kinetic equation are nothing but averages over samples of distribution of molecules. Therefore, because of the analogy between discrete and continuous kinetic equations, LBM can be treated as average of the distribution of artificial particles that live purely on the cubic grid. Molecules of the gas concerned can propagate through the lattice and collide with each other. The only difference from real particles is that velocity is parallel to lattice directions and there are certain restrictions on its magnitude. The scheme of lattice gas is presented in the Figure (2.4).

The interpretation concerned is extremely useful for formulation of boundary conditions. The number of degree of freedoms in LBM is usually higher than in macroscopic system that is described thereof. Therefore, it is typically that that macroscopic boundary conditions do not have enough information for setting correct boundary conditions for

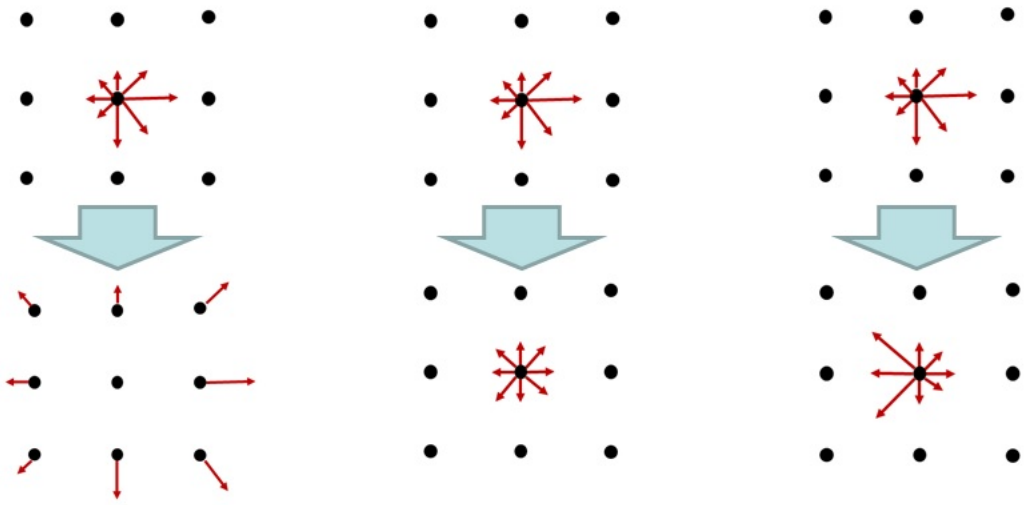

Figure 2.3: Illustration of each of the terms in the LBM Scheme. One time step is considered. The first one shows the effect of streaming during the time step concerned. It is simply propagation to the neighbour. The collision term or integral corresponds to the relaxation of particles to the equilibrium distribution and forcing term represents the change of distributions functions because of interaction with external world. In the given example the force acts from left to right.

LBM. This means that there are different alternatives for streaming rules at the boundary. The selection of the correct one is not a trivial problem. In such situations the intuition about distribution functions as flux of the artificial molecules is extremely useful: the idea about the interaction of particles with the boundary finally leads to the natural formulation of boundary conditions.

Historically, numerical methods for simulations of gas of artificial particles have been developed first. Typically they are referred to as Cellular Automata or Lattice Gas Automata (LGA) [54]. It can be shown that through appropriate selection of the set of velocities and by setting collision rules correctly, one can model the Navier-Stokes equation. Some of the advantages like small memory requirements and low computational costs, can be useful for practical implementations. What is more exciting is that LGA is free from

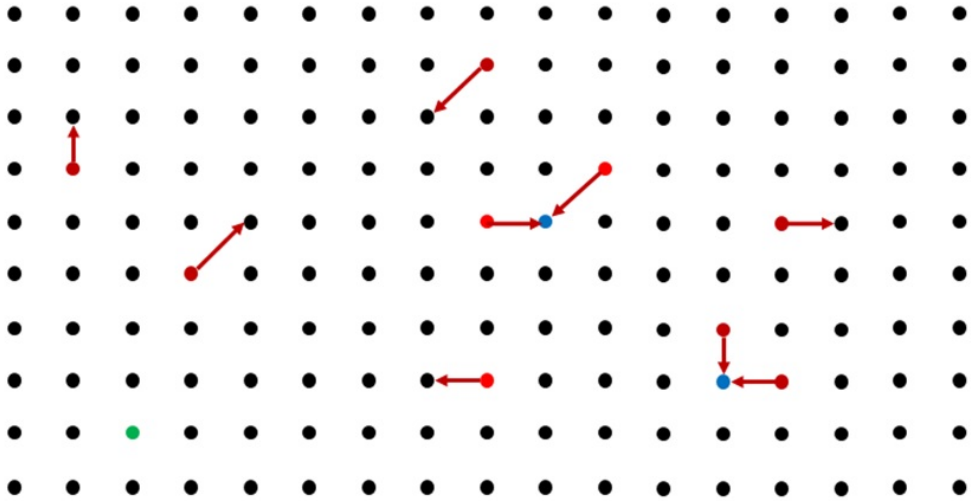

Figure 2.4: Schematic picture of lattice gas. Particles of the gas concerned travel with velocities parallel to lattice direction. They are allowed to move from one node to the neighbour during the time-step. If to particles come to the same node simultaneously the collision happens.

round-off errors. Despite the remarkable properties of LGA, high level of noise in the averaged macroscopic properties limits the applicability of the method. Actually, LBM has been developed as the tool for solving the problem with noises in LGA.

2.3 LBM and Modelling Frameworks

Despite the relatively short history, LBM has been applied to modelling vast variety of physical systems. The flexibility concerned is provided through the generic form of the governing equations:

$$\frac{\partial f_i}{\partial t} + c_i^\alpha \frac{\partial f_i}{\partial x^\alpha} + F_i = \Omega_i$$

$$f_i(t + \Delta T, x + \Delta X) - f_i(t, x) + F_i \Delta T = \Omega_i(f) \Delta T$$

It can be shown that up to issues with numerical stabilities almost any physical system can be described in terms of LBM if collision and forcing terms Ω_i and F_i respectively

have been chosen in appropriate way. For instance, Jianfeng Lu et al applied LBM for quantum systems [55]. Ryosuke Yano studied relativistic hydrodynamics with LBM [56]. And of course, a huge amount of works is dedicated to the Navier-Stokes Equation, that is the original purpose for which the method has been developed, for instance [57]. The essence of the discussion above is that almost any system from the Schröedinger Equation and dynamics of the magnetic to the hydrodynamics can be modelled within a unified numerical algorithm. That feature of the method concerned is remarkable by itself, what is more important that it gives a basis for seamless integration for problems with multiple scales. The later has a vital importance for the simulation of shale reservoirs.

Because of the properties of the LBM, there is no surprise that LBM has found its application in Petroleum Engineering. At the very beginning, LBM has been used as an auxiliary tool for preparation of data for conventional reservoir simulation. To the best of author's knowledge, calculation of permeability of various rock samples has been the first application of LBM in the field involved. Traditionally, permeability is obtained from core-flooding experiments. The latter is usually quite expensive and time-consuming. Because of such reasons, calculation of the rock properties concerned based on numerical experiments seems to be a prospective alternative to direct measurements. More precisely, the idea of the approach is to solve Navier-Stokes equations in the porous media with given geometry and calculate permeability based on results of the simulations. The geometry of the rock for the calculations can be obtained from the digital model of a real core [58] or it can be generated artificially [59]. It has happened that boundaries of complicated shape can be treated in LBM in a relatively simple but effective way. Therefore, LBM has found its applications in such type of numerical experiments. Permeability has a reasonably good scaling properties, therefore, there is no need for simulation of flow of real fluid in such type of problems. This means that one can use fluid with artificial physical properties and have a correct result after appropriate rescaling procedure, however, actual properties of

real fluids may be critical in multi-phase flow problems [60].

The less popular area of application of LBM is field-scale simulation, namely solution for mass and momentum conservation equations linked by Darcy Law. One of the first works regarding such type of models has been devoted to water-flooding simulations. The focus of the work concerned is prediction of the watercut curve from numerical simulation, therefore fluids with artificial equation of state have been considered [61]. Despite the flexibility and potential of the method to implemented for simulation of various physical systems, it is not quite trivial to introduce a given equation of state for reservoir-scale simulations, because of the construction of LBM. Therefore, a relatively common situation is such that various effects like deviations from Darcy Law, stress-dependent permeability of the rock like are taken into account, although the linear EOS is used, for instance [62]. Here linear means that pressure is proportional to density. By the present moment, there is a significant fraction of studies of simulation of flow of the fluid with given EOS via LBM. The most popular one is so-called Shan-Chen model [63]. The major part of such works is focused on multiphase behavior either in pores or in bulk volumes. That means that such LBM models are not designed for reservoir scale simulations. Successful attempt of developing macroscopic LBM model has been made by Q.Liu et al [64]. Finally, despite the useful features of LBM and advances in its development, the method is not very popular in field-scale reservoir simulations.

3. EOS OF THE FLUID IN PORE-SCALE SIMULATIONS

Shale reservoirs provide a typical example of a multi-scale system. One of the most common ways for modelling multiscale systems is so-called sequential upscaling. In general, simulations at fine scale are generalized to effective rock-properties for further application in simulations at coarse scale and so on. The present work follows this general idea in such a way that we look for an upscaling LBM method. In this chapter the upscaling procedure for the smallest scale or pore scale is discussed. Basically, LBM-scheme for simulation of fluid flow at the scale concerned is presented. Numerical examples provide the validation of the method and demonstrate applications of LBM to the problems involved. The novelty of the presented approach is the implicit LBM scheme with density dependent lattice wrights.

3.1 Problem Setup

The major difference of fluid behaviour inside pores of shale rock in comparison with the conventional rock comes from the volume-to-surface ratio. Simple calculations can show that the area of the surface of fluid-rock contact per unit volume of the fluid increases with the decrease of the mean size of the pores. That causes the increase of the energy of interaction of fluid with solid matrix of the rock leading to the significant impact on the overall flow pattern. This is known as adsorption and slippage effects. in reservoir engineering, the phenomena involved are modelled through Langmuir isotherm and Klinkenberg correction formula. It has been mentioned in the introduction that the corrections concerned work well in general, however significant deviations with experimental results have been observed in certain cases. Therefore, there is a need for the improvements of the LBM framework for handling more general phenomena.

One of the options is to upscale high resolution simulations that are based on first prin-

ciples to correlations similar to Langmuir isotherm or Klinkenberg correction formula. That is exactly the place where LBM can be applied. LBM has a relatively long history of application to modelling of slippage effects [67], however adsorption has not been considered in great details. That is the reason why the main focus of the present work is adsorption. It is well-known that the physical mechanism of adsorption is an attraction between molecules of the rock and fluid or gas. The interaction concerned can be represented through its energy. The latter quantity depends on the type of interacting molecules and on the distance between them. Therefore, for absolutely accurate simulations the distribution of all molecules of the rock in the space is required. However, it is not real to have all this data because of the technical limitations. One of the possible solutions is to use a relatively simple model for the potential of interaction that describes all the physics in average. The parameters of the potential can be tuned in order to obtain the agreement with the experimental data. If the geometry of the porous media is known, then one can compute the distribution of the potential of the interaction inside the pore space. It is well-known from high-school physics that the gradient of the field concerned with the inverse sign is the force of interaction. In other words, the energy of interaction of two molecules together with the geometry of the pore space gives the forcing field. The latter makes it possible to implement an LBM scheme with the forcing terms for simulation of adsorption effects.

The focus of the present work is the development of the LBM scheme that is capable to capture the effects concerned. To the best of author's knowledge this is the first work, where the semi-implicit LBM scheme is used for modelling the adsorption effects, starting from the first principles. The approach presented here can be applied to the pore network with real geometry. Therefore, the novel technique presented here can be easily implemented. However, in this work, the major attention is paid to the details of derivations of the numerical method itself rather then to involved interaction between molecules or com-

plicated geometry of the porous media. Because of the reasoning above, the step-function has been chosen as a model for the potential of interaction between molecules:

$$\phi(x) = \begin{cases} -\phi_0, & \text{if } |x| < r_0 \\ 0, & \text{if } |x| \geq r_0 \end{cases} \tag{3.1}$$

The potential concerned depends on two parameters: the overall potential energy of the interaction ϕ_0 and the effective radius of action r_0 or investigation radius. One can consider the plane wall of the rock and the single molecule of the gas that interacts with the molecules of the wall in the form that is prescribed by the potential $\phi(x)$. The geometry of the porous media is very simple as well: rectangular channel. The potential (3.1) and the shape of the channel concerned result in the following force of attraction of molecule to the wall [70]:

$$F_B = -\rho \frac{3Q}{2Mr_0} \left(1 - \frac{z^2}{r_0^2}\right) \tag{3.2}$$

Here Q is the heat of adsorption, ρ is the density of the gas, M is the molar mass, z is the distance to the wall. The advantage of the present approach is that the magnitude of the potential ϕ can be expressed in terms of measurable quantities like the heat of adsorption. Typically, the data on the value of radius of investigation r_0 is available from various physical and chemical measurements.

Finally, the force field (3.2) is incorporated into the LBM scheme through the forcing term. The exact formulation of collision integral and the forcing term concerned are shown below. Results of simulations are discussed in the end of the present chapter.

3.2 Chapman-Enskog Expansion

To the best of the author's knowledge, there is only one way of establishing relations between DKE and a real physical system: Chapman-Enskog Expansion. The goal of the

present section is to explain that in the case of LBM with BGK collision term the procedure concerned is equivalent to the representation of the equilibrium distribution function as a power series with respect to relaxation time.

The central equation of the present work is a so-called discrete kinetic equation.

$$\frac{\partial f_i}{\partial t} + c_i^{\alpha} \frac{\partial f_i}{\partial x^{\alpha}} + F_i = \Omega_i \tag{3.3}$$

Here f_i are discrete distribution functions, namely mass of the particles that moves with velocity c_i, F_i corresponds to the net forces, Ω_i is a collision term. It has been mentioned in the previous section that the range of systems described by the equation (3.3) is impressively wide. The key role in such flexibility belongs to the collision and the forcing terms. In the present work, only the BGK model will be considered:

$$\frac{f_i^{eq} - f_i}{\tau} = \Omega_i \tag{3.4}$$

Here f_i^{eq} is equilibrium distribution function and τ is a relaxation time. The physical meaning of relaxation time is the representative time-scale for the process of relaxation of distribution to equilibrium. Therefore, the following conclusion is valid: for small relaxation times distribution functions should be close to equilibrium. The mathematical expression of that statement is that the solution for the (3.3) can be expressed as power series with respect to the relaxation time:

$$f_i = f_i^{eq} + \tau^1 f_i^{(1)} + \tau^2 f_i^{(2)} + ... \tag{3.5}$$

The expression for each of the terms in (3.5) can be derived from the (3.3) with the BGK

collision term. Namely, simple algebraic manipulations show that:

$$f_i = f_i^{eq} - \tau\left(\frac{\partial f_i}{\partial t} + c_i^\alpha \frac{\partial f_i}{\partial x^\alpha} + F_i\right) \tag{3.6}$$

In other words, it is possible to express the solution in the form of its derivatives. The result of the application of (3.6) to itself is the following equation:

$$f_i = f_i^{eq} - \tau\left(\frac{\partial f_i^{eq}}{\partial t} + c_i^\alpha \frac{\partial f_i^{eq}}{\partial x^\alpha} + F_i\right) + \tau^2\left(\left(\frac{\partial}{\partial t} + c_i^\alpha \frac{\partial}{\partial x^\alpha}\right)^2 f_i + \left(\frac{\partial}{\partial t} + c_i^\alpha \frac{\partial}{\partial x^\alpha}\right) F_i\right) \tag{3.7}$$

Here the following notation is used:

$$\left(\frac{\partial}{\partial t} + c_i^\alpha \frac{\partial}{\partial x^\alpha}\right)^2 f_i = \frac{\partial^2 f_i}{\partial t^2} + 2c_i^\alpha \frac{\partial^2 f_i}{\partial t \partial x^\alpha} + c_i^\alpha c_i^\beta \frac{\partial^2 f_i}{\partial x^\alpha \partial x^\beta}$$

Comparison of (3.5) with (3.7) gives the following expression for the approximations of various orders in relaxation time:

$$\begin{aligned} f_i^{(1)} &= -\frac{\partial f_i^{eq}}{\partial t} + c_i^\alpha \frac{\partial f_i^{eq}}{\partial x^\alpha} + F_i \\ f_i^{(2)} &= \left(\frac{\partial}{\partial t} + c_i^\alpha \frac{\partial}{\partial x^\alpha}\right)^2 f_i + \left(\frac{\partial}{\partial t} + c_i^\alpha \frac{\partial}{\partial x^\alpha}\right) F_i \end{aligned} \tag{3.8}$$

Expressions (3.5) - (3.8) are heavily used in the computation of moments of distribution functions. The latter are defined in the same way as in classic statistic theory;

$$M_k^{\alpha_1 \ldots \alpha_k} = \sum_i f_i c_i^{\alpha_1} \ldots c_i^{\alpha_k} \tag{3.9}$$

Here $M_k^{\alpha_1 \ldots \alpha_k}$ is a component of moment of the order k, c_i is one of the possible discrete velocities. The summation in (3.9) is over the set of all velocities in the model. That set is finite as long as discrete kinetic equation is considered. The most important

moments for the present research are moments of orders 0, 1 and 2.

$$\rho = \sum_i f_i \tag{3.10}$$

$$\rho u^\alpha = \sum_i f_i c_i^\alpha \tag{3.11}$$

$$\rho u^\alpha u^\beta + \Pi^{\alpha\beta} = \sum_i f_i c_i^\alpha c_i^\beta \tag{3.12}$$

The moments concerned have their own specific names. ρ is the density, u^α is average or macroscopic velocity and in the next section it is shown that $\Pi^{\alpha\beta}$ is a stress-tensor. The approximation for the solution of (2.8) can be used for calculations of moments of distribution and related quantities via (3.10) (3.11) and (3.12). Therefore, one can show that the following expression holds for the density, for the average velocity, and for the stress-tensor:

$$\begin{aligned} \rho &= \rho^{eq} + \tau\rho^{(1)} + \tau^2\rho^{(2)} + ... \\ u^\alpha &= u^{(eq),\alpha} + \tau u^{(1),\alpha} + \tau^2 u^{(2),\alpha} + ... \\ \Pi^{\alpha\beta} &= \Pi^{(eq),\alpha\beta} + \tau\Pi^{(1),\alpha\beta} + \tau^2\Pi^{(2),\alpha\beta} + ... \end{aligned} \tag{3.13}$$

This way of deriving approximate values for the moments and the distribution function is referred to as Chapman-Enskog expansion. To be precise, the procedure concerned has much more involved form in general, but in the case of BGK collision integral or similar models it becomes the same thing as a power series with respect to the relaxation time. It is worth to mention that certain degree of simplification of (3.13) without loss of generality can be achieved. Such systems are considered in the next section.

3.3 Navier-Stokes Equation for the Free Fluid

A picture paints a thousand words or equivalently the best way to understand subtle details of mechanics of LBM is to consider one representative example, which is the flow of the free fluid. In this section it is shown via Chapman-Enskog expansion [54] that LBM reproduces the Navier-Stokes equation [57] for a compressible fluid if first four moments of the equilibrium distribution functions coincide with the moments of Maxwell's distribution:

$$\begin{aligned} \rho &= \sum_i f_i^{eq} \\ \rho u^\alpha &= \sum_i f_i^{eq} c_i^\alpha \\ \rho u^\alpha u^\beta + P(\rho)\delta^{\alpha\beta} &= \sum_i f_i^{eq} c_i^\alpha c_i^\beta \\ \rho u^\alpha u^\beta u^\gamma + P(\rho)\Big(u^\alpha \delta^{\beta\gamma} + u^\beta \delta^{\alpha\gamma} + u^\gamma \delta^{\alpha\beta}\Big) &= \sum_i f_i^{eq} c_i^\alpha c_i^\beta c_i^\gamma \end{aligned} \tag{3.14}$$

In other words, it is shown that for the approximation of the flow of the given fluid it is sufficient to design the equilibrium distribution functions in such a way that the have the same moments as Maxwell's distribution. This statement is one of the contributions of the present work.

It is well-known that in the case of the free-moving fluid the evolution of the system concerned is governed by mass and momentum conservation laws. Viscosity and equation of state of the fluid are given:

$$\begin{aligned} P &= P(\rho) \\ \mu &= \mu(\rho) \end{aligned} \tag{3.15}$$

Therefore, all the mathematical manipulations are performed around that equations. Because the free fluid is studied, there is no need to care about forcing terms in (3.3), because they are all zero. Therefore, the only undetermined object is the equilibrium distribution

function. For the simplicity reasons it is assumed that f^{eq} depends only on macroscopic density and velocity:

$$f_i^{eq} = f_i^{eq}(\rho, u) \tag{3.16}$$

The equilibrium distribution is the state, to which the system is evolving with time. Therefore, it does not have to coincide with the actual distribution of particles. Although, the moments of equilibrium distribution of order zero and one are defined through the same moments of the actual distribution of particles. Moreover, those moments coincide in the case of the free-moving fluid:

$$\begin{aligned} \sum_i f_i^{eq}(\rho, u) &= \sum_i f_i = \rho \\ \sum_i f_i^{eq}(\rho, u) c_i^\alpha &= \sum_i f_i c_i^\alpha = \rho u^\alpha \end{aligned} \tag{3.17}$$

Mass and momentum conservation laws can be derived from the discrete kinetic equation with the BGK collision term and zero forcing term:

$$\frac{\partial f_i}{\partial t} + c_i^\alpha \frac{\partial f_i}{\partial x^\alpha} = \frac{f_i^{eq} - f_i}{\tau} \tag{3.18}$$

The averaging of both sides of (3.18) gives the following equaiton:

$$\sum_i \left(\frac{\partial f_i}{\partial t} + c_i^\alpha \frac{\partial f_i}{\partial x^\alpha} \right) = \frac{\partial \sum_i f_i}{\partial t} + \frac{\partial \sum_i f_i c_i^\alpha}{\partial x^\alpha} = \sum_i \frac{f_i^{eq} - f_i}{\tau} \tag{3.19}$$

The equation concerned can be simplified if the definition of the equilibrium distribution is applied (3.17):

$$\frac{\partial \sum_i f_i}{\partial t} + \frac{\partial \sum_i f_i c_i^\alpha}{\partial x^\alpha} = 0$$

Using the definition of the density and the momentum (3.10) and (3.11) one can get a

well-known continuity equation:

$$\frac{\partial \rho}{\partial t} + \frac{\partial (\rho u^{\alpha})}{\partial x^{\alpha}} = 0 \tag{3.20}$$

The summary of derivations above is that one can end-up with macroscopic equations with a two-step procedure: compute distribution moments of both parts of (3.18) and than use the definition of moments in terms of macroscopic quantities. That logic works well for the continuity equation as it has been shown above. Therefore, the procedure concerned can be applied to the momentum conservation equation. Multiplication of both parts of (3.18) by c_i^{β} and together with averaging with respect to lattice velocities gives the following expression:

$$\sum_i c_i^{\beta} \left(\frac{\partial f_i}{\partial t} + c_i^{\beta} c_i^{\alpha} \frac{\partial f_i}{\partial x^{\alpha}} \right) = \frac{\partial \sum_i f_i c_i^{\beta}}{\partial t} + \frac{\partial (\sum_i f_i c_i^{\alpha} c_i^{\beta})}{\partial x^{\alpha}} = \sum_i \frac{f_i^{eq} - f_i}{\tau} c_i^{\beta} \tag{3.21}$$

The only new term in the equation concerned is $\sum_i f_i c_i^{\alpha} c_i^{\beta}$. However, it is possible to rewrite it in the convenient form:

$$\begin{aligned} \sum_i f_i c_i^{\alpha} c_i^{\beta} = \sum_i f_i (c_i^{\alpha} - u^{\alpha})(c_i^{\beta} - u^{\beta}) + \sum_i f_i (c_i^{\alpha} - u^{\alpha}) u^{\beta} + \sum_i f_i u^{\alpha} (c_i^{\beta} - u^{\beta}) + \\ + \sum_i f_i u^{\alpha} u^{\beta} = \rho u^{\alpha} u^{\beta} + \sum_i f_i (c_i^{\alpha} - u^{\alpha})(c_i^{\beta} - u^{\beta}) = \rho u^{\alpha} u^{\beta} + \Pi^{\alpha\beta} \end{aligned} \tag{3.22}$$

Here $\Pi^{\alpha\beta}$ is simply $\sum_i f_i (c_i^{\alpha} - u^{\alpha})(c_i^{\beta} - u^{\beta})$. Finally, definitions of the moments and the equilibrium distribution function give the following expression:

$$\frac{\partial (\rho u^{\alpha})}{\partial t} + \frac{\partial (\rho u^{\alpha} u^{\beta})}{\partial x^{\beta}} + \frac{\partial}{\partial x^{\beta}} \Pi^{\alpha\beta} = 0 \tag{3.23}$$

The latter means that $\Pi^{\alpha\beta}$ is nothing but the stress-tensor. Therefore, for the fluids it should

take the form:

$$\Pi^{\alpha\beta} = P\delta^{\alpha\beta} - \mu\left(\frac{\partial u^{\alpha}}{\partial x_{\beta}} + \frac{\partial u^{\beta}}{\partial x_{\alpha}} - \frac{2}{3}\frac{\partial u^{\gamma}}{\partial x^{\gamma}}\delta^{\alpha\beta}\right) \tag{3.24}$$

It is important to notice that (3.23) is exact and it looks like classic macroscopic momentum conservation equation. However, the stress tensor is expressed in terms of the distribution functions. That means that the closing relation is missing in general. On the other hand, it is reasonable to expect that for slow processes the stress-tensor and other moments of distribution should be close to the macroscopic one. In other words, high order terms in (3.13) should be negligible. It is worth to emphasize that because of the constraints on the equilibrium distribution only stress-tensor has non-trivial expansion. Density and momentum have only zero-order terms.

In other words, Chapman-Enskog procedure for the stress-tensor establishes certain restrictions on the parameters of the LBM scheme. The rest of the present section is devoted to the derivation of the first-order expression for the $\Pi^{\alpha\beta}$.

The formula for the second moment of distribution can be transformed as follows:

$$\sum_i f_i c_i^{\alpha} c_i^{\beta} = \sum_i f_i^{eq} c_i^{\alpha} c_i^{\beta} + \sum_i (f_i - f_i^{eq}) c_i^{\alpha} c_i^{\beta} \tag{3.25}$$

From (3.3) one can have

$$f_i^{eq} - f_i = \tau\left(\frac{\partial f_i}{\partial t} + \frac{\partial c_i^{\beta} f_i}{\partial x^{\beta}}\right)$$

This means that up to the terms of first order in relaxation time, an actual distribution function equals to the equilibrium distribution function. Therefore, the following equality holds:

$$\sum_i f_i c_i^{\alpha} c_i^{\beta} = \sum_i f_i^{eq} c_i^{\alpha} c_i^{\beta} + O(\tau)$$

That results immediately in a well-known stress-tensor for the fluid with zero viscosity:

$$\Pi^{\alpha\beta} = P\delta^{\alpha\beta} + O(\tau) \tag{3.26}$$

For the purposes of further derivations, expressions for the time derivative of density and velocity are required. Actually, there is no need for exact formula: it is enough to keep only leading term in relaxation time. Equation (3.26) gives Euler equation for compressible fluid up to higher orders in τ:

$$\frac{\partial \rho}{\partial t} + \frac{\partial \rho u^{\alpha}}{\partial x^{\alpha}} = 0 \tag{3.27}$$

$$\frac{\partial (\rho u^{\alpha})}{\partial t} + \frac{(\partial \rho u^{\alpha} u^{\beta})}{\partial x^{\beta}} = -\frac{\partial P}{\partial x_{\alpha}} + O(\tau) \tag{3.28}$$

For the purposes of further derivations first derivatives of velocity with respect to time is needed. It can be obtained from (3.27) - (3.28) with the usage of the following transformation:

$$\frac{\partial (\rho u^{\alpha})}{\partial t} + \frac{(\partial \rho u^{\alpha} u^{\beta})}{\partial x^{\beta}} = u^{\alpha}\frac{\partial \rho}{\partial t} + \rho\frac{\partial u^{\alpha}}{\partial t} + u^{\alpha}\frac{\partial \rho u^{\beta}}{\partial x^{\beta}} + \rho u^{\beta}\frac{\partial u^{\alpha}}{\partial x^{\beta}} = \rho\left(\frac{\partial u^{\alpha}}{\partial t} + u^{\beta}\frac{\partial u^{\alpha}}{\partial x^{\beta}}\right) \tag{3.29}$$

Finally,

$$\frac{\partial u^{\alpha}}{\partial t} + u^{\beta}\frac{\partial u^{\alpha}}{\partial x^{\beta}} = -\frac{1}{\rho}\frac{\partial P}{\partial x_{\alpha}} + O(\tau) \tag{3.30}$$

With the expressions for first derivatives with respect to time and with formulas for the first four moments of equilibrium distribution, the Chapman-Enskog expansion for the stress-tensor can be performed. It has been shown that the part of the stress tensor is nothing but spherical term that corresponds to the pressure. The remaining part

$$\sum_{i}(f_i - f_i^{eq})c_i^{\alpha}c_i^{\beta}$$

can be computed in the following way:

$$\sum_i (f_i - f_i^{eq}) c_i^\alpha c_i^\beta = -\tau \sum_i c_i^\alpha c_i^\beta \left(\frac{\partial f_i}{\partial t} + c_i^\gamma \frac{\partial f_i}{\partial x^\gamma} \right) =$$

$$= -\tau \sum_i c_i^\alpha c_i^\beta \left(\frac{\partial f_i^{eq}}{\partial t} + c_i^\gamma \frac{\partial f_i^{eq}}{\partial x^\gamma} \right) + O(\tau^2) = -\tau \frac{\partial}{\partial t} (\rho u^\alpha u^\beta + P\delta^{\alpha\beta}) -$$

$$-\tau \frac{\partial}{\partial x^\gamma} \left(\sum_i f_i^{eq} c_i^\alpha c_i^\beta c_i^\gamma \right) = -\tau u^\beta \frac{\partial \rho u^\alpha}{\partial t} - \tau \rho u^\alpha \frac{\partial u^\beta}{\partial t} - \tau \frac{\partial}{\partial x^\gamma} \left(\sum_i f_i^{eq} u^\alpha u^\beta u^\gamma \right) -$$

$$-\tau \frac{\partial}{\partial x^\gamma} \left(\sum_i f_i^{eq} (c_i^\alpha - u^\alpha) u^\beta u^\gamma \right) - \tau \frac{\partial}{\partial x^\gamma} \left(\sum_i f_i^{eq} u^\alpha (c_i^\beta - u^\beta) u^\gamma \right) -$$

$$-\tau \frac{\partial}{\partial x^\gamma} \left(\sum_i f_i^{eq} u^\alpha u^\beta (c_i^\gamma - u^\gamma) \right) - \tau \frac{\partial}{\partial x^\gamma} \left(\sum_i f_i^{eq} (c_i^\alpha - u^\alpha)(c_i^\beta - u^\beta) u^\gamma \right) -$$

$$-\tau \frac{\partial}{\partial x^\gamma} \left(\sum_i f_i^{eq} (c_i^\alpha - u^\alpha) u^\beta (c_i^\gamma - u^\gamma) \right) - \tau \frac{\partial}{\partial x^\gamma} \left(\sum_i f_i^{eq} u^\alpha (c_i^\beta - u^\beta)(c_i^\gamma - u^\gamma) \right) -$$

$$-\tau \frac{\partial}{\partial x^\gamma} \left(\sum_i f_i^{eq} (c_i^\alpha - u^\alpha)(c_i^\beta - u^\beta)(c_i^\gamma - u^\gamma) \right) - \tau \delta^{\alpha\beta} \frac{\partial P}{\partial \rho} \frac{\partial \rho}{\partial t} + O(\tau^2) =$$

$$= \tau u^\beta \left(\frac{\partial (\rho u^\alpha u^\gamma)}{\partial x^\gamma} + \frac{\partial P \delta^{\alpha\gamma}}{\partial x^\gamma} \right) + \tau \rho u^\alpha \left(u^\gamma \frac{\partial u^\beta}{\partial x^\gamma} + \frac{1}{\rho} \frac{\partial P \delta^{\beta\gamma}}{\partial x^\gamma} \right) + \tau \delta^{\alpha\beta} \frac{\partial P}{\partial \rho} \frac{\partial (\rho u^\gamma)}{\partial x^\gamma} -$$

$$-\tau \frac{\partial}{\partial x^\gamma} \left(\rho u^\alpha u^\beta u^\gamma \right) - \tau \frac{\partial}{\partial x^\gamma} \left(P u^\alpha \delta^{\beta\gamma} + P u^\beta \delta^{\alpha\gamma} + P u^\gamma \delta^{\alpha\beta} \right) + O(\tau^2) =$$

$$= \tau \frac{\partial \rho}{\partial x^\gamma} u^\alpha u^\beta u^\gamma + \tau \rho \frac{\partial u^\alpha}{\partial x^\gamma} u^\beta u^\gamma + \tau \rho u^\alpha \frac{\partial u^\beta}{\partial x^\gamma} u^\gamma + \tau \rho u^\alpha u^\beta \frac{\partial u^\gamma}{\partial x^\gamma} + \tau \frac{\partial P}{\partial x^\gamma} u^\beta \delta^{\alpha\gamma} +$$

$$+\tau \rho u^\alpha \frac{\partial u^\beta}{\partial x^\gamma} u^\gamma + \tau \frac{\partial P}{\partial x^\gamma} u^\alpha \delta^{\beta\gamma} + \tau \delta^{\alpha\beta} \rho \frac{\partial P}{\partial \rho} \frac{\partial u^\gamma}{\partial x^\gamma} + \tau u^\gamma \delta^{\alpha\beta} \frac{\partial P}{\partial \rho} \frac{\partial \rho}{\partial x^\gamma} -$$

$$-\tau \frac{\partial \rho}{\partial x^\gamma} u^\alpha u^\beta u^\gamma - \tau \rho \frac{\partial u^\alpha}{\partial x^\gamma} u^\beta u^\gamma - \tau \rho u^\alpha \frac{\partial u^\beta}{\partial x^\gamma} u^\gamma - \tau \rho u^\alpha u^\beta \frac{\partial u^\gamma}{\partial x^\gamma} -$$

$$-\tau \frac{\partial P}{\partial x^\gamma} u^\alpha \delta^{\beta\gamma} - \tau \frac{\partial P}{\partial x^\gamma} u^\beta \delta^{\alpha\gamma} - \tau \frac{\partial P}{\partial x^\gamma} u^\gamma \delta^{\alpha\beta} -$$

$$-\tau P \frac{\partial u^\alpha}{\partial x_\beta} - \tau P \frac{\partial u^\beta}{\partial x_\alpha} - \tau P \delta^{\alpha\beta} \frac{\partial u^\gamma}{\partial x \gamma} + O(\tau^2) =$$

$$= -\tau P \left(\frac{\partial u^\alpha}{\partial x_\beta} + \frac{\partial u^\beta}{\partial x_\alpha} + \delta^{\alpha\beta} \left(1 - \frac{\rho}{P} \frac{\partial P}{\partial \rho} \right) \frac{\partial u^\gamma}{\partial x^\gamma} \right) + O(\tau^2) =$$

$$= -\tau P \left(\frac{\partial u^\alpha}{\partial x_\beta} + \frac{\partial u^\beta}{\partial x_\alpha} - \frac{2}{3} \delta^{\alpha\beta} \frac{\partial u^\gamma}{\partial x^\gamma} \right) - \tau P \left(\frac{5}{3} - \frac{\rho}{P} \frac{\partial P}{\partial \rho} \right) \frac{\partial u^\gamma}{\partial x^\gamma} \delta^{\alpha\beta} + O(\tau^2) \tag{3.31}$$

Combining (3.22) and (3.31) one can reformulate the momentum conservation equation in the following way:

$$\frac{\partial\left(\rho u^{\alpha}\right)}{\partial t}+\frac{\partial\left(\rho u^{\alpha} u^{\beta}\right)}{\partial x^{\beta}}=-\frac{\partial P \delta^{\alpha \beta}}{\partial x^{\beta}}+ \\ +\frac{\partial}{\partial x^{\beta}}\left(\mu\left(\frac{\partial u^{\alpha}}{\partial x_{\beta}}+\frac{\partial u^{\beta}}{\partial x_{\alpha}}-\frac{2}{3} \delta^{\alpha \beta} \frac{\partial u^{\gamma}}{\partial x^{\gamma}}\right)+\zeta \delta^{\alpha \beta} \frac{\partial u^{\gamma}}{\partial x^{\gamma}}\right)+O(\tau^{2}) \tag{3.32}$$

Here μ and ζ are the viscosity and the second viscosity respectively, The expression for them is the following:

$$\mu=\tau P \tag{3.33}$$

$$\zeta=\mu\left(\frac{5}{3}-\frac{\rho}{P} \frac{\partial P}{\partial \rho}\right) \tag{3.34}$$

Typically, viscosity and pressure are given as a functions of density, therefore, equations (3.33) and (3.34) determine the relaxation time:

$$\tau=\frac{\mu}{P} \tag{3.35}$$

The summary of the following section is that with certain restrictions on the moments of the equilibrium distribution and relaxation time, compressible version of the Navier-Stokes equations can be reproduced up to the terms of the second order in relaxation time. Therefore, derivations above give a motivation for using LBM for Computational Fluid Dynamics (CFD) and demonstrate the work flow of the design of the LBM scheme in generic case. It should be mentioned that no assumptions regarding the equilibrium distribution functions have been made, except the expression for the moments. This means that the problem of the development of the LBM scheme is reduced to the construction of the equilibrium distribution functions with the specified moments. The proof of this statement demonstrated above is one of the contributions of the present study.

3.4 Equilibrium Distribution Functions

The outcome of the previous sections is that the moments of equilibrium distribution function determine the properties of the macroscopic systems that can be extracted from the dynamics of the particles. For instance, it has been shown that if first four moments of equilibrium distribution function coincide with Maxwell's distribution than the Navier-Stokes equation can be reproduced up to the terms of second order with respect to relaxation time. Therefore, the application of Chapman-Enskog expansion to the LBM systems with the same moments (3.14) of equilibrium distribution function results in the same macroscopic equations. The results of the present section are presented with the permission of the Society of Petroleum Engineering.

Equations (3.14) can be satisfied in different ways. The most common approach relies on the similarity between continuous and discrete kinetic equations. Namely, the equilibrium distribution in the continuous case is Maxwell's distribution, which is the product of Gaussian distributions for each of the spatial dimensions. Inspired by the analogy concerned the function similar to Taylor expansion of Maxwell's distribution has been suggested for the discrete kinetic equation:

$$f_i^{eq}(\rho, u) = w_i \rho \left(1 + \frac{u \cdot c_i}{c_s^2} + \frac{(u \cdot c_i)^2}{2c_s^4} - \frac{u^2}{2c_s^2} \right) \tag{3.36}$$

Here c_si is so-called lattice speed of sound. In standard LBM framework it is constant:

$$c_s = \frac{1}{\sqrt{3}} \frac{\Delta X}{\Delta T} \tag{3.37}$$

Here ΔX and ΔT are representative spatial and temporal scales. In the particular case its numerical interpretation and as of solution scheme those quantities are simply space and time steps. Such approach results in the fact that the equation of state becomes similar to

the ideal gas, which is not very common in the real world. In order to solve this issue, extra terms are introduced into equation (3.18). In this work the method that allows one to model correct equation of state without the presence of auxiliary terms is introduced. The central idea is to follow the route of the continuous theory as far as it possible and get values for weights and lattice speed of sound in (3.36). The results of the present section has been shown in [70]. However, the derivations were missing there. Therefore, the method for the solution of the equations (3.14) is presented first time.

It the previous section it has been shown that macroscopic equations of movement of a certain fluid are reproduced correctly if the constraints (3.14) on moments of equilibrium distribution are satisfied. With the given form of f_i^{eq}, each moment is nothing but polynomial function with respect to u. Therefore, applying method of uncertain coefficients, one can derive the following constraints on weights:

$$\begin{aligned}
\sum_i w_i &= 1 \\
\sum_i w_i c_i^\alpha &= 0 \\
\sum_i w_i c_i^\alpha c_i^\beta &= c_s^2 \delta^{\alpha\beta} \\
\sum_i w_i c_i^\alpha c_i^\beta c_i^\gamma &= 0 \\
\sum_i w_i c_i^\alpha c_i^\beta c_i^\gamma c_i^\delta &= c_s^4 \Big(\delta^{\alpha\beta}\delta^{\gamma\delta} + \delta^{\alpha\gamma}\delta^{\beta\delta} + \delta^{\alpha\delta}\delta^{\beta\gamma} \Big)
\end{aligned} \tag{3.38}$$

And an expression for the lattice speed of sound:

$$c_s^2 = \frac{P}{\rho} \tag{3.39}$$

Constraints (3.38) is the system of five equations and the number of weights is 27

for D3Q27 model or nine for D2Q9. Therefore, in theory there are many ways to satisfy (3.38). However, the physical nature of the problem allows one to narrow the set of possible options for weights. First of all, it can be observed from (3.36) that:

$$\rho w_i = f_i^{eq}(\rho, 0)$$

The latter means that value of weight is proportional to the mass of the particles that move with a given velocity for the equilibrium distribution function with zero mean velocity. it is immediately leads to the inequality:

$$\forall i \geq 0 \rightarrow w_i \geq 0 \tag{3.40}$$

More strong restrictions come from the rotational symmetry. It is easy to see that if lattice velocities c_i and c_j have the same absolute value than there is exist a rotation A such that $A(c_i) = c - j$ and that maps lattice vectors to lattice vectors. Macroscopic equations that are modeled preserve rotational symmetry, therefore, that symmetry should be preserved in LBM scheme. The consequence of the latter is the following statement:

$$|c_i| = |c_j| \Rightarrow w_i = w_j \tag{3.41}$$

In the case of D3Q27 model there are only four possibilities for the absolute value of lattice velocity vector:

$$\begin{aligned} i = 0 &\rightarrow |c_i| = 0 \\ i = 1...6 &\rightarrow |c_i| = \frac{\Delta X}{\Delta T} \\ i = 7...18 &\rightarrow |c_i| = \sqrt{2}\frac{\Delta X}{\Delta T} \\ i = 19...27 &\rightarrow |c_i| = \sqrt{3}\frac{\Delta X}{\Delta T} \end{aligned} \tag{3.42}$$

Up to the coefficient $\frac{2\Delta X}{\Delta T}$ lattice vectors c_i coincide with vectors that connect the center of unit cube with it's center, faces, edges and vertexes. Therefore, the following notation can be introduced naturally:

$$\begin{gathered} i = 0 \rightarrow w_i = w_c \\ i = 1...6 \rightarrow w_i = w_f \\ i = 7...18 \rightarrow w_i = w_e \\ i = 19...27 \rightarrow w_i = w_v \end{gathered} \tag{3.43}$$

Here indexes w_c, w_f, w_e, w_v correspond to center, faces edges and vertexes of the cube. Therefore, rotational symmetry reduces the number of degrees of freedom from 27 to 4. However, one can show that equations with odd degrees with respect to lattice velocities are satisfied automatically because of the symmetry of D3Q27 lattice. Therefore, only three equations remains:

$$\begin{gathered} \sum_i w_i = 1 \\ \sum_i w_i c_i^\alpha c_i^\beta = c_s^2 \delta^{\alpha\beta} \\ \sum_i w_i c_i^\alpha c_i^\beta c_i^\gamma c_i^\delta = c_s^4 \Big(\delta^{\alpha\beta}\delta^{\gamma\delta} + \delta^{\alpha\gamma}\delta^{\beta\delta} + \delta^{\alpha\delta}\delta^{\beta\gamma} \Big) \end{gathered} \tag{3.44}$$

The common way to solve the equations (3.44) is to perform the contraction of both parts of equations with appropriate power of Kronecker tensor in order to end up with scalar equations:

$$\sum_i w_i = 1$$
$$\sum_i w_i c_i^\alpha c_i^\beta \delta_{\alpha\beta} = c_s^2 \delta^{\alpha\beta}\delta_{\alpha\beta} \tag{3.45}$$
$$\sum_i w_i c_i^\alpha c_i^\beta c_i^\gamma c_i^\delta \delta_{\alpha\beta}\delta_{\gamma\delta} = c_s^4 \Big(\delta^{\alpha\beta}\delta^{\gamma\delta} + \delta^{\alpha\gamma}\delta^{\beta\delta} + \delta^{\alpha\delta}\delta^{\beta\gamma} \Big) \delta_{\alpha\beta}\delta_{\gamma\delta}$$

It easy to see that because of the high symmetry of the initial system of tensor equations (3.38) any solution of contracted system (3.45) is a solution of the initial one. Eventually, there are only three non-trivial constraints on weights. Therefore, the value of one of them can be kept arbitrary. in the present work the value of w_0 is selected in accordance with classic LBM models. With such choice of w_0 the following expression for weight can be derived:

$$\begin{aligned} w_c &= \frac{8}{27} \\ w_f &= \frac{1}{6}\left(3(1-w_c) - \frac{15}{2}\left(\frac{c_s\Delta T}{\Delta X}\right)^2 + \frac{15}{2}\left(\frac{c_s\Delta T}{\Delta X}\right)^4\right) \\ w_e &= \frac{1}{12}\left(3(w_c-1) + 12\left(\frac{c_s\Delta T}{\Delta X}\right)^2 - 15\left(\frac{c_s\Delta T}{\Delta X}\right)^4\right) \\ w_v &= \frac{1}{8}\left((1-w_c) - \frac{9}{2}\left(\frac{c_s\Delta T}{\Delta X}\right)^2 + \frac{15}{2}\left(\frac{c_s\Delta T}{\Delta X}\right)^4\right) \end{aligned} \tag{3.46}$$

3.4.1 Numerical Scheme

The term discrete kinetic equation assumes discretization in the speed of velocities or momentums of particles. However, the problem is still the system of PDE's. As it happens in general, it can not be solved analytically for the majority of the cases. Therefore, the numerical scheme is required. This leads in turn to the temporal and spatial discretization. The simplest way to do it is to introduce the cubic lattice with the period ΔX and fix the time-step ΔT.

The set of velocities of the particles is the same is the set of lattice directions. The

geometric way of thinking about D3Q27 model is to consider a cubic discretization of the space. In this case each of the cubes has 27 neighbors with common face edge or vertex or the cube itself. Therefore, let R_i is the vector that connects the center of a given cube with the center of one of his neighbors. If ΔX is the period of the lattice than

$$R_i = \Delta X e_i$$

Here e_i is called a lattice vector. It is easy to see that in the case of cubic lattice the absolute value of each of the coordinates of e_i is either one or zero. Having a set of lattice vectors one can construct the set of lattice velocities c_i

$$c_i = \frac{\Delta X}{\Delta T} e_i$$

It is important to keep in mind that the set of lattice velocities is dependent on the discretization, therefore, those quantities are not related to physical system directly. However, such set of lattice velocities results in a very natural discretization:

$$\frac{\partial f_i}{\partial t} + c_i^\alpha \frac{\partial f_i}{\partial x^\alpha} = \frac{f_i(t + \Delta T, x + e_i \Delta X) - f_i(t, x)}{\Delta T} + O(\Delta T, \Delta X) \tag{3.47}$$

An alternative form of the approximation of the combination for the derivatives is the following one:

$$\frac{\partial f_i}{\partial t} + c_i^\alpha \frac{\partial f_i}{\partial x^\alpha} = \frac{f_i(t, x) - f_i(t - \Delta T, x - e_i \Delta X)}{\Delta T} + O(\Delta T, \Delta X) \tag{3.48}$$

It will be shown later than those two ways of discretization correspond to explicit and semi-implicit schemes respectively. Approximations (3.47) and (3.48) lead to the

following numerical schemes, respectively:

$$f_i(t + \Delta T, x + e_i \Delta X) = f_i(t, x) + \Delta T \Omega_i(f(t, x)) \tag{3.49}$$

$$f_i(t, x) - \Delta T \Omega_i(f(t, x)) = f_i(t - \Delta T, x - e_i \Delta X) \tag{3.50}$$

The expression (3.49) represents nothing but the explicit scheme, and equation (3.50) corresponds to the implicit scheme. The explicit scheme is traditional for Lattice-Boltzmann Methods. It is widely used and have a clear mechanistic interpretation as a two-step process. The first step is called collision:

$$\tilde{f}_i(t, x) = f_i(t, x) + \Delta T \Omega(f(t, x)) \tag{3.51}$$

And streaming step:

$$f_i(t + \Delta T, x + e_i \Delta X) = \tilde{f}_i(t, x) \tag{3.52}$$

These two approaches allow the following generalization:

$$\frac{f_i(t, x) - f_i(t - \Delta T, x - e_i \Delta X)}{\Delta T} = (1 - \theta)\Omega_i(f(t, x)) + \theta \Omega_i(f(t - \Delta T, x - e_i \Delta X)) \tag{3.53}$$

Here θ is a real number from zero to one. To the best of author's knowledge this is the first time, when the schemes (3.49), (3.50), and (3.53) are used with density-dependent weights of the LBM model.

One of the most essential parts of the LBM scheme is forcing term, because it is usually designed in such a way, that all the physics of the model is hidden in the term concerned. In the present work the alternative point of view is used: behaviour of the fluid

is determined by the equilibrium distribution function. Such formulation of the method allows one to simplify the expression of the forcing term. In the present work external forces are included through the correction of the equilibrium velocity [72]:

$$u \to u + \tau G \tag{3.54}$$

Here G is the force acting on the unit mass of the fluid. It can be seen from the Chapman-Enskog expansion that the replacement (3.54) represents the external forces correctly. Therefore, the schemes (3.49), (3.50) and (3.53) with modification (3.54) describes the flow of the fluid subjected to the external forces. It is important to notice, the idea of representation of forces through the correction of the mean velocity is not novel. The purpose of the discussion above is to show that the LBM scheme with density-dependent weights admits the inclusion of external forces into the model.

The implicit schemes (3.50) and (3.53) do not have such natural interpretation. According to the authors knowledge, they have been published in [68]. However, the traditional expression for equilibrium distribution functions were considered in that paper. The novelty of the present work is in the implementation of the schemes (3.50) and (3.53) with density-dependent weights and presence of the external forces. It is shown that it is possible to use those numerical schemes without significant increase of computational time and with improved stability of the simulation.

It is important to keep in mind the difference between the proposed numerical scheme and common approaches. In the present work lattice weights are expressed as a functions of the density of the fluid. The density of the fluid can vary both in space and time. Despite that possibility there is no need for solution of systems of non-linear equations. Because of the construction of the BGK collision term, the simple averaging of both sides (3.49),

(3.50), or (3.53) gives the following expression for the density of the fluid at a given node:

$$\rho(t,x) = \sum_i f_i(t,x) = \sum_i f_i(t-\Delta, x-\Delta X e_i) \tag{3.55}$$

The similar equation holds for the mean velocity or for the momentum:

$$\rho u^\alpha = \sum_i f_i(t,x) c_i^\alpha = \sum_i f_i(t-\Delta T, x-\Delta X e_i) c_i^\alpha \tag{3.56}$$

Expressions (3.55) and (3.56) are valid because moments of order zero and one of the equilibrium distribution are the same as of the actual one. In the case of the modification (3.54) the collision term does not cancels out:

$$\sum_i \Omega_i c_i^\alpha = \sum_i \frac{f_i^{eq}(t,x) c_i^\alpha - f_i(t,x) c_i^\alpha}{\tau} = \frac{\rho u^\alpha + \tau \rho G^\alpha - \rho u^\alpha}{\tau} = \rho G^\alpha \tag{3.57}$$

Therefore, the calculation of the moments of both parts of the equation (3.50) results in the following equation:

$$\rho u^\alpha - \rho \Delta T G^\alpha = \sum_i f_i(t-\Delta T, x - e_i \Delta X) c_i^\alpha \tag{3.58}$$

Equation (3.55), (3.56), and (3.58) are shown for the semi-implicit scheme. However, the similar expression can be derived for other types of the schemes. The common feature of all of the algorithms described here is that density and mean velocity of the fluid can be determined after the streaming step. As long as both density and mean velocity are defined, one can compute equilibrium distribution functions and other terms of the model. The important thing is that all the calculations are performed locally even for the semi-implicit scheme. That is the reason why the semi-implicit scheme is beneficial in terms of performance: the improvements in stability are achieved through the minor increase

of the computational cost. What is more important is that the efficiency for the parallel computing remains the same as for the explicit scheme. This is the consequent of the observation that the communication between nodes in both schemes is exactly the same.

The other important property of the scheme with density-dependent weights is the restriction on the time step because of the issues with numerical stability. It has been mentioned in the introduction that the major source of instabilities in LBM is negative value of distribution function. The latter means that for the stable scheme at least equilibrium distribution functions should be positive for any possible mean velocity. In the case of zero mean velocity, equilibrium distribution functions are simply:

$$f_i^{eq} = w_i \rho \tag{3.59}$$

Therefore, for the stability of the scheme it is necessary that lattice weights are positive. From the plot for lattice weights below it can be seen, that there exist a certain range for the values of the λ-parameter $\frac{c_s \Delta T}{\Delta X}$ such that all of the lattice weights are positive simultaneously.

Moreover, if the spatial step ΔX is fixed then for a given density of the fluid there exist a range of time steps $[\Delta T_{min}, \Delta T_{max}]$ for which all the lattice weights are positive. The presence of the upper bound for the time step is not surprising. The lower bound is the unusual thing. The existence of lower bound on the time step impacts the overall work flow of the modelling.

The first feature is the choice of the time step. Actually, the restrictions on the time step creates certain difficulties. For instance, in traditional simulations one can always reduce the rime step, preserving the same spatial resolution. In the case of the LBM scheme one should reduce the spatial step as well. That means that the cost simulations can be increased dramatically.

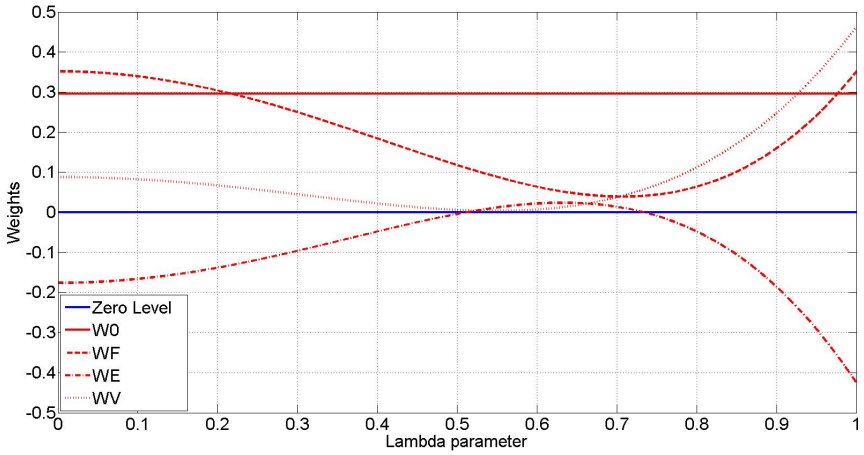

Figure 3.1: Plots of combination of the weights w_c, $6w_f$, $12w_e$, $8w_v$. Factors 1, 6, 12 and 8 correspond to the number of lattice directions in a given family of weights. It can be seen that there exist lower and upper bound for the value of the dimensionless λ-parameter.

The more important consequence is that in certain cases it is not possible to run the simulation. For instance, if the contrast in densities of the fluid is high enough then it can be impossible to adjust the temporal and spatial resolutions in such a way that the weights are positive for all possible densities of the fluid. The other example that illustrates this idea is a multi-phase flow. In this case the presence of two fluids with significant differences in PVT properties makes it impossible to adjust the size of the mesh and time step in order to design the stable LBM scheme.

Finally, the constraint on the time step demonstrates that the ratio between spatial step and temporal step is determined by PVT properties of the fluid. For gases, the ratio $\Delta X/\Delta T$ has the same order of magnitude as the speed of sound. The latter makes the approach developed impractical for field scale simulations, because it tends to resolve effects that occur at the temporal scale of sound waves in the gas. The latter is significantly smaller then the actual time-scale of the processes at the field-scale. The reasoning above establishes the need for the alternative tool for reservoir simulations via LBM.

3.4.2 Boundary Conditions

In LBM, the streaming step is defined as follows:

$$f_i(\hat{t}, x) = f_i(t - \Delta T, x - \Delta e_i) \tag{3.60}$$

In the equation (3.60) it is assumed both of the nodes concerned are inside the computational domain. The latter is the case of problems defined in the whole space. However, the vast majority of problems that are important for practical implementations are formulated for bounded domains. Therefore, the streaming step is not defined for all the nodes. That means that the streaming step should be redefined for the nodes that are close to the boundary of the computational domain. The latter can be done through the formulation of boundary condition (BC). The major challenge in the development of BC is that dynamic of the particles on the lattice should be related to a real physical system. The same statement applies for the BC as well. In other words, BC should be related to the physical processes that appear on the boundary of the system. In the case of hydrodynamics the physics concerned is described in terms of the velocity of the fluid. Typically, there are two possibilities for the speed of the fluid at the boundary: vanishing of only normal component of the velocity, and zero velocity. In any case, those two constraints can give only up to three equations. However, the number of the components of distribution functions that should be defined can be even 13 for D3Q27 model. The latter means that the formulation of BC for a given problem is typically not unique. That is the greatttention should be paid for the formulation of BC for LBM.

In the present work three boundary conditions are used: periodic, reflection and zero-velocity. The simplest BC to impose is the periodic one. In this case it is possible to imagine that PDE's are defined inside the infinite domain, however the solution is periodic with respect to the spatial coordinates. In other words, the solution satisfies the following

constraint:

$$f_i(t, x^1, x^2, x^3) = f_i(t, x^1 + n_1 L^1, x^2 + n_2 L^2, , x^3 + n_3 L^3) \tag{3.61}$$

Here n_1, n_2, and n_3 are integers. L^1, L^2, and L^3 are referred to as period with respect to the coordinate axes. The equation (3.61) means that all the information about the solution in the whole space is contained in the box $B = [0; L^1] \times [0; L^2] \times [0; L^3]$. It is simple to see that for any point in space x, there exist at least one point $p(x)$ inside the block B and integers n_1, n_2, and n_3, such that:

$$\begin{gathered} x - p(x) = n_1 L^1 + n_2 L^2 + n_3 L^3 \\ f_i(t, x) = f_i(t, p(x)) \end{gathered} \tag{3.62}$$

Equations (3.62) give the rule for the redefinition of the streaming step in the case of periodic boundary conditions:

$$f_i(\hat{t}, x) = f_i(t - \Delta T, p(x - \Delta e_i)) \tag{3.63}$$

From the discussion above it follows that the periodic problem in the infinite domain is equivalent to the problem in the box B with periodic BC. What is more important is that the solution for the problem in the infinite domain can be reconstructed from the finite one with the usage of three affine maps and inverse to them. Those maps are shifts by L^1 in 'X' direction, by L^2 in 'Y' direction, and by L^3 in 'Z' direction, which are referred to as S_1, S_2, and S_3 respectively. In other words, there are six maps or generators: three shifts S_1, S_2, and S_3 and three inverse maps S_4, S_5, and S_6. Therefore, for any point $x \in B$, for any composition of generators $A = S_{i_1} ... S_{i_n}$, the reconstruction procedure can be defined

as:

$$f_i(t, A(x)) = f_i(t, x) \tag{3.64}$$

The idea of the reconstruction of the solution using a single box and a set of generators can be applied for the derivation of reflection boundary conditions. In this case the set of generators is formed by reflections of the box B with respect to its faces. Therefore, there are six generators R_1, R_2, R_3, R_4, R_5, and R_6 as in the previous case. It is easy to see that for any point in space x there exist a point y in the box B, such that $y = r(x)$ and r is the composition of reflections. In other words, it is possible to put the point x in the box B by the finite number of reflections with respect to the faces of the box B. The latter allows one to redefine the streaming step as follows:

$$f_i(\hat{t}, x) = f_i(t - \Delta T, r(x - \Delta e_i)) \tag{3.65}$$

It can be shown that the result of the operation (3.63) is the same as long as $r(x-\Delta e_i) \in B$. It can be seen that because of symmetry of the procedure concerned, the component of the velocity normal to a given face of the box B vanishes at that edge. Therefore, the reflection BC is equivalent to the vanishing of normal component of the velocity at the boundary. The Figure (3.2) illustrates the idea of the implementation of the boundary condition.

Zero-velocity boundary condition is required for the numerical solution of the Navier-Stokes equation via LBM. The most popular boundary condition for such simulations is the Bounce-Back boundary condition [57]. The advantage of the BC concerned is that it is formulated in local terms. Basically, if the node $x - \Delta X e_i$ is outside the computational domain, then in the case of Bounce-Back boundary condition one should find lattice vector e_j such that $e_j = -e_i$. With such e_j the streaming step takes following form:

$$f_i(\hat{t}, x) = f_j(t - \Delta T, x) \tag{3.66}$$

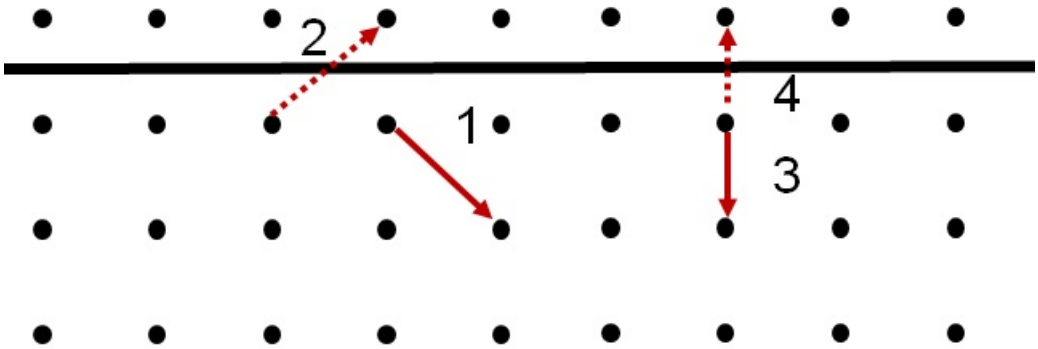

Figure 3.2: Illustration of the algorithm for application of the reflection boundary condition. Particles for the components 1 and 3 are streamed from 2 and 4 respectively.

Despite the simplicity and convenience in terms of implementations, the boundary condition concerned should be used with care. The reason is that it does not guarantee the vanishing of the tangent component of the velocity at the boundary [51]. Therefore, in the present work the modified version of Bounce-Back boundary condition is used.

The formulation of modified Bounce-Back rule is inspired by the analogy between LBM and FV methods. The analogy arises from the fact that LBM is one of the methods for numerical solution of system of hyperbolic equations, for DKE in particular. For the equations of that type the direction of the flux is one of the most essential things to take care about. This is expressed in the fact that the up-winding procedure presents in all of the FV schemes for hyperbolic equations. Roughly speaking, the idea of the up-winding procedure can be expressed as follows: fluxes that leave the given cell are computed based on the properties inside that cell, otherwise parameters of neighbouring grid blocks are used. The same principle is applicable to the cells on the boundary. In this case, the flux that leaves the computational domain is computed based on the values of properties inside that cell. For the flux that is coming from the boundary to the computational domain, the

boundary condition should be applied. In the case of DKE for D3Q27 model all of the lattice velocities except zero can be divided in pairs c_i and the opposite one $c_j = -c_i$. That means that for the boundary in general position to the lattice velocities exactly 14 can be computed from the streaming step and for another 13 a boundary condition should be applied. The latter happens because of the symmetry of the lattice: if particles with the speed c_i leave the computational domain, then the particles with the opposite velocity $-c_j$ should come from the exterior of the domain concerned and vice versa. However, it is very common in LBM to work with domains that have boundaries parallel to lattice directions. This situation is referred to as degeneration in the present work. It is worth to notice that the degeneration concerned can be eliminated by the arbitrary small perturbation of the shape of the boundary. If the boundary has been deformed, then exactly for the half of the distribution functions that correspond to the particles that propagate parallel to the boundary the boundary condition should be applied. However, the perturbation is arbitrary, therefore, it is not possible to prove which of the distribution functions should be streamed and which of them shoud be computed through BC. Because of the reasoning above it has been decided to compute the half of the distribution function via boundary condition and stream the remaining part:

$$f_i(t, x) = \frac{1}{2} f_j(t - \Delta T, x) + \frac{1}{2} f_i(t - \Delta T, x - \Delta X e_i) \tag{3.67}$$

Here j corresponds to the particles with the velocity $-e_i$. The rule (3.68) is applied only to the particles that have the speed parallel to the boundary. For the remaining distribution function the standard Bounce-Back boundary condition is applied:

$$f_i(t, x) = f_j(t - \Delta T, x) \tag{3.68}$$

It is worth to mention that in the modification concerned affect only the particles that travel parallel to the boundary. In the classic Bounce-Back scheme components of distribution functions that correspond to the particles concerned are simply streamed from the neighbours. Numerical simulations that are discussed below show that the modified Bounce-Back boundary condition leads to zero mean velocity at the wall. The idea of the algorithm is illustrated in the Figure (3.3):

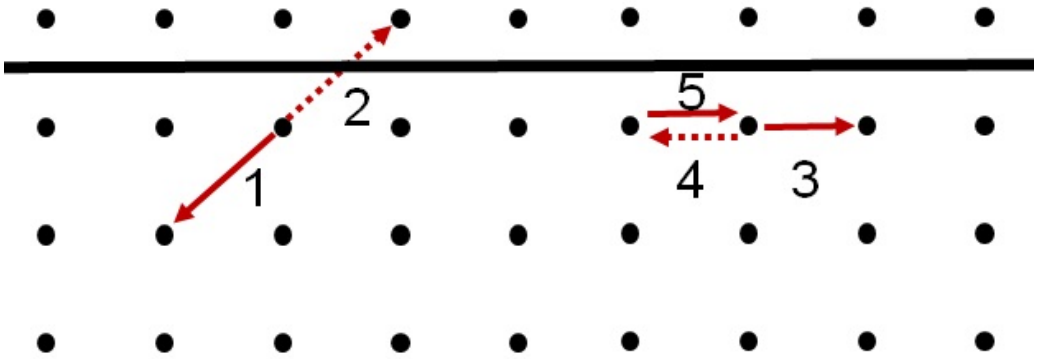

Figure 3.3: Illustration of the algorithm for application of the modified Bounce-Back boundary condition. For the particles 1 and 2 the classic Bounce-Back algorithm is applied. Distribution function 3 is a weighted sum of distribution functions 4 and 5.

3.5 Numerical Results

In the present section results of series of numerical simulations are presented. First two subsections are devoted to the validation of the developed approach. The last one illustrates one of the possible application of LBM to the problem of scale integration.

3.5.1 EOS Validation

One of the possible tests of the performance of the algorithm is test of the equilibrium in gravity field. In the present section the gas with the following EOS has been considered:

$$P = P_0 \left(\frac{\rho}{\rho_0} \right)^{\gamma} \tag{3.69}$$

Here P_0 and ρ_0 are reference pressure and density respectively. P is the value of pressure for the density ρ. γ is the parameter that controls the features of the EOS. It is simple to see that $\gamma = 1$ represents the ideal isothermal gas, and $\gamma = 7/5$ corresponds to the adiabatic process of the ideal two-atomic gas. For the validation purposes only those values of γ has been considered. The gas with the EOS described has been placed into the gravity field. The magnitude of the gravity acceleration has been considered to be constant and equal to $1000m/s^2$. The overall heights of the system is $100m$. The results are compared with the numerical solution for the following equation:

$$\frac{\partial \rho}{\partial z} = -\frac{\rho g}{\frac{\partial P}{\partial \rho}} \tag{3.70}$$

The equation (3.70) has been solved numerically on a tiny mesh. The initial condition for (3.70) is the following:

$$\rho(h = 0) = \rho_0 \tag{3.71}$$

In the present work five values of ρ_0 has been considered: $1kg/m^3$, $1.78kg/m^3$,$3.17kg/m^3$, $5.63kg/m^3$, $10kg/m^3$. The Figure (3.4) demonstrates that both solutions are close to each other. The results of both numerical methods are in the agreement with each other as it is demonstrated in Figures (3.4) and (3.5):

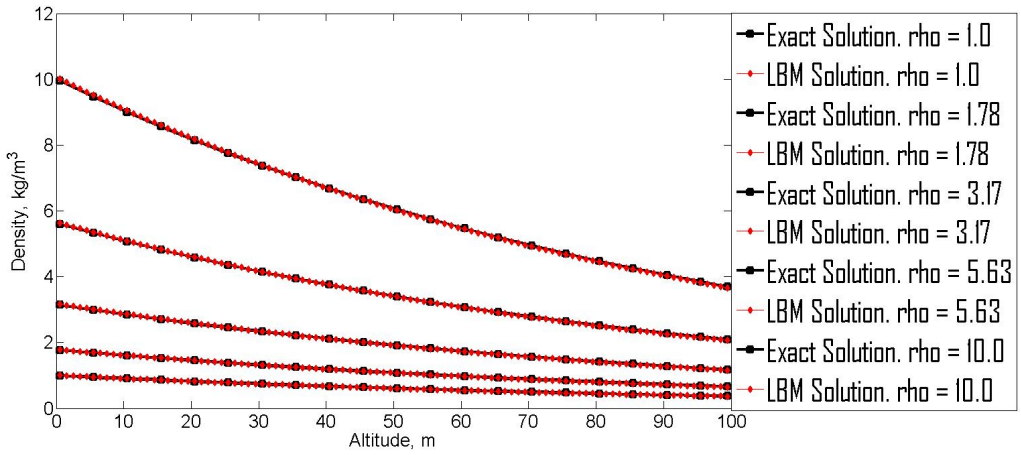

Figure 3.4: Validation for the LBM scheme developed for $\gamma = 1$. The solution derived through LBM (solid line) almost coincide with the solution obtained by conventional methods (line with dots).

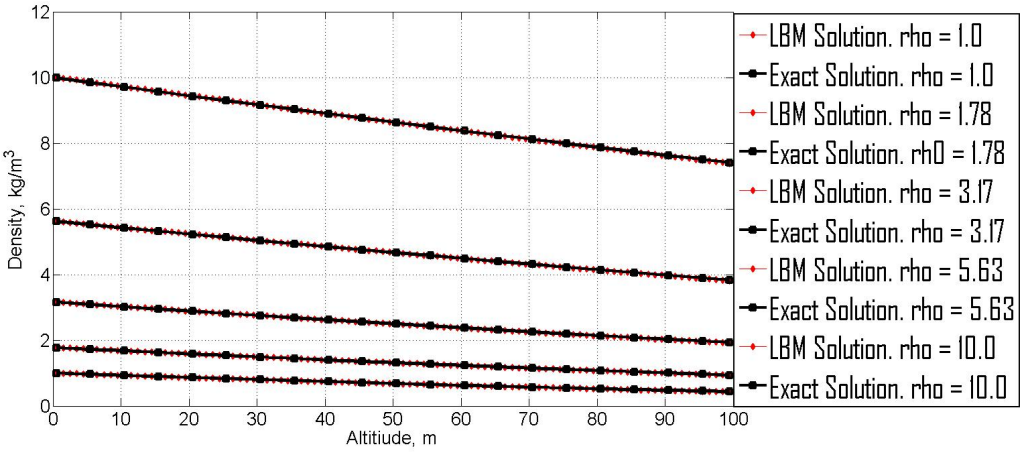

Figure 3.5: Validation for the LBM scheme developed for $\gamma = 7/5$. The solution derived through LBM (solid line) almost coincide with the solution obtained by conventional methods (line with dots).

3.5.2 Poiseuille Flow

The standard validation test for LBM is flow between parallel planes. The system concerned is modelled via LBM through imposing appropriate boundary conditions. Namely,

constant pressure or density BC is applied to inlet and outlet. Zero-velocity BC is applied to the parallel planes or walls. Periodic boundary condition is used in order to model 2D system using 3D code. In such setting, the driving force for the flow is pressure difference. In the present work that driving force is replaced by the uniform acceleration parallel to the walls. The latter is equivalent to the free-falling fluid bounded by parallel vertical planes. In this case constant pressure BC is replaced by the periodic BC. The main motivation for the this replacement it is convenience in terms of formulation of boundary conditions: there are certain difficulties with formulation of BC at the intersection of two surfaces with boundary conditions of different types in general. However, this procedure is simple for the case of intersection of surfaces with periodic BC and zero-velocity BC. The difference in the driving force is important for practical calculations. However, both of the systems are equivalent for the purposes of the validation of formulation of zero-velocity BC and for the relation (3.35) between the relaxation time τ and viscosity μ.

It is well-known that for the flow configuration concerned, the velocity field has parabolic profile:

$$u = \frac{\rho g z(d-z)}{2\mu} \tag{3.72}$$

Here ρ is the density of the fluid, u is a velocity of the flow, μ is the viscosity of the fluid, g is a magnitude of the acceleration field, d is the distance between planes, and z is the distance to one of the planes. For the purposes of validation, the simulation of the fluid flow with the following values of the parameters in (3.72): $\rho = 1kg/m^3$, $d = 10^{-6}m$, $g = 1000m/s^2$, has been performed. The time step in the simulation is $1.84 \cdot 10^{-3}s$, the relaxation time is in the range from $9.4 \cdot 10^{-4}s$ to $7.36 \cdot 10^{-3}s$. Numerical results demonstrate the agreement with the expression for the viscosity (3.35) and that the modified Bounce-Back boundary can be applied to the simulation of the fluid flow with zero velocity at the walls as it follows from the Figure (3.6):

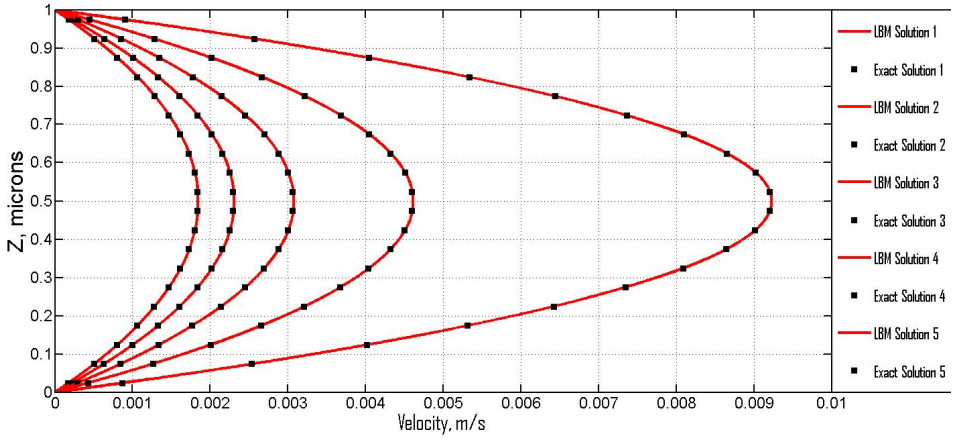

Figure 3.6: Impact of the relaxation time on the distribution of the velocity. Plots of the distribution of the velocity of the fluid in the direction normal to the wall are presented. Simulations have been performed for the following values of relaxation time in the range from $9.4 \cdot 10^{-4} s$ to $7.36 \cdot 10^{-3} s$. Numerical solution (solid line) is in the agreement with the analytic expression (solid dots). It can be seen that the zero-velocity boundary condition holds in the simulations.

From the Figure (3.6) it can be seen that both the velocity distribution in the cross-section between planes and the absolute value of the speed of the fluid are in the reasonable agreement with the analytic expression. Therefore, the LBM model developed can be applied to the numerical solution of the Navier-Stokes equations.

3.5.3 Example of Application

In the present section the application of the LBM scheme developed to the simulation of the fluid flow in shale reservoirs is considered. Basically, it is shown how the method can be integrated into the sequential upscaling work flow. Numerical simulations with LBM of the flow of methane between parallel planes are considered as it is shown in the figure (3.7). It has been assumed that the virial EOS allows one to compute PVT properties with reasonable accuracy.

It has been mentioned in the introduction to the present chapter that there are many

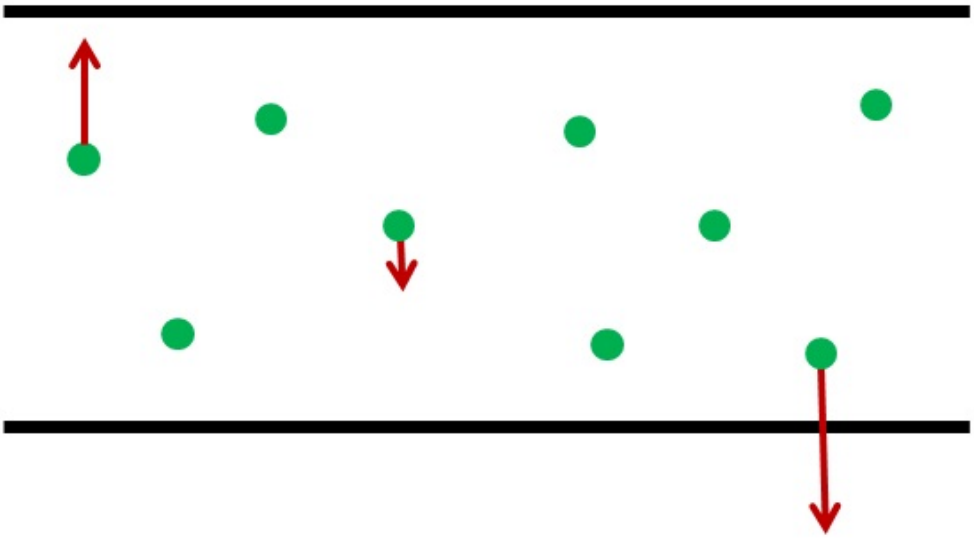

Figure 3.7: The schematic representation of the flow geometry. The flow between parallel planes is considered. The adsorption is represented as the force that pulls molecules of the gas to the wall. This force is represented via red arrow. The magnitude of the force is reflected through the lengths of the arrow.

research papers on the simulation of the slippage effects in small pores. The typical approach is the modification of the boundary conditions in such a way that the velocity of the fluid at the walls is not zero in general. The focus of the present study is the impact of the adsorption. Therefore, standard zero-velocity BC are applied. The adsorption is introduced through the force field through (3.2), (3.54), and (3.53). The introduction of the force concerned results in the redistribution of the fluid in the cross-section of the channel. Results of the simulations that demonstrate the effect concerned are shown in the Figure (3.8):

One of the effects of the adsorption is the attraction of some part of the fluid to the walls of the channel. The latter leads to the non-uniform distribution of the density of the fluid inside the channel. Moreover, the relation between the average or mean density and the macroscopic pressure of the fluid can be affected as well. The purpose of the present

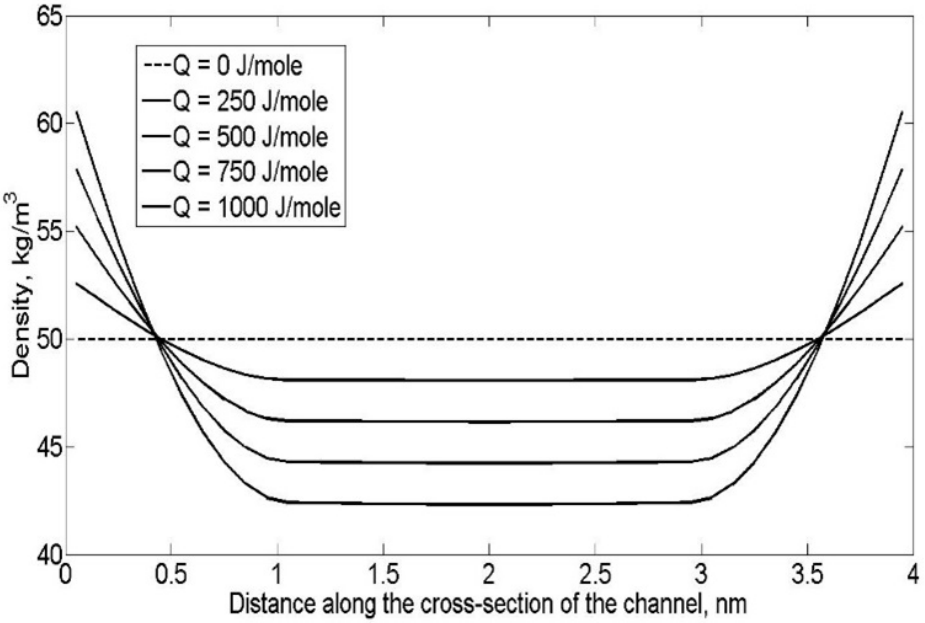

Figure 3.8: Density distribution inside the channel.

work is to compute corrections to the PVT properties of the fluid based on the results of numeral simulations. Therefore, the following relation is the subject of principal interest:

$$P = P(\rho, Q, d) \tag{3.73}$$

Here Q is the heat of adsorption, d is the diameter of the channel. The expression (3.73) can be used in a reservoir simulation for calculation of pressure or density of the fluid if the heat of adsorption and representative size of the pores are specified for a given rock. The more convenient form of the (3.73) is the representation of pressure change as a multiplication by a certain correction factor:

$$P = K(\rho, Q, d)P_0(\rho) \tag{3.74}$$

Here K is the correction factor, and P_0 is the pressure of the fluid when the adsorption is negligible. In the work series of simulations have been performed in order derive a correlation for the correction factor K. The diameter of the channel d has been varied from 4 nm to 12 nm. The radius of investigation is assumed to be $1\ nm$ and is the same in all of the simulations. Heat of adsorption is $Q = 1000.0\ J/mole$.

One can see that because of the geometry of the system concerned, the fluid that is close to the center or far away from the walls is not subjected to the attraction force. The latter means that the fluid in the region concerned should follow the standard EOS. Moreover, simple physical reasoning shows that the pressure it the middle of the channel is exactly the pressure, that can be measured in the experiments. That is the reason why the pressure that corresponds to the density of the fluid in the center of the channel is considered as an actual one. Therefore, the algorithm of the calculation of K is the following: the first step is the computation of the distribution of the density of the fluid in the cross-section of the channel for the given mean velocity ρ. The second step is the evaluation of the correction factor using the formula:

$$K = \frac{P_0(\rho_C)}{P(\rho)} \tag{3.75}$$

Here ρ_c is the density of the fluid in the center of the channel. The dependency of the correction factor on the parameters of the adsorption is hidden inside the value of ρ_C, because the latter number is fully controlled by the strength of the interaction.

Finally the coefficient $K(Q, d)$ can be computed based on the series of numerical simulations. With such coefficient it is possible to derive the effective EOS for the fluid in the porous media with a given size of the pores. The example of the results of such calculations for methane with Peng-Robinson EOS is shown in the Figure (3.9):

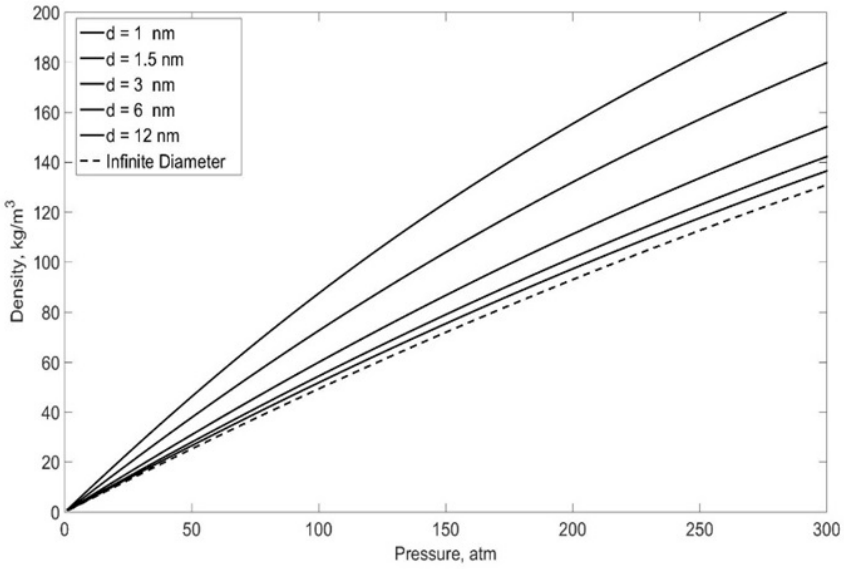

Figure 3.9: Plots of the dependency of the density on the pressure are presented for several values of the diameter of the channel. As expected, the role of the adsorption becomes more and more important as the diameter of the channel approaches to zero. The other important observation is that the limit of the infinite diameter of the channel coincides with the standard EOS for the fluid in a big volume.

3.6 Summary

in the present chapter the approach for the simulation of the fluid flow at the pore-scale has been presented. Standard numerical tests provide the validation for the developed technique. The potential of the new LBM scheme for the upscaling of PVT properties of fluids has been demonstrated. It should be mentioned that the central idea of the technique has been published as a conference paper [70]. However, several significant improvements have been introduced.

The first improvement is the replacement of the explicit LBM-scheme by the semi-implicit one. The latter increases the numerical stability of the method. The second important thing to mention is the derivation of the expression for weights, for the lattice

speed of sound and for the relaxation time for the scheme with density-dependent lattice weights. In the [70] only the central idea regarding the way of how that expressions can be derived has been presented. The third improvement is modified of the Bounce-Back boundary condition for the simulation of fluid flow with zero-velocity boundary condition at the walls of the channel. Finally, validation tests together with the correlation for the correction factor for the pressure are novel results.

In the present work the limitations of the technique developed are discussed as well. It has been shown that the issues with numerical stability lead to the strong limitations on the robustness of the approach. The issues concerned is the major reason for the remaining part of the work.

4. FIELD SCALE SIMULATIONS

In the previous section the LBM model for the simulation of fluid flow at the pore-scale has been developed. It has been emphasized that the approach concerned imposes severe restrictions on the time-step (4.17). One of the possible interpretations of the constraint observed is that the time-step is related to the PVT properties, in particular to the speed of sound. Simple calculations show that in this case the time-step should be of the order of seconds for the typical size of the mesh that is used in reservoir simulations. The latter is not practical because the time scale concerned can be several years. Therefore, an additional work for the improvement of the method is required. Despite the disadvantage in terms of the restriction on the time-step, the approach developed has a self-consistent mathematical structure. The latter motivates one to continue the development of the scheme for the field-scale simulations, for example by introducing additional lattice vectors. Moreover, there are prospectives of the extension of the technique to the irregular lattices.

The natural way for the generalization involved comes from the similarity between LBM and standard finite volume methods. One can consider the lattice node as the cube with the center that coincides with the location of the node. In this case any distribution function multiplied by the volume of the node is the total mass of particles that move in a given direction. It is clear that the streaming step is simply mass-exchange between nodes or between cubic volumes associated with them. Therefore, distribution functions correspond to the fluxes in standard finite-volume schemes. However, the difference from the finite volume schemes is that in conventional methods pressures and densities are primary objects. Fluxes are computed based on the values of those primary variables. In LBM, the inverse situation can be observed. In this approach mass fluxes are primary objects and

physical quantities are calculated based on the fluxes, for instance, through the application of the averaging procedure (3.11). The other important difference is that in LBM the mass exchange occurs not only between blocks with common faces. Moreover, it is clear from the Figure (4.1), that lattice vectors correspond to the vectors that connect the centres of elements with common points:

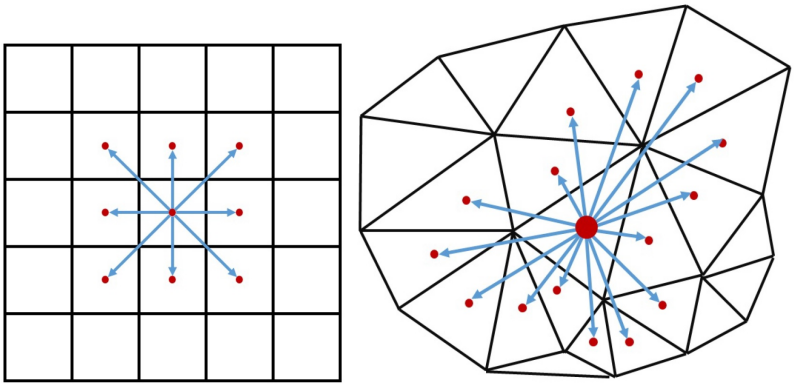

Figure 4.1: Finite Volume Nature of Lattice Boltzmann Method. Each lattice node can be considered as the center of the cubic volume. In this case lattice vectors connect centers of cubes with common points. The mass exchange occurs between the volumes concerned.

Despite the differences mentioned above, the finite-volume interpretation of LBM is quite useful for the theoretical analysis of the numerical scheme. For example, one of the benefits of the interpretation concerned is direct translation of the language of finite volume methods to LBM. For instance, the growth of the instability in the LBM scheme when one of the components of the distribution function becomes negative, can be explained in terms of the violation of up-winding procedure in the corresponding finite volume scheme.

The other benefit of the "finite volume" way of thinking about LBM is a natural generalization of the method to the irregular lattice geometry. The idea is simple: in the case of the regular mesh geometry nodes correspond to the grid blocks and streaming step is

equivalent to the mass-exchange or flux. The statement above is a direct sequence of the formulation of the equations for LBM (3.50). In this case nodes are simply centres of the grid-blocks and lattice vectors correspond to the vectors that connect centres of the grid blocks. In other words, lattice vectors can be defined in terms of the grid geometry in the case of rectangular mesh. The definition concerned can be extended to the case of the unstructured grid geometry as it shown in the figure (4.1). From the previous section it follows that as long as lattice velocities are defined, the only missing ingredient of the LBM scheme is the equilibrium distribution function. Basically, for the simulation of the Navier-Stokes equations with LBM it is enough to satisfy the constraints for the moments of the equilibrium distribution functions as it shown in the Figure 3.1. That reduces the problem to the purely algebraic one. Finally, it can be formalized as the system of linear equation in the finite dimensional subspace in tensor algebra of R^3:

$$M_0 + M_1^{\alpha} e_{\alpha} + M_2^{\alpha\beta} e_{\alpha} \otimes e_{\beta} + M_3^{\alpha\beta\gamma} e_{\alpha} \otimes e_{\beta} \otimes e_{\gamma} = \sum_i f_i^{eq} \eta_i \tag{4.1}$$

Here e_{α} are basis vectors in R^3. M_k is the moment of order k. η_i are defined as follows:

$$\eta_i = 1 + c_i^{\alpha} e_{\alpha} + c_i^{\alpha} c_i^{\beta} e_{\alpha} \otimes e_{\beta} + c_i^{\alpha} c_i^{\beta} c_i^{\gamma} e_{\alpha} \otimes e_{\beta} \otimes e_{\gamma} \tag{4.2}$$

Finally, the problem of finding appropriate equilibrium distribution functions can be reduced to the problem of finding the decomposition of the tensor sum of the moments as a convex combination of vectors η_i. It is worth to mention that the system of equations (4.1) is not simple for analysis, because the number of equations can be less than the dimension of space and some of them can be linearly dependent. However, it has a potential to solve the problem with constraints on the time step that has been indicated in the previous chapter (4.17). The latter is the main motivation for further investigation.

Summarizing the discussion above, further development of the approach developed in the previous section is beneficial in two ways: it makes it possible to extend LBM to the unstructured grid geometry and gives promise for resolving the issue with the restriction on the time-step. Unfortunately, the latter is not the case. Detailed analysis shows that the constraints on the time-step involved are inherit for LBM. This statement is formalized as a theorem and proved in the present section. The limitations observed make that approach impractical for reservoirs simulations. Pseudo-potential models can be one of the possible solutions for the problems concerned. In the present section an LBM scheme for pseudo-potential models is described. The limitations of the approach are observed.

4.1 Proof of the Limitations

In the previous section the algorithm for the construction of lattice vectors has been discussed. It has been mentioned that the theoretical analysis can be complicated for the lattice of general connectivity. Therefore, in the present section the case of the lattice with high spatial symmetry is studied. The letter means that lattice should preserve its shape under a given transformation of coordinates. The set concerned should include the central symmetry with respect to the lattice vector that represents zero velocity. Rotations to 90 degrees with respect to all coordinate axes should preserve the lattice as well. Moreover, the set of lattice velocities should include D3Q27 lattice. It is possible to show that for such lattices there is no such choice of equilibrium distribution functions that guarantees positivity of the latter for any temporal step in the range from zero to a certain positive critical value.

For the proof of the statement concerned it is enough to construct at least one that violates the constraint on the time step. The latter can be done directly, however some preliminary work is required. The first thing that should be done for the simplification of the analysis is a renormalization of the equilibrium distribution function. Traditionally, the

equilibrium distribution is normalized to the density:

$$\rho = \sum_i f_i^{eq}$$

It is convenient to renormalise it to unit. The next step is the reformulation of the constraints on the moments of the equilibrium distribution function. It has been mentioned that for the simulation of the fluid flow governed by the Navier-Stokes equation, it is enough to have the moments of equilibrium distribution M_0,M_1,M_2,M_3 in the form given by (3.14). Initially, the distribution concerned has only three parameters: density, average velocity and pressure as function of density. However, after the normalization to unit, only velocity and so-called lattice speed of sound $c_s^2 = P/\rho$.

The latter means that renormalized distribution functions should satisfy equations (3.14) for any average velocity in a reasonable range, and at least for zero mean velocity. The case of zero velocity is simple for analysis because of the spatial symmetry. As a consequence on the symmetry concerned, the magnitude of the equilibrium distribution function that corresponds to the lattice velocity c_i depends only on the absolute value of c_i. Therefore, the situation is almost identical to the weights of semi-Gaussian or quadratic equilibrium distribution. The difference is in the presence of extra terms that correspond to lattice velocities beyond the D3Q27 model. Because of the symmetry of the lattice, the similar reasons to (3.44) are applicable. Therefore, one equation on vectors in the subspace in tensor algebra of R^3 can be reduced to the system of three algebraic equations:

$$\begin{aligned} \sum_i \frac{f_i^{eq}}{\rho} &= 1 \\ \sum_i \frac{f_i^{eq}|c_i|^2}{\rho} &= 3c_s^2 \\ \sum_i \frac{f_i^{eq}|c_i|^4}{\rho} &= 15c_s^4 \end{aligned} \tag{4.3}$$

Here dimensionless units can simplify the expression significantly. Namely, lattice velocities can be expressed through lattice vectors:

$$c_i = \frac{\Delta X}{\Delta T} e_i$$

Dimensionless speed of sound can be introduced:

$$\lambda = \frac{c_s \Delta T}{\Delta X} \tag{4.4}$$

Moreover, it is convenient to denote normalized distribution functions as ϕ_i:

$$\phi_i = \frac{f_i^{eq}}{\rho} \tag{4.5}$$

In this case the system (3.44) transforms to:

$$\begin{aligned} \sum_i \phi_i &= 1 \\ \sum_i \phi_i |e_i|^2 &= 3\lambda^2 \\ \sum_i \phi_i |e_i|^4 &= 15\lambda^4 \end{aligned} \tag{4.6}$$

One can divide summations above into summation over D3Q27 lattice and over the remaining part:

$$\sum_i \phi_i = \sum_{i \in D3Q27} \phi_i + \sum_{i \notin D3Q27} \phi_i = 1$$

The second term of the summation can be denoted as x_1:

$$x_1 = \sum_{i \notin D3Q27} \phi_i$$

The similar notation can be introduced for other equations in (4.6):

$$x_2 = \sum_{i \notin D3Q27} \phi_i |e_i|^2$$

$$x_3 = \sum_{i \notin D3Q27} \phi_i |e_i|^4$$

Eventually, the summation over the lattice velocities has been divided into the summation over the D3Q27 and over the remaining part of the set. It has been mentioned that because of the symmetry $\phi_i = \phi_j$ if and only if $|e_i| = |e_j|$. Therefore, the summation over D3Q27 lattice can be transformed to:

$$\sum_{i \in D3Q27} \phi_i = \sum_{i:|e_i|=0} \phi_i + \sum_{i:|e_i|=\sqrt{1}} \phi_i + \sum_{i:|e_i|=\sqrt{2}} \phi_i + \sum_{i:|e_i|=\sqrt{3}} \phi_i$$

According to the notations introduced in the previous section for the D3Q27 model, one can denote terms in the summation above as:

$$\begin{aligned} \Phi_c &= \sum_{i:|e_i|=0} \phi_i \\ \Phi_f &= \sum_{i:|e_i|=\sqrt{1}} \phi_i \\ \Phi_e &= \sum_{i:|e_i|=\sqrt{2}} \phi_i \\ \Phi_v &= \sum_{i:|e_i|=\sqrt{3}} \phi_i \end{aligned} \tag{4.7}$$

The direct substitution shows that constraints (3.44) can be transformed to the form:

$$\begin{aligned}
\Phi_c + \Phi_f + \Phi_e + \Phi_v + x_1 &= 1 \\
\Phi_f + 2\Phi_e + 3\Phi_v + x_2 &= 3\lambda^2 \\
\Phi_f + 4\Phi_e + 9\Phi_v + x_3 &= 15\lambda^4
\end{aligned} \tag{4.8}$$

The system of equation concerned can be solved with respect to Φ_f, Φ_e, Φ_v:

$$\begin{aligned}
\Phi_f &= 3 - 3\lambda^2 + \frac{15}{2}\lambda^4 - 3(\Phi_c + x_1) + \frac{5}{2}x_2 - \frac{1}{2}x_3 \\
\Phi_e &= -3 + 12\lambda^2 - 15\lambda^4 + 3(\Phi_c + x_1) - 4x_2 + x_3 \\
\Phi_v &= 1 - \frac{9}{2}\lambda^2 + \frac{15}{2}\lambda^4 - (\Phi_c + x_1) + \frac{3}{2}x_2 - \frac{1}{2}x_3
\end{aligned} \tag{4.9}$$

From the definition of ϕ_i, $\phi_i|e_i|^2$, $\phi_i|e_i|^4$ it follows that all of the terms in(4.9) are positive. Moreover, the following inequality holds:

$$0 < \Phi_c + x_1 < 1 \tag{4.10}$$

It has been mentioned that all of the Φ_f, Φ_e, Φ_v should be positive. The latter results in a system of inequalities:

$$\begin{aligned}
0 &< 3 - 3\lambda^2 + \frac{15}{2}\lambda^4 - 3(\Phi_c + x_1) + \frac{5}{2}x_2 - \frac{1}{2}x_3 \\
0 &< -3 + 12\lambda^2 - 15\lambda^4 + 3(\Phi_c + x_1) - 4x_2 + x_3 \\
0 &< 1 - \frac{9}{2}\lambda^2 + \frac{15}{2}\lambda^4 - (\Phi_c + x_1) + \frac{3}{2}x_2 - \frac{1}{2}x_3
\end{aligned} \tag{4.11}$$

Standard rules of taking weighted sums of inequalities give the following constraint:

$$0 < \frac{15}{2}\lambda^4 - \frac{3}{2}\lambda^2 + \frac{1}{2}x_2 - \frac{1}{2}x_3 \tag{4.12}$$

The latter can be converted to:

$$\frac{1}{2}x_3 - \frac{1}{2}x_2 < \frac{15}{2}\lambda^4 - \frac{3}{2}\lambda^2 \tag{4.13}$$

It is easy to see that because of the definition of x_2 and x_3 the difference $x_3 - x_2$ is positive, therefore (4.13) results in the constraint on λ:

$$0 < \frac{15}{2}\lambda^4 - \frac{3}{2}\lambda^2 \tag{4.14}$$

Finally,

$$\frac{1}{\sqrt{5}} < \lambda \tag{4.15}$$

The latter sets the restriction on the time-step:

$$\frac{\Delta X}{c_s\sqrt{5}} < \Delta T \tag{4.16}$$

The existence of the upper bound for λ and for ΔT follows the expectations. As long as only positive distribution functions are of the interest, then each of the variables x_1, x_2, x_3, Φ_c,Φ_f,Φ_e,Φ_v should be in the interval $[0; 1]$. However for big enough λ or ΔT the value of Φ_e becomes negative because of (4.9).

From the discussion above it follows that the only way to keep all the components of the equilibrium distribution functions positive is to establish an upper and lower bounds for both λ and ΔT.

$$\lambda_{min} < \lambda < \lambda_{max}$$

The values of lower and upper boundary for λ are determined by the connectivity of the lattice but not by the spatial step. The latter constraint on λ leads to the constraint on the

time step:

$$\Delta T_{min} = \frac{\Delta X \lambda_{min}}{c_s} < \Delta T < \frac{\Delta X \lambda_{max}}{c_s} = \Delta T_{max} \tag{4.17}$$

It is important to notice that the ΔT_{min} and ΔT_{max} are determined both by the size of the mesh and by the PVT properties of the fluid. The latter imposes severe limitations on the robustness of the method especially for multiphase flow. If the ranges of time steps for two fluids do not overlap, then it is not possible to design a stable LBM scheme. The latter is one of the reasons for the development of the alternative ways of treatment of EOS in LBM. The second reason comes from the field scale simulations in Petroleum Engineering. With such incorporation of PVT into the lattice scheme the method becomes sensitive to what happens at temporal and spatial scales of sound waves in the fluid. The latter is not the case in reservoir simulations. At that types of problem typical time scales are significantly higher. With all that reasoning it is clear that an alternative way of modelling of PVT properties of fluid is highly desired. One of the solutions is discussed below.

4.2 LBM Model for Field-Scale Simulations

The outcome of previous sections is that there exist principal limitations of the method that result in the severe restriction on the time step. Therefore, an alternative approach for field-scale or REV-scale simulations is required. The fact that the only impact of PVT properties on the dynamics of the process is through the viscosity of the fluid, and forces that appear due to the gradient of the stress-tensor or pressure gradients. Therefore, if spatial derivatives of pressure can be computed effectively, then it is possible to design an alternative LBM model that can have more advanced properties in terms of numerical stability and accuracy. Finally, the central idea is to select lattice speed of sound independently from the PVT properties and introduce PVT-data into the scheme through the appropriate approximation of the gradients. In the present work the magnitude of the

lattice speed of sound is selected in accordance with the tradition in LBM:

$$c_s = \frac{1}{\sqrt{3}} \frac{\Delta X}{\Delta T}$$

Such choice corresponds to the value of λ in the middle of the stability range of the system. Values of lattice weights are in the agreement with the constraints (3.45). In other words, weights and lattice speed of sound are standard for D3Q27 model.

Summarizing the discussion above, the LBM scheme for field scale simulations can be derived from the classic LBM formulation with appropriate calculation of pressure gradients. The diffusion equation can be used for the purpose concerned. The mathematics behind the latter statement is explained in the next section.

4.2.1 Diffusion Equation in LBM

In the previous chapter the situation when the first several moments of discrete and continuous distribution coincide. In that case it is possible to derive Navier-Stokes equation from the LBM scheme. It is worth to investigate the scenario when the assumption about the equality of the moments does not hold. The example of such lattice system is shown below:

$$\begin{aligned} \frac{\partial g_i}{\partial t} + c_i^\alpha \frac{\partial g_i}{\partial x^\alpha} &= \Omega_i \\ \Omega_i &= \frac{w_i \psi(t,x) - g_i}{\tau_g} \end{aligned} \tag{4.18}$$

Here g_i is a certain distribution function. ψ is a given function of space and time. The expected behaviour of the lattice system concerned is the relaxation to $w_i\psi$. The characteristic scale of such process is the relaxation time. In this case the Chapman-Enskog expansion is still applicable. That technique gives the following expression for distribution functions:

$$g_i = w_i\psi - \tau\left(w_i \frac{\partial \psi}{\partial t} + w_i c_i^\alpha \frac{\partial \psi}{\partial x^\alpha}\right) + O(\tau^2) \tag{4.19}$$

Chapman-Expansion for the distribution functions leads to the expansion for the moments of the distribution concerned:

$$\sum_i g_i = \psi - \tau \frac{\partial \psi}{\partial t} + O(\tau^2) \tag{4.20}$$

$$\sum_i c_i^\alpha g_i = -\sum_i \tau w_i c_i^\alpha c_i^\beta \frac{\partial \psi}{\partial x^\beta} + O(\tau^2) = -\sum_i \tau c_s^2 \delta^{\alpha\beta} \frac{\partial \psi}{\partial x^\beta} + O(\tau^2) \tag{4.21}$$

The latter formula is of critical importance for the further work, because it relates the second moment of the distribution g_i with the gradient of ψ

$$\frac{\partial \psi}{\partial x^\beta} = -\frac{1}{\tau c_s^2} \delta_{\alpha\beta} \sum_i g_i c_i^\alpha + O(\tau) \tag{4.22}$$

The equation above tells that for small relaxation times the first moment of distribution function can be considered as a reasonably good approximation to the gradient of ψ.

One remark should be made. The equation (4.18) does not model the diffusion exactly as it can be concluded from Chapman-Enskog analysis. However, it can be shown that in the expansion concerned for the zero moment of g_i the principal term with spatial derivatives is proportional to Laplacian of ψ.

4.2.2 Temporal and Spatial Discretization

The numerical scheme for the discrete kinetic equation (4.18) can be developed in the same way as for (3.18). It has been mentioned earlier that the first moment of the distribution g_i approximates the gradient as long as the relaxation time is small enough. Therefore, the implicit scheme is of particular interest. That is the reason why only implicit

scheme is considered here:

$$g_i(t,x) - g_i(t-\Delta T, x - e_i \Delta X) = \frac{\Delta T\big(w_i \psi(t,x) - g_i(t,x)\big)}{\tau} \tag{4.23}$$

In this particular case, the equation (4.23) can be solved analytically, therefore there is no need in Newton-Rapson iterations or similar methods:

$$g_i(t,x) = \frac{\Delta T}{\Delta T + \tau} w_i \psi(t,x) + \frac{\tau}{\Delta T + \tau} g_i(t - \Delta T, x - e_i \Delta X) \tag{4.24}$$

The expression above can be applied recursively:

$$\begin{aligned} g_i(t,x) = \frac{\Delta T}{\Delta T + \tau} w_i \psi(t,x) + \frac{\tau \Delta T}{(\Delta T + \tau)^2} w_i \psi(t - \Delta T, x - e_i \Delta X) + \\ + \left(\frac{\tau}{\Delta T + \tau} \right)^2 g_i(t - 2\Delta T, x - 2\Delta X e_i) \end{aligned} \tag{4.25}$$

The first moment of distribution g_i can be computed directly:

$$\begin{aligned} \sum_i g_i c_i^\alpha = \sum_i c_i^\alpha \frac{\tau \Delta T}{(\Delta T + \tau)^2} w_i \psi(t - \Delta T, x - e_i \Delta X) + O(\tau^2) = \\ = -\sum_i \tau w_i c_i^\alpha c_i^\beta \frac{\Delta T^2}{(\Delta T + \tau)^2} \frac{\partial \psi}{\partial x^\beta} + O(\Delta T^2 + \tau^2) = -\tau c_s^2 \delta^{\alpha\beta} \frac{\partial \psi}{\partial x^\beta} + O(\Delta T^2 + \tau^2) \end{aligned} \tag{4.26}$$

The latter means that the expression (4.22) for the gradient of ψ in the case of discrete kinetic equation is valid up to second order terms in ΔT and first order terms in τ even for the spatial and temporal discretization. In other words gradients can be expressed through moments of distribution even in the discrete case.

4.2.3 Reservoir Simulation Model

In the previous section the flow of fluid in a void space has been discussed. In such situation the evolution of the system is completely determined by the fluid properties. The

case of the flow in porous media is different because of the obvious reasons. For the sake of simplicity it is better to introduce two notions of the density of the fluid: the physical density ρ_{phys} and "real" density ρ. ρ_{phys} is the quantity that appears in the equation of state for evaluation of pressure or viscosity of fluid:

$$P = P(\rho_{phys})$$

$$\mu = \mu(\rho_{phys})$$

The "real" or apparent density refers to the mass distribution of the fluid. In other words, the mass of the fluid in domain G is given by the following expression

$$M(G) = \int_G \rho dV \equiv \int_G \rho d^3x$$

It is clear that because of the definitions above both densities are related through the porosity ϕ:

$$\rho_{phys} = \phi\rho \tag{4.27}$$

One more remark regarding the terminology. In this work the actual velocity is used instead of the superficial one. With such notations for actual density and velocity the continuity equation has the same form as for the fluid without porous media:

$$\frac{\partial\rho}{\partial t} + \frac{\partial(\rho u^\alpha)}{\partial x^\alpha} = 0 \tag{4.28}$$

It has been shown by Coussy et al [69] that under certain assumptions the momentum conservation of fluid in the porous media can be described by Brinkman equation:

$$\frac{\partial(\rho u^\alpha)}{\partial t} + \frac{\partial(\rho u^\alpha u^\beta)}{\partial x^\beta} = -\delta^{\alpha\beta}\frac{\partial P}{\partial x^\beta} - \phi\mu(K^{-1})^\alpha_\beta u^\beta \tag{4.29}$$

Here K is a permeability tensor. Therefore, K^{-1} is its inverse. The term

$$-\phi\mu(K^{-1})^{\alpha}_{\beta}u^{\beta}$$

Is responsible for the viscous friction of fluid and solid matrix that forms porous rock. It is different from the classic expression for Darcy's friction because the actual velocity of the fluid is used instead of the superficial one.

In general, the gravity force should be included into (4.29), but it is not the focus of the present work. Despite the latter remark, one can see that the approach proposed in the present work can be naturally generalized to the system with gravity forces.

It has been mentioned that the lattice speed of sound for the field scale simulations is selected in accordance with temporal and spatial steps only. That means that dimensionless speed of sound is constant as well as weights of equilibrium distribution. The latter fact in couple with equation (3.38) gives a natural way of transformations from ordinary vector in Euclidian Space to lattice particle distributions. Namely, if the vector η is in R^3, then one can construct the following set of distribution functions:

$$\eta \to \frac{w_i}{c_s^2} c_i \cdot \eta = L_i(\eta) \tag{4.30}$$

The transformation L_i concerned has certain important properties that follow from (3.38):

$$\begin{gathered} \sum_i L_i\eta = \sum_i \left(\frac{w_i}{c_s^2} c_i \cdot \eta\right) = \eta^{\beta}\delta_{\alpha\beta}\sum_i \frac{w_i}{c_s^2} c_i^{\alpha} = 0 \\ \sum_i L_i(\eta)c_i^{\gamma} = \sum_i \left(\frac{w_i}{c_s^2} c_i \cdot \eta\right)c_i^{\gamma} = \eta^{\beta}\delta_{\alpha\beta}\sum_i \frac{w_i}{c_s^2} c_i^{\alpha}c_i^{\gamma} = \eta^{\beta}\delta_{\alpha\beta}\delta^{\alpha\gamma} = \eta^{\gamma} \end{gathered} \tag{4.31}$$

From the calculations above, it follows that the transformation (4.30) gives a lattice distribution or lattice vector that has zero moment of order zero, and that has the moment of

order one, which is equal to the initial vector in Euclidian space. The same thing can be done with the scalar function Q:

$$Q \to \frac{w_i}{c_s^2} Q = S_i(Q) \tag{4.32}$$

The similar calculation shows that for the transformation of the scalar $S_i(Q)$ the following equalities are valid:

$$\begin{aligned} Q &= \sum_i S_i(Q) = \sum_i w_i Q \\ 0 &= \sum_i S_i(Q) c_i^\alpha = \sum_i w_i c_i^\alpha Q \end{aligned} \tag{4.33}$$

The properties of scalar and vector transformations discussed above give a natural way for inclusion of forcing terms and sources in the DKE and LBM models:

$$\frac{\partial f_i}{\partial t} + c_i^\alpha \frac{\partial f_i}{\partial x^\alpha} = \frac{f_i^{eq} - f_i}{\tau} + L_i(\eta) + S_i(Q) \tag{4.34}$$

Equations (4.31) and (4.33) can be used in order to derive mass and momentum conservation laws from (4.34):

$$\begin{aligned} \frac{\partial \rho}{\partial t} + \frac{\partial (\rho u^\alpha)}{\partial x^\alpha} &= Q \\ \frac{\partial (\rho u^\alpha)}{\partial t} + \frac{\partial (\rho u^\alpha u^\beta)}{\partial x^\beta} + \frac{\partial (\Pi^{\alpha\beta})}{\partial x^\beta} &= \eta^\alpha \end{aligned} \tag{4.35}$$

From the Chapman-Enskog procedure, it follows that if lattice speed of sound is constant, then the stress tensor is simply:

$$\Pi^{\alpha\beta} = \rho c_s^2 \delta^{\alpha\beta} + O(\tau)$$

Finally, if the following condition holds:

$$\eta^{\alpha} = \delta^{\alpha\beta}\frac{\partial(\rho c_s^2 - P)}{\partial x^{\beta}}$$

then the LBM scheme represents the Brinkman equation up to the terms of order one in τ. The latter means that the following system of discrete kinetic equations describes the Brinkman equation up to $O(\tau)$:

$$\begin{aligned} \frac{\partial f_i}{\partial t} + c_i^{\alpha}\frac{\partial f_i}{\partial x^{\alpha}} &= \frac{f_i^{eq} - f_i}{\tau_f} + L_i\left(\frac{\sum_j g_j c_j}{\tau_g c_s^2}\right) + S_i(Q) \\ \frac{\partial g_i}{\partial t} + c_i^{\alpha}\frac{\partial g_i}{\partial x^{\alpha}} &= \frac{w_i(P - \rho c_s^2) - g_i}{\tau_g} \end{aligned} \tag{4.36}$$

Here τ_f and τ_g are relaxation times for distributions f_i and g_i respectively. The relaxation times concerned does not have to be equal. Moreover, as long as the desired accuracy is of zero order with respect to relaxation time, than τ_f and τ_g can be chosen to be arbitrary but sufficiently small numbers. For instance, the degree of freedom in magnitude of the relaxation time can be used for the control of the stability and convergence of the method. In the scheme concerned (4.34) Q represents source terms. In the case of reservoir simulation it is responsible for performance of the well. in this work Q is the function of the density in the cell and bottom-hole pressure:

$$Q = Q(P, P_{bh}) = Q(P(\rho_{phys}), P_{bh}) = Q(P(\rho/\phi), P_{bh})$$

4.2.4 Numerical Scheme

The arguments similar to the case of free moving fluid are applicable for the case of the system of discrete kinetic equations. It has been mentioned earlier that the implicit scheme is of particular interest. Therefore, only that scheme is considered in the details

here. It can be formulated in the same way as (3.48):

$$\begin{aligned} f_i(t,x) - f_i(t-\Delta T, x-\Delta X e_i) &= \Delta T \frac{f_i^{eq}(t,x) - f_i(t,x)}{\tau_f} + \\ &+ \Delta T S_i(Q(t,x)) + \Delta T L_i \left(\frac{\sum_j g_j(t,x) c_j}{\tau_g c_s^2} \right) \\ g_i(t,x) - g_i(t-\Delta T, x-\Delta X e_i) &= \Delta T \frac{w_i(P(t,x) - \rho(t,x)c_s^2) - g_i(t,x)}{\tau_g} \end{aligned} \tag{4.37}$$

The system of equations (4.37) consists of several non-linear equations coupled with each other, however, it can be solved even analytically if there is no source term. Otherwise, the only equation that should be solver numerically is one-dimensional equation for density or for mass conservation. The algorithm of the solution is described below.

The first step is solving equations for the density based on the equation for the f_i. Namely, one can compute the moment of order zero of both parts of the (4.37):

$$\rho(t,x) - \sum_i f_i(t-\Delta T, x-\Delta X e_i) = Q(t,x)$$

As long as the source term is the function of the pressure and the density of the fluid and the bottom-hole pressure, one can obtain the following equation for the density:

$$\rho(t,x) - Q(P(\rho(t,x)/\phi(t,x)), P_{bh}) = \sum_i f_i(t-\Delta T, x-\Delta X e_i) \tag{4.38}$$

The second step is computation of the pressure using EOS for the fluid. That means that all of the quantities $P, c_s^2\rho, \rho$, become known for each of the cell at new time step. It is simple to see that for known pressures and densities the equation for g-distribution in (4.37) becomes a simple linear equation and can be easily solved:

$$g_i(t,x) = \frac{\Delta T}{\Delta T + \tau_g} w_i(P(t,x) - c_s^2\rho(t,x)) + \frac{\tau_g}{\Delta T + \tau_g} g_i(t-\Delta T, x-\Delta X e_i) \tag{4.39}$$

The latter means that it is possible to solve for the components of the distribution g_i. That means that gradients of the combination $P - c_s^2\rho$ can be computed based on the expression through the first moments, in other words, the vector η is simply:

$$\eta = \frac{1}{\tau_g c_s^2} \sum_j g_j(t,x) c_j$$

Finally, it is possible to come back to the equation for f-distribution functions and determine the first momentum of equilibrium distribution function or mean velocity:

$$\sum_i f_i(t,x) c_i^\alpha - \sum_i f_i(t - \Delta T, x - \Delta X e_i) c_i^\alpha = \eta^\alpha$$

As long as η is known and first moments of both distributions f_i and f_i^{eq} are the same by the definition, then the value of each of the coordinates of the first moment can be determined. With the knowledge of the density and the mean velocity, $F_i eq$ can be computed. Therefore, the situation is almost the same as with g-distribution functions:

$$f_i(t,x) = \frac{\Delta T}{\Delta T + \tau_f} f_i^{eq}(t,x) + \frac{\tau_f}{\Delta T + \tau_f} \Big(f_i(t - \Delta T, x - \Delta X e_i) + S_i(Q(t,x)) + L_i(\eta) \Big) \tag{4.40}$$

The important fact regarding that algorithm is that its performance is comparable with the performance of the explicit scheme. Indeed, there are no matrix-vector multiplications and all calculations are local, in other words, the efficiency for parallel computing of both schemes should be comparable. One of the major motivations for the development of such implicit scheme is that the limit of zero relaxation times is of particular interest for the field-scale simulations. It is easy to see that the algorithm above is stable as long as $\tau_f \geq 0$ and $\tau_g \geq 0$.

Together with the stability with respect to the relaxation time, the implicit scheme

has one more important feature: the numerical solution allows higher density or pressure contrasts if compared with the traditional explicit LBM scheme.

4.2.5 Grid Geometry for Field-Scale Simulations

In the previous section the numerical LBM scheme for field scale simulations has been presented. The algorithm concerned can be applied to simulations of realistic models, however only uniform cubic grid has been considered. The latter is not practical, because a typical reservoir has a typical contrast in vertical and horizontal scales. Therefore, non-cubic geometry of the mesh is of important for applications. One of the ways to introduce more involved grid geometry into LBM has been discussed in the previous section. However, one of the disadvantages of the approach concerned is the difficulty of solution for the equation for the equilibrium distribution functions (3.14). In this case an alternative solution can be found. Instead of deforming the mesh, one can "deform" the equation. Formally, this means the introduction of another coordinate system, called the reference one. That coordinates might be non-linear, but the computational mesh should be uniform and cubic in that coordinates. In other words, the idea is to solve the equations in the reference coordinate system instead of the original or the natural one. In the present section specific notations are introduced. The apparent density of the fluid, the value of the a-th coordinate and the value of the component b of the velocity vector are denoted as r, x^a, u^brespectively. The same quantities can be introduced for the reference system: ρ, ξ^α and υ^β. The following notations are used for the transformation from natural coordinates to reference and for the inverse map:

$$x^a = x^a(\xi)$$

$$\xi^\alpha = \xi^\alpha(x)$$

The Jacobi matrices of direct and inverse maps are simply:

$$\frac{\partial x^a}{\partial \xi^\alpha}, \frac{\partial \xi^\alpha}{\partial x^a}$$

The rule for the transformation of the velocity vectors is well-known form the calculus:

$$u^a = \frac{\partial x^a}{\partial \xi^\alpha} \upsilon^\alpha \tag{4.41}$$

The rule for the transformation of densities can be derived from simple change of variables:

$$\int_G r d^3x = \int_\Omega r \, det\left(\frac{\partial x}{\partial \xi}\right) d^3\xi = \int_\Omega \rho d^3\xi$$

Therefore:

$$r = det\left(\frac{\partial \xi}{\partial x}\right)\rho \tag{4.42}$$

With the notations introduced, it is possible to study the properties of mass and momentum conservation equations under the transformation of coordinates:

$$\begin{gathered} \frac{\partial r}{\partial t} + \frac{\partial (r u^\alpha)}{\partial x^\alpha} = 0 \\ \frac{\partial (r u^\alpha)}{\partial t} + \frac{\partial (r u^\alpha u^\beta)}{\partial x^\beta} = -\delta^{\alpha\beta}\frac{\partial P}{\partial x^\beta} + r G^\alpha \end{gathered} \tag{4.43}$$

From the technical point of view it is easier to start with the transformation of the mass conservation equation using rules of the transformation of densities and velocities (4.41) - (4.42):

$$\begin{gathered} \frac{\partial}{\partial t}\left(\rho \; det\left(\frac{\partial \xi}{\partial x}\right)\right) + \frac{\partial \xi^\alpha}{\partial x^a}\frac{\partial}{\partial \xi^\alpha}\left(\rho \; det\left(\frac{\partial \xi}{\partial x}\right)\upsilon^\beta \frac{\partial x^a}{\partial \xi^\beta}\right) = \\ = \left(\frac{\partial \rho}{\partial t} + \frac{\partial (\rho \upsilon^\alpha)}{\partial \xi^\alpha}\right) \; det\left(\frac{\partial \xi}{\partial x}\right) + \rho \upsilon^\beta \frac{\partial \xi^\alpha}{\partial x^a}\frac{\partial}{\partial \xi^\alpha}\left(\; det\left(\frac{\partial \xi}{\partial x}\right)\frac{\partial x^a}{\partial \xi^\beta}\right) \end{gathered} \tag{4.44}$$

Direct calculation of the derivatives of the determinant shows that the last term in the equation (4.44) vanishes. Therefore, one can end up with the following equation:

$$Q = \frac{\partial r}{\partial t} + \frac{\partial (r u^a)}{\partial x^a} = \left(\frac{\partial \rho}{\partial t} + \frac{\partial (\rho \upsilon^\alpha)}{\partial \xi^\alpha} \right) det \left(\frac{\partial \xi}{\partial x} \right)$$

Here Q represents the sources. Finally, the equation for mass conservation preserves its form even in the reference coordinate system:

$$\frac{\partial \rho}{\partial t} + \frac{\partial (\rho \upsilon^\alpha)}{\partial \xi^\alpha} = Q \; det \left(\frac{\partial x}{\partial \xi} \right) \tag{4.45}$$

The similar arguments can be applied to the momentum conservation equation. Calculations are more involved in this case, and the form of final equation differs from the initial one. It is better to consider each of the terms separately:

$$\frac{\partial (r u^a)}{\partial t} = \frac{\partial}{\partial t} \left(\rho \upsilon^\alpha \; det \left(\frac{\partial \xi}{\partial x} \right) \frac{\partial x^a}{\partial \xi^\alpha} \right) = \frac{\partial (\rho \upsilon^\alpha)}{\partial t} \; det \left(\frac{\partial \xi}{\partial x} \right) \frac{\partial x^a}{\partial \xi^\alpha} \tag{4.46}$$

The similar expression can be derived for the convection term:

$$\begin{gathered}
\frac{\partial (r u^a u^b)}{\partial x^b} = \frac{\partial \xi^\gamma}{\partial x^b} \frac{\partial}{\partial \xi^\gamma} \left(\rho \upsilon^\alpha \upsilon^\beta \frac{\partial x^a}{\partial \xi^\alpha} \frac{\partial x^b}{\partial \xi^\beta} \; det \left(\frac{\partial \xi}{\partial x} \right) \right) = \\
= \frac{\partial (\rho \upsilon^\alpha \upsilon^\beta)}{\partial \xi^\beta} \frac{\partial x^a}{\partial \xi^\alpha} det \left(\frac{\partial \xi}{\partial x} \right) + \rho \upsilon^\alpha \upsilon^\beta \frac{\partial x^a}{\partial \xi^\alpha} \frac{\partial \xi^\gamma}{\partial x^b} \frac{\partial}{\partial \xi^\gamma} \left(\frac{\partial x^b}{\partial \xi^\beta} \; det \left(\frac{\partial \xi}{\partial x} \right) \right) + \\
+ \rho \upsilon^\alpha \upsilon^\beta \frac{\partial \xi^\gamma}{\partial x^b} \frac{\partial x^b}{\partial \xi^\beta} \; det \left(\frac{\partial \xi}{\partial x} \right) \frac{\partial^2 x^a}{\partial \xi^\alpha \partial \xi^\gamma} = \\
= \frac{\partial x^a}{\partial \xi^\alpha} det \left(\frac{\partial \xi}{\partial x} \right) \left(\frac{\partial (\rho \upsilon^\alpha \upsilon^\beta)}{\partial \xi^\beta} + \rho \upsilon^\beta \upsilon^\gamma \frac{\partial \xi^\alpha}{\partial x^b} \frac{\partial^2 x^b}{\partial \xi^\beta \partial \xi^\gamma} \right) = \\
= \frac{\partial x^a}{\partial \xi^\alpha} det \left(\frac{\partial \xi}{\partial x} \right) \left(\frac{\partial (\rho \upsilon^\alpha \upsilon^\beta)}{\partial \xi^\beta} + \rho \Gamma^\alpha_{\beta\gamma} \upsilon^\beta \upsilon^\gamma \right)
\end{gathered} \tag{4.47}$$

Here $\Gamma^\alpha_{\beta\gamma}$ is a Christoffel symbol. Using (4.46), (4.47) and (4.43), one can derive the mass

and momentum conservation equations in the reference coordinate system:

$$\begin{aligned} \frac{\partial \rho}{\partial t} + \frac{\partial (\rho \upsilon^{\alpha})}{\partial \xi^{\alpha}} &= Q \; det\left(\frac{\partial x}{\partial \xi}\right) \\ \frac{\partial (\rho \upsilon^{\alpha})}{\partial t} + \frac{\partial (\rho \upsilon^{\alpha} \upsilon^{\beta})}{\partial \xi^{\beta}} + \rho \Gamma^{\alpha}_{\beta\gamma} \upsilon^{\beta} \upsilon^{\gamma} &= -det\left(\frac{\partial x}{\partial \xi}\right) \Theta^{\alpha\beta} \frac{\partial P}{\partial \xi^{\beta}} + \rho \frac{\partial \xi^{\alpha}}{\partial x^{a}} G^{a} \end{aligned} \tag{4.48}$$

Here $\Theta^{\alpha\beta}$ is a metric tensor. It is defined as follows:

$$\Theta^{\alpha\beta} = \frac{\partial \xi^{\alpha}}{\partial x^{a}} \frac{\partial \xi^{\beta}}{\partial x^{b}} \delta^{ab} \tag{4.49}$$

It is easy to see that mass conservation equation has not changed at all. There are two changes in the form of momentum conservation. The first one is the presence of curvature of the coordinate transformation through the extra forcing term: $\rho \Gamma^{\alpha}_{\beta\gamma} \upsilon^{\beta} \upsilon^{\gamma}$. The second change is the factor in front of the gradient term. Acceleration field G^{a} has changed as well, but it follows the rule of transformation for vectors. In the case of flow in porous media, the acceleration or forcing field is simply:

$$rG^{a} = -\phi \mu (K^{-1})^{a}_{b} u^{b}$$

The forcing term in the reference coordinate system is given by the following expression:

$$\rho \frac{\partial \xi^{\alpha}}{\partial x^{a}} G^{a} = -det\left(\frac{\partial x}{\partial \xi}\right) \phi \mu \frac{\partial \xi^{\alpha}}{\partial x^{a}} (K^{-1})^{a}_{b} \frac{\partial x^{b}}{\partial \xi^{\beta}} \upsilon^{\beta}$$

It is easy to see that the latter is equivalent to the replacement of permeability tensor:

$$K^{b}_{a} \rightarrow \frac{\partial \xi^{\beta}}{\partial x^{b}} \frac{\partial x^{a}}{\partial \xi^{\alpha}} K^{b}_{a} = \kappa^{\beta}_{\alpha}$$

Finally, for the flow in the porous media one can get the equation for momentum conser-

vation:

$$\frac{\partial(\rho\upsilon^{\alpha})}{\partial t}+\frac{\partial(\rho\upsilon^{\alpha}\upsilon^{\beta})}{\partial\xi^{\beta}}+\rho\Gamma^{\alpha}_{\beta\gamma}\upsilon^{\beta}\upsilon^{\gamma}=-det\left(\frac{\partial x}{\partial\xi}\right)\left(\Theta^{\alpha\beta}\frac{\partial P}{\partial\xi^{\beta}}+\phi\mu(\kappa^{-1})^{\alpha}_{\beta}\upsilon^{\beta}\right) \tag{4.50}$$

The transformation of time can be considered as well. Basically, the dimensionless time θ can be introduced in the following way:

$$t=\Delta T\theta \tag{4.51}$$

The transformation of time impacts the velocity in the following way:

$$\hat{v}=v/\Delta T \tag{4.52}$$

Here $\hat{v}$ is a dimensionless velocity. With such notations the equation (4.50) is transformed as follows:

$$\begin{aligned}\frac{\partial(\rho\hat{\upsilon}^{\alpha})}{\partial\theta}+\frac{\partial(\rho\hat{\upsilon}^{\alpha}\hat{\upsilon}^{\beta})}{\partial\xi^{\beta}}+\rho\Gamma^{\alpha}_{\beta\gamma}\hat{\upsilon}^{\beta}\hat{\upsilon}^{\gamma}=-\Delta T^{2}det\left(\frac{\partial x}{\partial\xi}\right)\Theta^{\alpha\beta}\frac{\partial P}{\partial\xi^{\beta}}+\\ +\Delta T\,det\left(\frac{\partial x}{\partial\xi}\right)\phi\mu(\kappa^{-1})^{\alpha}_{\beta}\hat{\upsilon}^{\beta}\end{aligned} \tag{4.53}$$

It is easy to see that the numerical scheme for LBM (4.37) can be applied for reservoir simulations at the field scale almost without any changes. The only modification is that the gradient computed through the moments of g distribution functions should be multiplied by the metric tensor.

4.2.6 Numerical Diffusion

Classic LBM schemes has demonstrated a reasonable agreement with analytical tools in the simulation of steady-state flow [71]. Simple simple calculations can show that the novel LBM model is applicable for such types of simulations as well. Despite this

advantage of the method, there exist a significant numerical error in the simulation of transient processes. Namely, the numerical diffusion of the scheme is too high leading to overestimate of the speed of propagation of the fluid. The latter can be shown with the one dimensional example problem. One can consider a 1D reservoir of length L, with permeability k, and porosity ϕ. The viscosity of the fluid is supposed to be constant and equal to μ. For the purposes of simplicity, an ideal gas can be considered. The EOS of the fluid is:

$$P = \frac{\rho_p RT}{M} \tag{4.54}$$

Here P is the pressure, ρ_p is a real of physical density of the fluid, T is the temperature, M is the molar mass. In terms of the notations introduced at the beginning of the present chapter the EOS can be written in the form:

$$P = \frac{\rho RT}{M\phi} \tag{4.55}$$

The evolution of the system is determine by the combination of mass conservation equation and Darcy Law:

$$\frac{\partial \rho}{\partial t} = \frac{\partial}{\partial x_\alpha}\left(\frac{\rho k}{\phi \mu}\frac{\partial P}{\partial x^\alpha}\right) \tag{4.56}$$

That expression be transformed to the following:

$$\frac{\partial \rho}{\partial t} = \frac{\partial}{\partial x_\alpha}\left(\frac{\rho k}{\phi^2 \mu}\frac{RT}{M}\frac{\partial \rho}{\partial x^\alpha}\right) \tag{4.57}$$

The equation (4.57) is non linear. However, it can be linearised if the deviation of the density is small if compared with the mean value. The latter means that terms with derivatives of the density that have an order higher then two are negligible:

$$\frac{\partial \rho}{\partial t} = \frac{\rho k}{\phi^2 \mu} \frac{RT}{M} \Delta \rho \tag{4.58}$$

This equation is a well-known heat-conductivity equation. In the case of one dimension, the expression (4.58) is simply:

$$\frac{\partial \rho}{\partial t} = \frac{\rho k}{\phi^2 \mu} \frac{RT}{M} \frac{\partial^2 \rho}{\partial x^2} \tag{4.59}$$

If the initial condition is:

$$\rho = \rho_0 + \Delta \rho_0 cos\left(\frac{2\pi x}{L}\right) \tag{4.60}$$

then the solution for (4.59) has the following form:

$$\rho = \rho_0 + \Delta \rho_0 e^{-\lambda t} cos\left(\frac{2\pi x}{L}\right) \tag{4.61}$$

The physical meaning of the solution concerned is that the small harmonic perturbation of the initial distribution of density decays exponentially with time. Moreover, the harmonic shape of the perturbation is preserved and only the amplitude of the perturbation changes. The latter observation is extremely useful for the analysis of the conversion of the method.

The direct substitution of (4.61) into (4.59) gives the following expression for λ:

$$\lambda = \frac{4\pi^2 \rho_0 k}{\mu \phi^2 L^2} \frac{RT}{M} \tag{4.62}$$

Finally, equations (4.57) - (4.62) allow one to compare the LBM scheme with analytical solution. In the present work the following values of the parameters have been used:

It can be seen easily from (4.61) that the perturbation decreases by the factor e^{-1} after the period of time of duration $1/\lambda$. The plots of the perturbation at the moment $1/\lambda$ are shown below. The numerical solution is computed for the several values of time steps ΔN

L, m	k, D	ϕ	ρ_0, kg/m^3	μ, cP	T, K	M, kg/mol
2000	1	0.01	1	0.01	350	0.016

Table 4.1: Values of the parameters used in simulations.

in such a way that the final moment of time for all simulations is the same:

$$\frac{1}{\lambda} = \Delta N \Delta T \tag{4.63}$$

The number of time steps for each simulation is summarized in the table below: It can

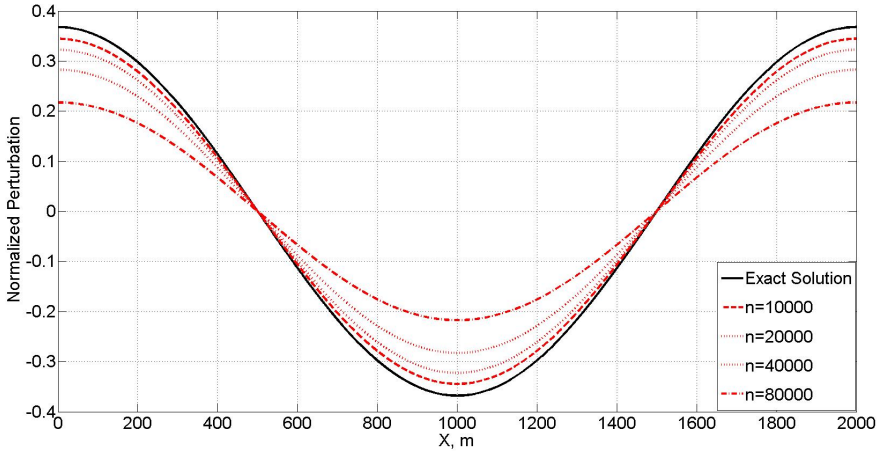

Figure 4.2: This figure illustrates the effect of numerical diffusion on numerical results. Analytical solution is compared with numerical simulations for the same moment of time but for the different number of time stes

Number of simulation	1	2	3	4
Number of time steps	10000	20000	40000	80000

Table 4.2: Total number of time steps in simulations.

be seen from the Figure (4.2) that the rate of the decay of the perturbation for numerical solution is significantly higher then for the analytical one. The latter effect is the evidence of high numerical diffusion of the scheme. The numerical error can be estimated via Chapman-Enskog Expansion. For that purpose the term $f_i(t,x) - f_i(t-\Delta T, x - e_i \Delta X)$ in the equation (4.37) can be approximated as a polynomial function through the Taylor expansion:

$$\begin{gathered} f_i(t,x) - f)i(t-\Delta T, x - e_i\Delta X) = \Delta T \frac{\partial f_i}{\partial t} + \Delta T c_i^\alpha \frac{\partial f_i}{\partial x^\alpha} - \\ -\frac{\Delta T^2}{2}\left(\frac{\partial^2 f_i}{\partial t^2} + 2c_i^\alpha \frac{\partial^2 f_i}{\partial t \partial x^\alpha} + c_i^\alpha c_i^\beta \frac{\partial^2 f_i}{\partial x^\alpha \partial x^\beta}\right) + O(\Delta T^3) \end{gathered} \tag{4.64}$$

With such expression, the equation (4.37) can be transformed as follows:

$$\begin{gathered} \frac{\partial f_i}{\partial t} + c_i^\alpha \frac{\partial f_i}{\partial x^\alpha} - \frac{\Delta T}{2}\left(\frac{\partial^2 f_i}{\partial t^2} + 2c_i^\alpha \frac{\partial^2 f_i}{\partial t \partial x^\alpha} + c_i^\alpha c_i^\beta \frac{\partial^2 f_i}{\partial x^\alpha \partial x^\beta}\right) + O(\Delta T^2) = \\ = \Omega_i(t,x) + F_i(t,x) \end{gathered} \tag{4.65}$$

The summation over the set of lattice velocities of both sides of (4.65) gives the following equation:

$$\frac{\partial \rho}{\partial t} + \frac{\partial(\rho u^\alpha)}{\partial x^\alpha} - \frac{\Delta T}{2}\left(\frac{\partial^2 \rho}{\partial t^2} + 2\frac{\partial^2(\rho u^\alpha)}{\partial t \partial x^\alpha} + \frac{\partial^2(\rho c_s^2 \delta^{\alpha\beta} + \rho u^\alpha u^\beta)}{\partial x^\alpha \partial x^\beta}\right) = O(\Delta T^2) \tag{4.66}$$

One of the outcomes of the expression (4.66) is that material balance in its canonical form is satisfied up to the terms of order one with respect to the time step ΔT. More precisely, in the numerical scheme, the mass is conserved up to the round-off errors. The error occurs in closing relation. In other words, the deviation from the Darcy law is of order one with respect to the ΔT. The latter observation can be applied to (4.66). First of all, the terms

with second order derivatives can be grouped as follows:

$$\frac{\partial \rho}{\partial t}+\frac{\partial(\rho u^{\alpha})}{\partial x^{\alpha}}-\frac{\Delta T}{2}\left(\frac{\partial}{\partial t}\left(\frac{\partial \rho}{\partial t}+\frac{\partial(\rho u^{\alpha})}{\partial x^{\alpha}}\right)+\frac{\partial^2(\rho u^{\alpha})}{\partial t \partial x^{\alpha}}+\frac{\partial^2(\rho c_s^2 \delta^{\alpha\beta}+\rho u^{\alpha}u^{\beta})}{\partial x^{\alpha}\partial x^{\beta}}\right)=O(\Delta T^2) \tag{4.67}$$

Here $c_s = 1/sqrt(3)\Delta X/\Delta T$ is the lattice speed of sound. From the discussion above it follows that mass conservation equation is satisfied up to the terms of order one with respect to ΔT. The latter means that the term is of the second order with respect to the temporal step:

$$\frac{\Delta T}{2}\left(\frac{\partial \rho}{\partial t}+\frac{\partial(\rho u^{\alpha})}{\partial x^{\alpha}}\right)=O(\Delta T^2) \tag{4.68}$$

Equation (4.68) tells that the combination of terms with second order derivatives discussed above can be neglected.

Equation (4.66) allows further simplification that can be derived form the physics of the process. Typically, the acceleration of the fluid in the case of flow in porous media is negligible [69]. The mathematical interpretation of the latter statement is that time derivatives of the velocity of the fluid and together with the absolute value of the velocity is negligible. With the reasoning above, the equation (4.66) can be transformed as follows:

$$\frac{\partial \rho}{\partial t}+\frac{\partial(\rho u^{\alpha})}{\partial x^{\alpha}}+\frac{\Delta}{2}c_s^2\nabla^2\rho=O(\Delta T^2) \tag{4.69}$$

In the case of the flow in porous media the velocity of the fluid is related to the pressure or density gradient through the Darcy Law:

$$rhou=-\frac{\rho k}{\phi\mu}\nabla P=-\frac{\rho k}{\phi^2\mu}\frac{\partial P}{\partial \rho_p}\nabla\rho \tag{4.70}$$

The last equality in the formula above holds only if the reservoir is uniform. Finally, if square of the gradient of the density is negligible, then the numerical scheme approximates

the solution to the following equation:

$$\frac{\partial \rho}{\partial t} = \left(\frac{\rho k}{\phi^2 \mu} \frac{\partial P}{\partial \rho_p} + \frac{1}{6} \frac{\Delta X^2}{\Delta T} \right) \nabla^2 \rho + O(\Delta T^2) \tag{4.71}$$

The equation (4.71) is important for understanding of the performance of the LBM. It imposes controversial restrictions on the time step. One hand, the small time step results in a small magnitude of the dimensionless velocity of the fluid. Therefore, all the components of the equilibrium distribution functions are positive. That means that the numerical solution is far away from oscillations because of the major source of numerical instability. On the other hand, small time step results in a high value of numerical diffusion, because the numerical error occurs because of the term:

$$\frac{1}{6} \frac{\Delta X^2}{\Delta T} \nabla^2 \rho \tag{4.72}$$

In other words, the situation is similar to what have been observed in the previous section with the self-consistent LBM model. It is easy to see that the numerical effect concerned can be fixed if the predictor-corrector LBM scheme is considered at least in the case when the assumptions regarding the magnitude of the velocity and gradient of the pressure are valid. However, the reason for the numerical diffusion is fundamental for LBM and it is caused by the nature of the streaming step in LBM. For example, if the distribution is close to equilibrium and the velocity of the fluid is small, then each of the distribution functions f_i is approximately equal to $w_i \rho$. The latter means tha during each time step, only a small part of the overall mass of the system remains at rest. Obviously, the mass fraction of the part concerned is w_0. The remaining particles participate in mass exchange. The fraction of the overall mass that participates in mass exchange concerned does not depend on the magnitude of the time step. Therefore, the mass exchange between the cells

can be significant even if the time step is small.

The important conclusion from the discussion above is the presence of significant difficulties of application of LBM to field-scale problems with multiphase flow. For instance, it is easy to see that because of the numerical diffusion the distribution of phases in the pores space can appear even if pressure gradient is zero everywhere. The latter reasoning indicate the need for the alternative formulation of LBM scheme for field scale simulations. The novel LBM scheme is the subject of the discussion of the next chapter.

5. NOVEL LBM SCHEME FOR FIELD SCALE SIMULATIONS

In the previous chapter the LBM pseudo-potential model for field-scale simulations has been described. It has been shown that the numerical diffusion introduces a significant numerical error. It has been indicated that the main reason for such phenomenon is the form of the equilibrium distribution. Namely, the fraction of the particles that are streamed to the neighbouring nodes does not depend on the magnitude of the time step. Moreover, that fraction of the particles is calculated from local quantities. In other words, the total flux of the particles leaving the given node has no information regarding gradients. This causes problems for field-scale simulations, where the pressure gradient is the main driving force. The reasoning above indicates the need for fundamental revisions of the formulation of LBM models.

In the present chapter an alternative formulation of the LBM scheme is presented. The novelty of the model is in the expression for the equilibrium distribution functions. Those functions are designed in such a way that only two moments of the distribution coincide with the moments of the Maxwell distribution. The immediate consequence of such formulations is that the LBM scheme can be applied only to field-scale simulations but not to the numerical solving for the Navier-Stokes equations. However, the novel approach does not suffer from numerical diffusion if compared with the pseudo-potential scheme discussed previously.

5.1 Derivation of the Expression for Equilibrium Distribution Functions

The flow in porous media is governed by the Darcy law, that states that the velocity of the fluid is a linear function of the pressure gradient. That means that zero pressure gradient results in the absence of any movement of the fluid. Such relation between the pressure gradient and the velocity of the fluid motivates to design equilibrium distribution

functions with similar properties. In other words, components of the equilibrium distribution that correspond to the particles with non-zero speed should be linear with respect to pressure gradient and should vanish together with the pressure gradient.

It is important to notice that this formulation leads to the deviations of the second order moments of the distribution from the Maxwell distribution. Namely, if pressure gradient and velocity are both equal to zero, then the second moment of the distribution is zero:

$$\sum_i f_i^{eq} c_i^\alpha c_i^\beta = f_0^{eq} c_0^\alpha c_0^\beta = 0 \tag{5.1}$$

The other important observation that narrows the set of options for equilibrium distribution functions comes from the numerical stability. It has been mentioned previously that equilibrium distribution functions should be positive for the stability of the LBM scheme. Therefore, the expression for equilibrium distribution functions can not be a simple linear function because it changes the sign with change of the sign of the mean velocity. Therefore, linearity and positivity seems to be controversial requirements. However, this can be resolved if only convex combination of vectors are considered. To this end, if the density and the moment or mean velocity are given, then the idea is to select the triplet of lattice velocity vectors c_{i_1}, c_{i_2}, c_{i_3} in such a way that:

$$\rho u^\alpha = f_{i_1} c_{i_1}^\alpha + f_{i_2} c_{i_2}^\alpha + f_{i_3} c_{i_3}^\alpha \tag{5.2}$$

All other equilibrium distribution functions are considered to be zero. The only exception is the component that corresponds to the particles with zero velocity. It is defined in the accordance with the given density of the fluid at the point concerned:

$$f_0 = \rho - f_{i_1} - f_{i_2} - f_{i_3} \tag{5.3}$$

It is clear that for D3Q27 model it is always possible to find the triplet of lattice velocities such that all the coefficients in the decomposition (5.2) are non-negative. The only issue is that the triplet may not be unique. Therefore, the algorithm for the generation of the triplet is required. Therefore, only specific triplets of lattice vector are considered in the present work, we refer them as natural. The triplet $(e_{i_1}, e_{i_2}, e_{i_3})$ is called natural if two conditions are satisfied. The first condition is on the magnitude of the vectors:

$$\begin{aligned} |e_{i_1}| &= 1 \\ |e_{i_2}| &= 2 \\ |e_{i_3}| &= 3 \end{aligned} \tag{5.4}$$

The second condition is related to the coordinates of the vectors. The first vector of the natural triplet is e_{i_1} and it is a face vector. Therefore, only one coordinate of the vector concerned is non-zero. In this case we denote the coordinate as α_1. The second vector of the natural triplet is e_{i_2}. It is an edge vector. Therefore, exactly two coordinates of the vector are non-zero. One of them is forced to be α_1. In other words, α_1 and α_2 are two different coordinates of vector e_{i_2} that are different from zero. The similar construction is applied to the third vector e_{i_3}. As before, this vector has three non-zero coordinates. Two of them forced to be α_1 and α_2. The remaining non-zero coordinate is α_3. Finally the constrained can be formulated as the existence of three distinct coordinate indexes α_1, α_2, and α_3 such that:

$$\begin{aligned} e_{i_1}^{\alpha_1} = e_{i_2}^{\alpha_1} = e_{i_3}^{\alpha_1} \\ e_{i_2}^{\alpha_2} = e_{i_3}^{\alpha_2} \end{aligned} \tag{5.5}$$

There is a convenient way to think about the way of construction of natural triplet. One can start with the face vector e_{i_1}. This vector has one non-zero coordinate and two zero coordinates. The vector e_{i_2} is derived from e_{i_1} by the replacement of one of the zero

coordinates of e_{i_1} by the -1 or $+1$. e_{i_3} is constructed in the similar way: the remaining non-zero coordinate of e_{i_2} is replaced by the -1 or $+1$. Therefore, for every natural triplet the sequence α_1, α_2, α_3 of three different ordered numbers can be constructed. It is simple to show, that the inverse statement is valid as well: for each ordered set of three different numbers the natural triplet can be constructed. In other words, there is a one-to-one correspondence between natural triplets and ordered combinations of coordinate indexes.

In the novel LBM model described here, the equilibrium distribution functions are expressed through the density ρ and mean velocity u. The density is simply a way of normalization of the equilibrium distribution (3.10). The mean velocity is treated in more complicated way.

The first step of the evaluation of the equilibrium distribution function is the construction of the natural triplet. From the discussion above it follows that it is sufficient to generate the sequence of coordinate indexes. In the present work that sequence is constructed in such a way that for the given mean velocity the following is valid:

$$|u^{\alpha_1}| \geq |u^{\alpha_2}| \geq |u^{\alpha_3}| \tag{5.6}$$

The second step is to determine values of distribution functions. From the construction of the natural triplet of lattice vector velocities, one can derive the following system of equations:

$$\begin{aligned} \rho\frac{\Delta T}{\Delta X}|u^{\alpha_1}| &= f_{i_1}^{eq} + f_{i_2}^{eq} + f_{i_3}^{eq} \\ \rho\frac{\Delta T}{\Delta X}|u^{\alpha_2}| &= f_{i_2}^{eq} + f_{i_3}^{eq} \\ \rho\frac{\Delta T}{\Delta X}|u^{\alpha_3}| &= f_{i_3}^{eq} \end{aligned} \tag{5.7}$$

The solution for the system (5.7) is given by the expressions below:

$$\begin{aligned} f_{i_1}^{eq} &= \rho \frac{\Delta T}{\Delta X} \left(|u^{\alpha_1}| - |u^{\alpha_2}| \right) \\ f_{i_2}^{eq} &= \rho \frac{\Delta T}{\Delta X} \left(|u^{\alpha_2}| - |u^{\alpha_3}| \right) \\ f_{i_3}^{eq} &= \rho \frac{\Delta T}{\Delta X} |u^{\alpha_3}| \end{aligned} \tag{5.8}$$

We can see that the components of the equilibrium distribution functions are non-negative because of (5.6). The zero-velocity component of the distribution is calculated from (5.3). Therefore, equations (5.3) and (5.8) completely define the equilibrium distribution. Moreover, density and mean velocity obtained through the averaging procedure are the same as the input values ρ and u.

5.2 Numerical Scheme

In the previous section an algorithm of the calculation of equilibrium distribution has been proposed. The input for the algorithm is density and mean velocity of the fluid:

$$f_i^{eq} = f_i^{eq}(\rho, u) \tag{5.9}$$

In the case of the flow in porous media that velocity is determined by the Darcy Law:

$$u = -\frac{k}{\mu\phi} \nabla P$$

The velocity can be substituted into the expression for the equilibrium distribution function (5.9), as:

$$f_i^{eq} = f_i^{eq} \left(\rho, -\frac{k}{\mu\phi} \nabla P \right) \tag{5.10}$$

Therefore, in the case of the flow in the porous media, the equilibrium distribution function

is determined by the density of the fluid and by the pressure gradient. We can see from (5.8) that zero value of the pressure gradient results in the absence of the motion of the fluid. Therefore, such approach for the calculation of the equilibrium distribution functions is reasonable from the physical point of view.

The moments of the equilibrium distribution are given by the expressions:

$$\begin{aligned} \rho &= \sum_i f_i^{eq} \\ \rho u^\alpha &= \sum_i f_i^{eq} c_i^\alpha = -\frac{\rho k}{\mu\phi}\nabla P \end{aligned} \tag{5.11}$$

In this case, as long as (5.11) holds, the standard Chapman-Enskog expansion shows that the DKE or LBM model developed recovers the standard mass conservation law:

$$\frac{\partial \rho}{\partial t} = \nabla\left(\frac{\rho k}{\mu\phi}\nabla P\right) \tag{5.12}$$

It readily follows that the DKE model approximates the behaviour of the desired macroscopic system. Therefore, the only missing step for the development of the numerical LBM scheme is spatial and temporal discretization. Approximation of the derivatives of the distribution functions is the same as in schemes (3.49) or (3.50). The difference from the previous schemes is that the pressure gradient should be computed numerically. The latter can be done in a natural way with the standard weights w_i for D3Q27 model [51] based on the values of pressure at neighbouring nodes $P(x+e_i\Delta X)$. Namely, the standard Taylor expansion together with (3.38) gives the following expression:

$$\begin{aligned} &\sum_i w_i P(x+e_i\Delta X)e_i^\alpha = \\ &= \sum_i w_i\left(P(x)e_i^\alpha + \frac{\partial P}{\partial x^\beta}\Delta X e_i^\alpha e_i^\beta\right) + O(\Delta X^2) = c_s^2\delta^{\alpha\beta}\frac{\partial P}{\partial x^\beta}\Delta X + O(\Delta X^2) \end{aligned} \tag{5.13}$$

In other words, the pressure gradient can be approximated as follows:

$$\frac{\partial P}{\partial x^{\alpha}} = \delta_{\alpha\beta}\frac{1}{cs_2\Delta X}\sum_i P(x + e_i\Delta X)e_i \tag{5.14}$$

The similar formula can be derived for the second derivatives of the pressure:

$$\begin{gathered}\sum_i w_i(e_i^{\alpha}e_i^{\beta} - c_s^2\delta^{\alpha\beta})P(x + e_i\Delta X) = \\ = \Delta X^2 c_s^4\frac{1}{2}(\delta^{\alpha\beta}\delta^{\gamma_1\gamma_2} + \delta^{\alpha\gamma 1}\delta^{\beta\gamma_2} + \delta^{\alpha\gamma 2}\delta^{\beta\gamma_1})\frac{\partial^2 P}{\partial x^{\gamma_1}\partial x^{\gamma_2}} + O(\delta X^4)\end{gathered} \tag{5.15}$$

Therefore, the matrix of the second derivatives of the pressure can be approximated as:

$$\frac{\partial^2 P}{\partial x_{\alpha}x_{\beta}} = \frac{1}{c_s^4\Delta X^2}\sum_i P(x + e_i\Delta X)e_i^{\alpha}e_i^{\beta} \tag{5.16}$$

Expressions (5.14) and (5.16) allow one to compute the pressure gradient at the given lattice node. Therefore, the velocity of the fluid and equilibrium distribution can be computed as well. In other words, the relation (5.14) can be used in the numerical simulations with LBM. However, the direct implementation of the approximation of the pressure gradient can introduce additional numerical noise, since the equilibrium distribution functions are piece-wise linear with respect to pressure gradient. Moreover, in the case of local minimum or maximum of the pressure, the application of the expression (5.14) can result in the significant decrease of the overall flow velocity. This is of critical importance for the near-well region, where pressure has a local minimum or maximum. In order to resolve the issues with the noise and numerical error, the equilibrium distribution function is averaged over the cell, which is the neighbourhood of the node. For that purposes, the pressure gradient is approximated by the linear function using the Taylor expansion and derivatives (5.14) and (5.16). Thus, in the numerical scheme the following replacement

has been made:

$$f_i^{eq} \rightarrow \frac{\int_{cell} f_i d^3x}{\int_{cell} d^3x} \tag{5.17}$$

In the numerical scheme the quadrature rule is used in the numerical integration (5.17). It should be mentioned the integration should be performed over the subspace of three dimensional space. In the present work the geometry of the cells is rectangular or cubic. Therefore, the quadrature rule can be considered as the product of quadrature rules for one dimensional space. In the present work the quadrature rule for three dimensional integration is obtained from the one-dimensional rule with three weights and three points. Therefore, the quadrature rule in 3D has 27 weights and 27 points.

5.3 Numerical Results

The novel approach is validated against a FV reservoir simulator. A rectangular reservoir with a single vertical well in the middle has been considered (5.1).

The flow of the gas has been considered. PVT properties of the gas are described by the following EOS:

$$P = \rho \frac{P_0}{\rho_0} \tag{5.18}$$

Here p_0 is the pressure of the gas for the reference density ρ_0. In this particular section $P_0 = 1.0atm$ for the $\rho_0 = 1.0$. In other words, the gas with the unit density has the pressure of one atmosphere. The viscosity of the gas is constant and $\mu = 0.01cP$. The dimensions of the reservoir are the following: $2000m \times 2000m \times 20m$. The permeability is $k = 1mD$, the porosity is $\phi = 0.01$.

The two-years production from the reservoir has been modelled. Numerical tests has been made with the following values of the bottom-hole pressure (BHP): $10\ atm$, $30\ atm$, $50\ atm$, $70\ atm$ and $90\ atm$. Plots of recovery factor vs time have been compared with each other (5.2). The result of simulations with the novel approach are in the agreement

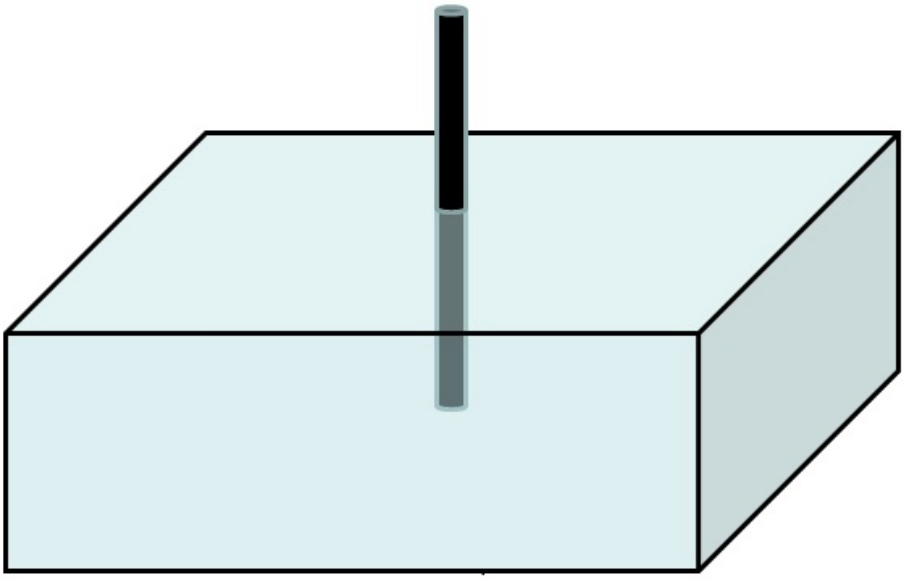

Figure 5.1: The scheme of the reservoir model that has been used in simulations. In fact, the reservoir is 2D despite the fact that the code has been designed for 3D models. The periodic boundary condition has been applied in the direction parallel to the well. This trick makes it possible to use 3D code for 2D simulations.

with ones obtained with a conventional FV simulations.

5.4 Properties of the Novel Approach

The first important thing to mention is the constraint on the time step. The equilibrium distribution is a piece-wise linear function of the pressure gradient as it follows from (5.3), (5.8) in couple with the Darcy law. This means that for f_0^{eq} to be positive, there is an upper boundary for the time step. One can show that the constraint on the time step is the same as for the explicit numerical scheme for reservoir simulations. Therefore, at the present stage of the development the method is far away from real implementations because of the high run-times.

Despite the disadvantage concerned, the method indicates the prospects of the development of LBM schemes for reservoir simulations. It is important to keep in mind that in

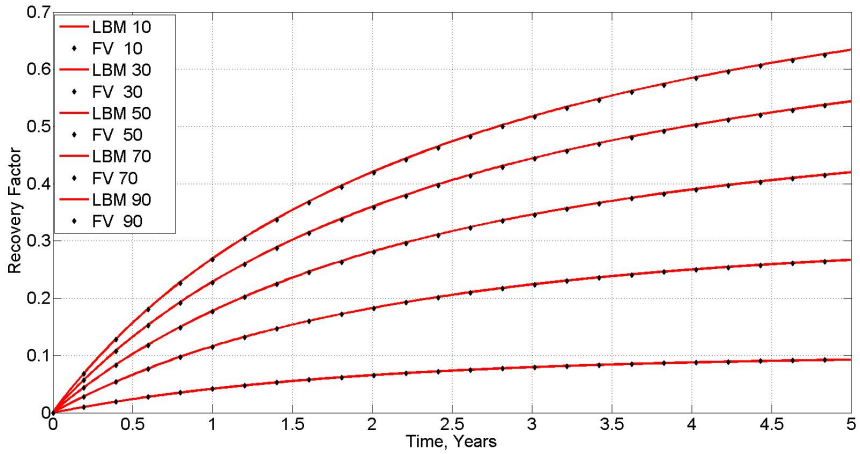

Figure 5.2: Plots of the recovery factor vs time for five values of BHP:. The BHP takes the following values: $10\ atm$, $30\ atm$, $50\ atm$, $70\ atm$ and $90\ atm$. The production profiles derived with the novel LBM scheme (solid line) and with the standard FV simulation (solid dots) are in the reasonable agreement with each other.

the approach discussed the equilibrium distribution functions that correspond to the particles with non-zero velocity are become zero together with the pressure gradient. This means a significant reduction of the numerical diffusion if compared with the standard pseudo-potential LBM schemes. Thus, the feature concerned is beneficial for the accurate modelling of transient processes.

The other advantage of the novel LBM scheme is a potential for the numerical solution of the Navier-Stokes equations. The equilibrium distribution of the form (5.3), (5.8) can be considered as the representation of the pure convection in terms of the distribution of the particles. In other words, this equilibrium distribution represents the pure convection. In this case the question arises: is it possible to add the diffusion part so that it is possible to model the flow of the gas without any porous media? Such separation of the diffusion and the convection has a potential to represent transport phenomena and EOS separately from each other. Moreover, the idea of representation of the mean velocity of the fluid as

the convex combination of lattice velocity vectors has a potential to solve the issue with the Galilean invariance in LBM, which is of fundamental importance.

Finally, the new approach described here can be applied to the simulation of the reservoirs with complex geometry. This happens because all the techniques of formulation of boundary conditions for LBM schemes can be used in simulations with the novel LBM scheme. Therefore, the method inherits the remarkable property of the classic LBM schemes to work with the systems with complex geometry.

6. CONCLUSION AND FUTURE RESEARCH

The first result of the present work is related to the so-called self-consistent LBM models. Here self-consistent means that the EOS of the fluid is introduced through the equilibrium distribution functions in contrast to the conventional LBM models. We have introduced a new LBM scheme using an implicit solver, which shows good accuracy and demonstrates the applicability to the modelling of shale reservoirs. This has been shown through the derivation of the modified EOS for the gas inside the nano-pores as it is illustrated with a Figure (3.9). Therefore, the method can be used for integration of various scales in simulations of shale reservoirs.

The most significant contribution of the present work is the observation of the limitations of the LBM as a computational method. The first restriction on the applicability of the LBM has been derived for the self-consistent model. It has been shown that for a given spatial resolution there exist both lower and upper bound for the time step. The upper bound is common in numerical methods. However, the presence of the lower bound on the time-step is surprising. This restriction limits the applicability of the method given its numerical stability. Basically, the self-consistent LBM model can be hardly extended to the multiphase flow, especially for the fluid with high contrast in density. Namely, the ranges of time steps for which the scheme is stable for each of the fluids may have an empty intersection. Therefore, in certain cases it is not possible to design any self-consistent LBM system for two-phase flow of fluids with a high contrast in PVT properties. Moreover, even for the single phase flow, high contrast in pressures within the computational domain can result in the negative equilibrium distribution functions, which typically leads to the blow-up of the solution.

The central result of the present work is that that limitations are fundamental for the

formulation of LBM. It has been shown that the extension of the lattice can not solve the problem with the existence of the lower bound for the time step. As long as the time step is related to the ratio between pressure and density, it follows that the self-consistent LBM scheme can not be applied for reservoir simulations, because of the impractically small time step.

From the discussion above, it can be concluded that the for the field-scale simulations a pseudo-potential model should be used. In the present work, a novel pseudo-potential model has been proposed. The advantage of the model is that it uses the semi-implicit scheme in the simulations. The feature concerned of the model is beneficial for the numerical stability of the scheme. That pseudo-potential LBM model follows the Darcy Law in the case of steady-state flow. Significant deviations from the results of simulations with FV schemes has been observed. In the present work it has been shown that the reason for that difference is the numerical diffusion. It has been demonstrated that the coefficient of the diffusion concerned is proportional to $\Delta X^2/\Delta T$. That relation imposes the lower bound for the time step, however, in the case of the pseudo-potential model the constraint on the magnitude of the time step comes not only from the stability reasons, but is caused by the issues with the accuracy. Moreover, it has been indicated that the numerical diffusion is an inherit property of standard LBM pseudo-potential methods. This happens because the mass fraction of the particles that participate in the mass exchange process during each time step does not vanish when the time step is going to zero. The latter causes significant difficulties in simulations of multiphase flow.

The third important contribution of the present work is the formulation of the alternative LBM model for field-scale simulations. The method can be applied to reservoir simulation as it has been demonstrated through the validation against the FV method. The major feature of the new approach is that components of the equilibrium distribution that correspond to the particles with non-zero velocities are proportional to the velocity of the

fluid or to the pressure gradient in the case of flow in porous media. The latter means that there is no mass flux, when the pressure gradient is zero, which is reasonable from the physical point of view. Therefore, the approach concerned has a potential for applications in reservoir simulations.

The robustness of the novel LBM scheme is comparable with standard FV explicit schemes for reservoir simulations. Therefore, at the present stage of the research the method is far away from real reservoir simulations. However, the method has a fundamental meaning for the theory of LBM. The central idea of the novel approach can be formulated as the explicit calculation of the convective part of the fluid motion. In the case of the flow of the fluid in porous media, the latter is the only available type of motion. It is worth to explore the possibility of the application of the method to the simulation of gas flow without any porous media. One of the possible ways is to separate convection and diffusion parts of the fluid motion and use the developed approach for the calculation of the convective part. In this case the novel technique is required for the calculation of the diffusion of the fluid. The research developed here can benefit the solution of the issue with the EOS in LBM simulations without the introduction of pseudo-potentials of different types.

Finally, the research concerned can be considered as the revision of the potential of the LBM for practical simulations. One of the outcomes is exploration of the boundaries for the applications of LBM, caused by the problems with numerical stability and accuracy. However, the conceptually new LBM scheme that has a potential to go beyond the indicated boundaries has been presented.

REFERENCES

[1] K. C. Samir , L. Wolfgang, “The Human Core of the Shared Socioeconomic Pathways: Population Scenarios by Age, Sex and Level of Eduaction for all Conutries to 2100,” Global Enviromental Change, vol. 42, pp. 181–192, 2017.

[2] A. E. Kontorovich, M. I. Epov, L. V. Eder, “Long Term and Medium-Term Scenarios and Factors in World Energy Perspectives for the 21st Century,” Russian Geology and Geophysics, vol. 55, pp. 534–543, 2014.

[3] B. B. Hughes, “International Futures and Integrated, Long-Term Forecasting of Global Transformations,” Futures, vol. 81, pp. 98–118, 2016.

[4] “Memorandum to Senate Environment and Public Works Committee”, Congressional Research Service, October 20, 2009.

[5] Joaquim José da Costa e Simas, “Simulation of fluid flows with Lattice Boltzmann on GPU’s"" Instituto Superior Técnico. Master Thesis, December 2010.

[6] C. R. Clarkson, N. Solano, R. M. Bustin, A. M. M. Bustin, G. R. L. Chalmers, L. He, Y. B. Melnichenko, A. P. Radlinski, T. P. Blach, “Pore Structure Characterization of North American Shale Gas Reservoirs Using USANS/SANS, gas adsorption, and mercury intrusion”, Fuel, vol. 103, pp. 606–616, 2013.

[7] P. Wang, Z. Jiang, L. Chen, L. Yin, Z. Li, C. Zhang, X. Tang, G. Wnag, “Pore Structure Characterization for the Longmazi and Niutitang Shales in the Upper Yangtze Platform, South China: Evidence from Focused Ion Beam - He Ion Miscroscopy, Nano-Computerized Tomography and Gas Adsorption Analysis”, Marine and Petroleum Geology, vol. 77, pp. 1323–1337, 2016.

[8] M. Schmitt, C. P. Fernandes, F. G. Wolf, J. A. Bellini, C. P. Rahner, V. S. Santiago dos Santos, "Characterization of Brazilian tight gas sandstones relating permeability and Angstrom-to micron-scale pore structures", Journal of Natural Gas Science and Engineering, vol. 27, pp. 789–807, 2015.

[9] M. Sheng, G. Li, Z. Huang, S. Tian, S. Shah, L. Geng, "Pore-Scale Modeling and Analysis of Surface Diffusion Effects on Shale-Gas Flow in Kerogen Pores", Journal of Natural Gas Science and Engineering, vol. 27, pp. 979–985, 2015.

[10] C. Shangbin, H. Yufu, F. Changqin, Z. Han, S. Yanming, Z. Zhaoxi, "Micro and Nano-Size Pores of Clay Minerals in Shale Reservoirs: Implication for the Accumulation of Shale Gas" Sedimentary Geology, vol. 342, pp. 180–190, 2016.

[11] D. Fan, A. Ettehadtavakkol, "Semi-Analytical Modeling of Shale Gas Flow through Fractal Induced Fracture Networks with Microseismic Data", Fuel, vol. 193, pp. 444–459, 2017.

[12] T. Guo, S. Zhang, Z. Qu, T. Zhou, Y. Xiao, H. Gao. "Experimental Study of Hydraulic Fracturing for Shale by Stimulated Reservoir Volume", Fuel, vol. 128, pp. 373–380, 2014.

[13] W. Yonggui, C. Linsong, H. Shijun, J. Oin, Z. Jin, L. Xiang, H. Hongliang, "A Practical Method for Production Data Analysis from Lultistage Fractured Horizontal Wells in Shale Gas Reservoirs", Fuel, vol. 186, pp. 821–829, 2016.

[14] Z. Zhang, X. Li, J. He, Y. Wu, G. Li. "Numerical Study on the Propagation of Tensile and Shear Fracture Network in Naturally Fractured Shale Reservoirs", Journal of Natural Gas Science and Engineering, vol. 37, pp.1–14, 2017.

[15] Y. Cho, E. Ozkan, O. G. Apaydin, "Pressure-Dependent Natural-Fracture Permeability in Shale and its Effect on Shale-Gas Well Production", SPE Reservoir Evalution &

Engineering, vol. 16, 2013.

[16] Z. Z. Li, T. Min, Q. Kang, Y. Ling-He, W. Q. Tao, “Investigation of Methane Adsorption and its Effect on Gas Transport in Shale Matrix through Microscale and Mesoscale Simulations”, International Journal of Heat and Mass Transfer, vol. 98, pp. 675-686, 2015.

[17] J. Kiang, R. M. Younis, “Compositional Modeling of Enhanced Hydrocarbons Recovery for Fractured Shale Gas-Condensate Reservoirs with Effects of Capillary Pressure and Multicomponent Mechanism”, Journal of Natural Gas Science and Engineering, vol. 34, pp. 1262–1275, 2016.

[18] A. S. Pour, S. Bryant. “Gas Permeability of Shale”, SPE Reservoir Evaluation and Engineering, vol. 15, 2012.

[19] Q. Cao, R. Banerjee, S. Gupta, J. Li, W. Zhou, B. Jeyachandra. “Data Driven Production Forecasting Usine Machine Learning”, SPE Argentina Exploration and Production of Unconventional Resources Symposium, 2016.

[20] H. Klie, “Physics-Based and Data-Driven Surrogates for Production Forecasting”, SPE Reservoir Simulation Simposium, 2012.

[21] O. Samandarli, H. A. Al-Ahmadi, R. A. Wattenbarger, “A Semi-Analytic Method for History Matching Fractured Shale Gas Reservoirs”, SPE Western North American Regional Meeting, 2011.

[22] A. Negara, A. Salama, S. Sun, M. Elgassier, Y. S. Wu, “Numerical Simulation of Natural Gas Flow in Anisotropic Shale” Abu Dhabi Internetional Petroleum Exhipition and Conference, 2015.

[23] W. Yu, K. Sepehrnoori, T. W. Patzek, “Evaluation of Gas Adsorption in Marcellus Shale”, SPE Annual Technical Conference and Exhibition, 2014.

[24] C. Li, P. Xu, S. Qiu, Y. Zhou, "The Gas Effective Permeability of Porous Media with Klinkenberg Effect", Journal of Natural Gas Science and Engineering, vol. 34, pp. 534–540, 2016.

[25] J. Li, A. S. Sultan, "Klinkenberg Slippage Effect in the Permeability Computations of Shale Gas by the Pore-Scale Simulations", Journal of Natural Gas Science and Engineering, vol. 30, pp. 1–6, 2016.

[26] K. I. Madiebo, H. Nasrabadi, E. Gildin, "Mesoscopic Simulation of Slip Motion for Gas Flow in Nanochannels", Fluids Engineering Systems and Technologies, vol. 7B, 2015.

[27] R. Kou, Y. Akkutlu, "A Molecular Dynamic Simulation Approach in Estimating Organic-Rich Shale Permeability", SPE International Conference and Exhibition, 2016.

[28] B. Jin, H. Nasrabadi, "Phase Behavior of Multi-Component Hydrocarbon Systems in Nano-Pores Using Gauge-GCMC Molecular Simulation", Fluid Phase Equilibria, vol. 425, pp. 324–334, 2016.

[29] B. Zhou, R. Xu, P. Jiang, "Novel Molecular Simulation Process Design of Adsorption in Realistic Shale Kerogen Spherical Pores", Fuel, vol. 180,pp. 718–726, 2016.

[30] Y. Ning, Y. Jiang, H. Liu, G. Qin, "Numerical modeling of slippage and adsorption effects on gas transport in shale formations using the lattice Boltzmann method", Journal of Natural Gas Science and Engineering, vol. 26, pp. 345–355, 2015.

[31] O. Samandarli, B. McDonald, G. Barzola, M. Murray, P. Richmond, "Understanding Shale Performance: Performance Analysis Workflow with Analytical Models in Eagle Ford Shale Play", SPE Unconventional Resources Conference, 2014.

[32] J. Guo, J. Zeng, X. Wang, “Analytical Model for Multifractured Horizontal Wells in Heterogeneous Shale Reservoirs”, SPE Asia Pacific Oil & Gas Conference and Exhibition, 2016.

[33] D. Zheng, B. Yuan, R. G. Moghanloo, “Analytical modeling dynamic drainage volumes for transient flow towards multi-stage fractured wells in composite shale reservoirs”, Journal of Petroleum Science and Engineering, vol. 149, pp. 756–764, 2017.

[34] H. Sun, A. Chawathe, H. Hoteit, X. Shi, L. Li, “Understanding Shale Gas Flow Behavior Using Numerical Simulation”, SPE Journal, 2015.

[35] J. Andrade, F. Civan, D. Devegowda, R. Sigal, “Accurate Simulation of Shale-Gas Reservoirs”, SPE Annual Technical Conference and Exhibition, 2010.

[36] N. Li, Q. Ran, J. Li, J. Yuan, C. Wang, Y. S. Wu, “A Multiple-Continuum Model for Simulation of Gas Production from Shale Reservoirs” SPE Reservoir Characterization and Simulation Conference and Exhibition, 2013.

[37] P. N. Azom, F. Javadpour, “Dual-Continuum Modeling of Shale and Tight Gas Reservoirs”, SPE Annual Technical Conference and Exhibition, 2012.

[38] B. Rubin, “Accurate Simulation of Non-Darcy Flow in Stimulated Fractured Shale Reservoirs”, SPE Western Regional Meeting, 2010.

[39] M. Limsukhon, K. Ghorayeb, R. M. Aziz, S. R. Narhari, S. Chakraborty, “Calibration of DFN Model with Well Test Data - A Case Study of The North Kuwait Jurassic Complex”, SPE/EAGE Reservoir Characterization and Simulation Conference, 2009.

[40] L. Guaiquirian, P. Gonzalez, A. Gonzalez, M. M. Hernandez, “Use of Discrete Fracture Network "DFN" to Characterise and Model a Naturally Fractured Sandstone Reservoirs: A case Study of Orocual Field, San Juan Formation, Venezuela"", SPE Latin American and Caribbean Petroleum Engineering Conference, 2007.

[41] Y. Wang, “A Hybrid Dual-Continuum Discrete Fracture Modeling Approach for Numerical Simulation of Production from Unconventional Plays”, SPE International Student Paper Contest at the SPE Annual Technical Conference and Exhibition, 2015.

[42] A. Kumar, D. Carnilleri, M. Brewer, “Comparative Analysis of Dual Continuum and Discrete Fracture Simulations Approaches to Model Fluid Flow in Naturally Fractured, Low-Permeability Reservoirs”, SPE Low Perm Symposium, 2016.

[43] C. Du, X. Zhang, B. Melton, D. Fullilove, B. Suliman, S. Gowelly, D. Grant, J. L. Calvez, “A Workflow for Integrated Barnett Shale Gas Reservoirs Modeling and Simulation”, SPE Latin American and Caribbean Petroleum Engineering Conference, 2009.

[44] G. Ren, J. Jiang, R. M. Younis, “A Fully Coupled XFEM-EDFM Model for Multiphase Flow and Geomechanics in Fractured Tight Gas Reservoirs”, Procedia Computer Science, vol. 80, pp. 1404–1415, 2016.

[45] A. G. Ramm, “Global Existence, Uniqueness and Estimates of the Solution to the NavierStokes Equations”, Applied Mathematics Letters, vol. 74, pp. 154–160, 2017.

[46] H. Zhang, D. Cao, “Molecular Simulation of Displacement of Shale Gas by Carbon Dioxide at Different Geological Depths”, Chemical Engineering Science, vol. 156, pp. 121-127, 2016.

[47] E. Schröedinger, ”An Undulatory Theory of the Mechanics of Atoms and Molecules”, Phys. Rev, vol. 28, (6): pp. 1049–1070, 1926.

[48] W. Hwang, “Mecahnics of Kinesin-Based Transport: From Single-Molecule to Multi-Motor Behaviors, to Cell Division”, IMAG Interagency Modeling and Analysis Group, webinar, 2013.

[49] S. Harris, “An Introduction to the Theory of the Boltzmann equation”, Dover Books, p. 221.

[50] T. Xue-lin, Y. Xin, C. Zhi-Cong, S. Xaio-Yan, “Application of LBM-SGS Model to Flows in a Pumping-Station Forebay”, Journal of Hydrodynamics, vol. 22, pp. 196–206, 2010.

[51] H. Cheng, Y. Qiao, C. Liu, Y. Li, B. Zhu, Y. Shi, D. Sun, K. Zhang, “Extended Hybrid Pressure and Velocity Boundary Conditions for D3Q27 Lattice Boltzmann Model”, Applied Mathematical Modeling, vol. 36, pp. 2031–2055, 2012.

[52] F. Calabro, A. C. Esposito, G. Mantica, T. Radice, “Refinable Functions, Functionals, and Iterated Function Systems”, Applied Mathematics and Computation, vol. 272, pp. 199–207, 2016.

[53] S. Palpacelli, “Quantum Lattice Boltzmann Methods for the Linear and Nonlinear Schrödinger Equation in Several Dimensions”, Iniversita delgi Studi Roma Tre, PhD Thesis, 2009.

[54] D. A. Wolf-Gladrow, “Lattice-Gas Cellular Automata and Lattice-Boltzmann Models - An Introduction”, Springer, 2000.

[55] J. Lu, C. B. Mendl, “Numerical Scheme for a Spatially Inhomogeneous Matrix-Valued Quantum Boltzmann Equation”, Journal of Computational Physics, vol. 291, pp. 303–316, 2015.

[56] R. Yano, “From Conduction to Convection of Thermally Relativistic Fluids between two Parallel Walls under Gravitational Force”, Physica A: Statistical Mechanics and its Applications, vol. 465, pp. 384-402, 2017.

[57] L. Pan, K. Xu, Q. Li, J. Li, “An Efficient and Accurate Two-Stage Fourth-Order Gas-Kinetic Scheme for the Euler and Navier-Stokes Equation”, Journal of Computational

Physics, vol. 326, pp. 197–221, 2016.

[58] Y. Keehm, T. Mukerji, M. Prasad, A. Nur, “Permeability Prediction from Thin Sections Using the Lattice-Boltzmann Flow Simulation”, Society of Exploration Geophysics Conference, 2003.

[59] Y. Jin, X. Li, M. Zhao, X. Liu, H. Li, “A mathematical Model of Fluid Flow in Tight Pores Media Based on Fractal Assumptions”, International Journal of Heat and Mass Transfer, vol. 108, pp. 1078–1088, 2017.

[60] T. Ramstad, P. E. Oren, S. Bakke, “Simulation of Two Phase Flow in Reservoir Rocks Using Lattice-Boltzmann Method”, SPE Annual Technical Conference and Exhibition 2009.

[61] J. Jiao, K. V. Paulson, “A Lattice-Boltzmann Automation for the Simulation of Two-Dimensional Waterflooding”, PETSOC Conference, 1993.

[62] L. Liu, J. Yao, L. Zhang, S. An, J. Zhao, H. Sun “REV-Scale Simulation of Micro-Fractured Unconventional Gas Reservoir”, Journal of Natural Gas Science and Engineering, vol. 30, pp. 1–11, 2017.

[63] D. Hessling, Q. Xie, J. Harting “Diffusion Dominated Evaporation in Multicomponent Lattice-Boltzmann Simulation”, Cornell University Library, arXiv:1701.03637v2, 2017.

[64] Q. Liu, Y. L. He, Q. Li, W. Q. Tao, “Multiple-Relaxation-Time Lattice Boltzmann Model for Convection Heat Transfer in Porous Media Under Local Thermal non-Equilibrium Condition”, International Journal of Heat and Mass Transfer, vol. 73, pp. 761–775, 2014.

[65] Y. Kuwata, K. Suga, “Anomally of the Lattice Boltzmann Methods in Three-Dimensional Cylindrical Flows”, Journal of Computational Physics, vol. 280,

pp. 563–569, 2015.

[66] A. Yagub, H. Fahrat, S. Kondaraju, T. Singh, “A Lattice Boltzmann for Substrates with Regularly Structured Surface Roughness”, Journal of Computational Physics, vol. 301, pp. 402–414, 2015.

[67] Y. Ning, Y. Jiang, H. Liu, G. Qin, “Numerical Modeling of Slippage and Adsorption Effects on Gas Transport in Shale Formations Using the Lattice Boltzmann Method”, Journal of Natural Gas Science and Engineering, vol. 26, pp. 345–355, 2015.

[68] P. R. Rao, L. A. Schaefer, “Numerical Stability of Explicit off-Lattice Boltzmann Schemes: A Comparative Study”, Journal of Computational Physics, vol. 285, pp. 251–264, 2015.

[69] O. Coussy, “Poromechanics”, John Wiley and Sons Ltd, pp. 37-82, 2004.

[70] A. Tarakanov, E. Gildin, H. Nasrabadi, “Simulation of Flow in the Solid Matrix of Shale Reservoirs Using Lattice-Boltzmann Method”, SPE Europec featured at 78th EAGE Conference and Exhibition, 2016.

[71] Z. Benamram, A. Tarakanov, H. Nasrabadi, E. Gildin, “Efficient Fractured Reservoir Simulation Using Lattice Boltzmann Method”, SPE Latin American and Caribbean Petroleum Engineering Conference, 2015.

[72] A. A. Mohamad, A. Kuzmin, “A Critical Evaluation of Force Term in Lattice Boltzmann Method, Natural Convection Problem”, International Journal of Heat and Mass Transfer, vol. 53, pp. 990-996, 2010.